UNIVERSITY OF BATH

PHD

Aspects of wave propagation in fluid-loaded structures.

Eatwell, G. P.

Award date:
1981

Awarding institution:
University of Bath

[Link to publication](#)

Alternative formats

If you require this document in an alternative format, please contact:
openaccess@bath.ac.uk

ASPECTS OF WAVE PROPAGATION IN

FLUID-LOADED STRUCTURES

submitted by G.P. Eatwell for the

degree of Ph.D. of the University of Bath

1981

G.P. Eatwell

ProQuest Number: U321669
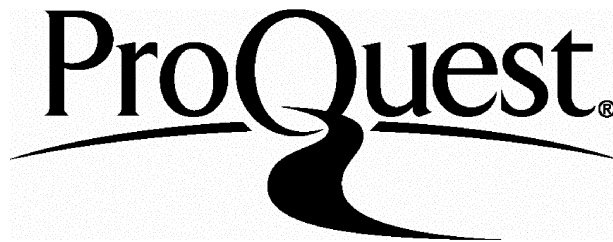
ProQuest U321669

ABSTRACT

This thesis is concerned with the study of two independent

problems. Chapter 2 is devoted to the development of a new

representation for the dynamic Green's tensor for a layered

medium. No completely closed solution is possible and the

objective here is to develop a representation that is more

amenable to computation than the existing representations

(Cagniard (39), Willis (73)). The representation derives from

a reduction of the integrals required for the inversion of the

terms in a"generalized ray" series. For the three-dimensional

(point source) problem the final solution requires either a

single integration (isotropic layers) or two integrations

(anisotropic layers) over contours that are independent of time

t and position x. The integrand is a simple explicit function,

much of which is independent of x and t and may be tabulated

when the solution is required for a range of values of x and t.

The remainder of this thesis examines the time-harmonic

response of thin, elastic, fluid-loaded plates stiffened by

attached parallel beams. The sound radiated by such structures

has been studied by many authors but few have been concerned with

the motion of the plate. Chapters 3, 4 and 5 of this thesis

examine plates stiffened, respectively, by finite, infinite,

and semi-infinite arrays of beams. In chapter 3, Fourier transforms

are used to obtain a set of simultaneous equations for the

transformed displacements and rotations at the beams. The inverse

transform of the solution to this set of equations is evaluated

asymptotically.

In chapters 4 and 5 the stiffening beams are equally spaced.

The equations are formulated in terms of discrete convolutions and a transform, related to the modified Z-transform, is used (together with the Wiener-Hopf technique in chapter 5) to obtain the solution. Asymptotically, the motion of the stiffened regions of the plate has the form of a Floquet wave.

ACKNOWLEDGEMENT

CONTENTS

Chapter 1.   INTRODUCTION

This thesis is concerned with the study of two independent problems. Chapter 2 is devoted to the development of a new representation for the transient response of a layered medium. Although applicable to problems in geophysics and acoustic emission, the method may also be used to find the response of a structure overlaid by a fluid half-space or a fluid layer. The remainder of the thesis is concerned primarily with particular fluid-loaded structures and examines the time-harmonic response of a thin, elastic, fluid-loaded plate stiffened by attached parallel beams.

No completely closed solution for the transient response of a layered medium is possible and so the objective of chapter 2 of this thesis is to develop a representation that is more amenable to computation than the existing representations. The waves that travel along various ray paths in the medium, because of multiple reflections and refractions, are represented as a series of "generalized rays". This series is obtained by the use of a suitable integral transform in the plane of the layers which produces a set of equations for the transformed variable. This set of equations is then solved by iteration to generate the "generalized ray" series. (See, for example, Spencer (60)). The integrals required for the inversion of the transforms in the series may be reduced by utilization of the structure of the terms. Chapter 2 describes an alternative to the existing methods of reduction (Cagniard (39), Willis (73)).

For the three dimensional (point source) problem the method of Cagniard (39) requires the evaluation of an integral over a

contour that is associated with an algebraic equation which
depends upon time t and position x. The method of Willis (73)
requires integration around a fixed contour but explicit
evaluation of the integrand requires the solution of an
algebraic equation for each time t and position x. The
representation developed here requires integration around two
fixed contours of a simple, explicit integrand; however, for
problems involving isotropic layers the order of integration may
be reversed and the first integration is elementary. Much of the
integrand is independent of x and t and may be tabulated when
the solution is required for a range of values of x and t. The
equation solving required by Cagniard (39) and Willis (73) is
avoided and the representation here is likely to be
computationally more efficient.

For simplicity the method is described for an anisotropic
half-space. Explicit expressions and results are given for an
isotropic half-space which is either free or overlaid by a
fluid. Each term in the generalized ray expansion for a layered
medium can be treated in a similar fashion.

The sound radiated by thin, elastic, beam-stiffened plates
is of interest in the analysis of aircraft and marine structures
and has been studied by many authors (see section 3.1). However,
few have been concerned with the motion of the plate. Chapters
3,4 and 5 of this thesis examine plates stiffened, respectively,
by finite, infinite and semi-infinite arrays of beams (and
combinations thereof).

Chapter 3 studies the response of a fluid-loaded plate
stiffened by arbitrarily spaced parallel beams which are modelled
as line attachments capable of exerting forces and moments on

the plate. A Fourier transform parallel to the beams produces a
finite set of equations for the transformed displacements and
rotations at the beams. Inversion of the transform to find the
displacement of the plate (or the fluid pressure) requires the
evaluation of integrals, which is a lengthy computation since
evaluation of the integrand at each point requires the solution
of a set of simultaneous equations. However, at large distances
from the beams the integrals can be evaluated asymptotically.
In chapter 3 results are given for line and point excitation of
a plate stiffened with equally spaced beams. As a natural
extension, chapter 4 examines the response of a periodically
stiffened plate. Solutions to the problem already exist (for
example, Evseev (73)), but apart from calculation for the input
impedance by Mace (80a) results have again been confined to
calculation of the radiated sound. In chapter 4 the problem is
formulated in terms of discrete convolution equations which
expose the structure of the problem. A transform, termed the
modified discrete Fourier transform, is introduced which is
related to the modified Z transform. Rather than representing
the displacement as a superposition of harmonic waves, as in the
ordinary Fourier transform, this discrete transform represents
the displacement as a superposition of Floquet waves. (after
G. Floquet (1883) who studied linear differential equations with
periodic coefficients). Application of the modified discrete
Fourier transform reduces the convolution equations to algebraic
equations which can be solved. The transform is inverted
asymptotically to show that the wave in the plate is
(asymptotically) a Floquet wave. The corresponding problem
without fluid loading is also considered and for this problem

the inversions may be performed exactly to show that the displacement field is made up of two forward- and two backward-going Floquet waves.

Chapter 5 uses the techniques developed in chapter 4 together with the Wiener-Hopf technique to study a plate stiffened on one half by a semi-infinite array of equally spaced beams. A real structure may possibly have some discontinuity in the periodicity of the stiffening. Some discontinuities, such as gaps or additional beams, are discussed in the extensions to chapter 4, but chapter 5 studies the simplest case of a complete change in structure. The general response of a plate stiffened on one half by a semi-infinite array of beams is discussed and explicit expressions and results are derived for the case when the excitation takes the form of a free plane wave in the unstiffened half of the plane, incident upon the array of beams. Once again the transforms are inverted asymptotically to give the reflected, transmitted and radiated fields. It is shown that, asymptotically, the transmitted field has the form of a Floquet wave which may or may not propagate unattenuated, whereas, again asymptotically, the reflected field has the same form as the incident wave. The incident wave, which is acoustically slow, is scattered by the beams and radiates sound into the fluid.

The techniques developed in chapters 4 and 5 may well have applications in the solution of other problems involving periodic or "semi-periodic" systems, although many simple systems may be studied by assuming the solution to be a linear combination of the free Floquet waves.

The work of chapter 2 is the subject of a paper which has been accepted for publication by the Journal of Wave Motion.

CHAPTER 2 THE DYNAMIC GREEN'S TENSOR FOR A LAYERED MEDIUM

2.1 INTRODUCTION

In this chapter a new representation for the dynamic Green's tensor for an elastic half-space or layered medium is developed. The representation is derived from a method for inverting the transforms which occur in a "generalized ray" expansion of the Green's tensor. The theory of generalized rays was developed for analysing transient waves in a layered medium and has applications in geophysics (Spencer (60), Knopoff et al (60), Pekeris (65)) and in the analysis of signals in acoustic emission (Pao and Gajewsky (77)).

Study of the dynamic Green's tensor for a layered medium usually proceeds from finding an appropriate integral transform for which equations are easy to generate. If the ultimate objective is to produce a representation amenable to computation, then a major effort is devoted to the efficient solution of these equations. The resulting transforms are then inverted numerically, which inevitably leads to some loss of accuracy near to wave-fronts. Recent examples are provided by the work of Kennett and Kerry (79) and Kennett (80). If high accuracy at wavefronts is required, then it is preferable to solve the equations that define the transform by iteration, to produce a series of "generalized rays". The integrals required for inverting the transform are then reduced by exploiting the particular structure of the individual terms in the series. One such method for reducing the integrals is that of Cagniard (39). For the two-dimensional (line source) problems this leads to a solution that is explicit

apart from the need to solve algebraic equations, while for the three-dimensional problem, there remains an integral over a contour that is dependent on time and position. The method requires the discussion of the structure of a complicated algebraic function and, apart from the study of the two-dimensional Lamb's problem for an anisotropic half-space by Burridge (71), the use of the method is effectively limited to problems involving isotropic layers. The two-dimensional problem has been studied by de Hoop (60) and the three-dimensional Green's tensor has been studied by Johnson (74) for a half-space and by Pao and Gajewsky (77) for a plate.

An alternative method for the reduction of the integrals in a "generalized ray" series is given by Willis (73), which is applicable to the more general problem of anisotropic layers. An example for an anisotropic layer embedded in a half-space is given by Bedding and Willis (80). For the three-dimensional problem the solution requires integration around a fixed unit circle of a function obtained by solving algebraic equations, while for the two-dimensional problem only the solution of algebraic equations is required.

The representation here gives the solution of the two-dimensional problem as an integral around a contour that is independent of time, t, and position, x, the integrand for which is a simple explicit function of x and t. Much of the integrand is also independent of x and t and may be tabulated when evaluating the solution for a range of values of x and t. For the three-dimensional case, the solution is in terms of the integral around a unit circle of a function which is itself defined by a contour integral as described above. Repeated evaluation of this

integral is likely to be competitive with the equation solving required in Willis (73). However, if the layers are isotropic the order of integration may be reversed. The integral over the unit circle is elementary and the final solution is given by the integral over a contour, independent of x and t, of an explicitly defined function with simple x and t dependence. Thus, the method avoids the equation solving of Willis (73) and the integration over contours with complicated x and t dependence, required by Cagniard (39).

In this chapter the method is described for the simple case of an anisotropic half-space. Explicit expressions and results are given for an isotropic half-space and the results of Johnson (74) reproduced apart from small discrepancies which are explained.

Finally, as a simple example of a fluid-loaded structure, expressions and results are given for the Green's tensor in an elastic half-space overlaid by a fluid.

2.2   THE REPRESENTATION

Consider the half-space $x_3 < 0$ relative to Cartesian coordinates (x_1, x_2, x_3), excited by a point force at $(0,0,z)$ with step function time dependence. The force has components

$$f_i = F_i H(t)\, \delta(x_1)\, \delta(x_2)\, \delta(x_3-z), \qquad (2.2.1)$$

where $H(\ )$ denotes the Heaviside step function and $\delta(\ )$ is the Dirac delta. The resulting displacement field has components

$$u_i(t,x,z) = G_{ij}(t,x,z)F_j \quad , \qquad (2.2.2)$$

where G_{ij} are the components of the Green's tensor and the summation convention is employed so that repeated suffixes are summed from 1 to 3. G_{ij} represents the ith component of displacement produced by a unit force in the j direction.

It is convenient to introduce matrix notation, as in Bedding and Willis (80), and to define matrices K and C so that they have components

$$K_{ik}(\omega, \xi) = -c_{ijkm}\, \xi_j\, \xi_m + \rho\omega^2 \delta_{ik} \qquad (2.2.3)$$

and

$$C_{ik}(\xi) = c_{i3km}\, \xi_m \quad , \qquad (2.2.4)$$

where c_{ijkm} are the elastic moduli of the half-space and ρ its density. The Green's tensor G then satisfies the equation of motion

$$K(\partial/\partial t, \nabla)G + I\, H(t)\delta(x_1)\delta(x_2)\delta(x_3-z) = 0, \quad t > 0, \ x_3 < 0, \qquad (2.2.5)$$

where I is the identity matrix. G also satisfies the boundary
condition

$$c(\nabla)G = 0, \quad x_3 = 0. \tag{2.2.6}$$

Additionally $G = 0$ for $t < 0$ and $G \to 0$ as $x_3 \to -\infty$.

The Green's tensor G can be written as

$$G = G^{\infty} + G^{1}, \tag{2.2.7}$$

where G^{∞} represents the associated infinite-body Green's tensor
and G^{1} is the "image" tensor induced by the boundary condition
(2.2.6). The Fourier transform $\bar{G}^{\infty}$ of G^{∞} is defined as

$$\bar{G}^{\infty}(\omega,k,z) = \int_{0}^{\infty} dt \iiint dx_1 dx_2 dx_3 G^{\infty}(t,x,z) e^{i(\omega t + k_a x_a + p x_3)}, \tag{2.2.8}$$

where Greek suffixes take the values 1,2 only. $\bar{G}^{\infty}$ is an analytic
function of ω for $Im(\omega) > 0$ for any real $k = (k_1, k_2, p)$. G^{∞}
satisfies (2.2.5) for all z, which transforms to give

$$K(\omega,k)\bar{G}^{\infty}(\omega,k,z) = \frac{i}{\omega} I e^{ipz}. \tag{2.2.9}$$

The eigen-vectors U_n of K are defined by

$$K(\omega,k)U_n = \rho(\omega^2 - \omega_n^2)U_n, \quad n=1,2,3, \tag{2.2.10}$$

where

$$\det K(\omega_n,k) = 0. \tag{2.2.11}$$

If the eigen-vectors are normalized so that $U_n^T U_n = 1$, (no
summation) then we have

$$I = \sum_{n=1}^{3} U_n U_n^T \tag{2.2.12}$$

and

$$\tilde{G}^{\infty}(\omega,k,z) = \frac{i}{\omega} \sum_{n=1}^{3} \frac{U_n U_n^T e^{ipz}}{\rho(\omega^2 - \omega_n^2(k))}$$ (2.2.13)

This inverts to give

$$\tilde{G}^{\infty}(\omega,k_1,k_2,x_3,z) = \frac{i}{2\pi\omega} \int dp \sum_{n=1}^{3} \frac{U_n U_n^T e^{-ip(x_3-z)}}{\rho(\omega^2 - \omega_n^2)} ,$$ (2.2.14)

where $\tilde{G}^{\infty}$ is the Fourier transform of G^{∞} with respect to x_1, x_2 and t. For $x_3 > z$ we can close the contour in the lower half plane and evaluate the integral using Cauchy's theorem, to give

$$\tilde{G}^{\infty}(\omega,k_1,k_2,x_3) = -\sum_{n=1}^{3} \frac{U_n(k,p_n)U_n^T(k,p_n)e^{-ip_n(x_3-z)}}{\rho\omega(\partial\omega_n^2/\partial p)(k,p_n)} ,$$ (2.2.15)

where p_n is a root of the equation

$$\omega_n(k_1,k_2,p_n) = \omega$$ (2.2.16)

so that $p_n(\omega,k_1,k_2)$ is inverse to $\omega_n(k)$ and satisfies

$$\det K(\omega,k_1,k_2,p_n) = 0.$$ (2.2.17)

Equation (2.2.11) has six roots $\pm \omega_n$, n=1,2,3 and, correspondingly (2.2.17) has six roots $p_n, r_n, n = 1,2,3$. Collectively, they define an algebraic function, $p(\omega,k_1,k_2)$ whose Riemann surface has six sheets. This is discussed in Willis (73). The branches p_n are those that have negative imaginary part when ω has positive imaginary part and it is possible, by

making cuts in the ω-plane along those segments of the real

axis where any p_n (and its associated r_n) is real, to ensure

that p_n has negative imaginary part throughout the cut ω-plane.

The branches r_n likewise have positive imaginary part throughout

the cut ω-plane.

For $x_3 < z$ we can close the contour for (2.2.14) in the

upper half-plane to give

$$\tilde{G}^{\infty}(\omega, k_1, k_2, x_3) = \sum_{n=1}^{3} \frac{U_n(k, r_n) U_n^T(k, r_n) e^{-ir_n(x_3-z)}}{\rho \omega (\partial \omega_n^2 / \partial p)(k, r_n)}, \quad x_3 < z. \tag{2.2.18}$$

This represents a sum of down-going plane waves travelling in

the direction (k_1, k_2, r_n), whilst (2.2.15) represents a sum of

up-going plane waves.

The image tensor G^1 satisfies the homogeneous wave equation

associated with (2.2.5), namely

$$K(\partial/\partial t, \nabla) G^1 = 0 \quad x_3 < 0. \tag{2.2.19}$$

Correspondingly $\tilde{G}^1$ satisfies a system of second-order ordinary

differential equations whose general solution is composed of

up- and down-going waves. However, $\tilde{G}^1$ is bounded as $x_3 \to -\infty$

so only down-going waves are permitted and

$$\tilde{G}^1 = \sum_{n=1}^{3} \left\{ U_n(k_1, k_2, r_n) W_n^T e^{-ir_n x_3} \right\}, \tag{2.2.20}$$

for some values of the amplitude vectors W_n. Imposition of the

boundary condition (2.2.6) gives

$$\sum_{n=1}^{3} \left\{ C(k, r_n) U_n(k, r_n) W_n^T + C(k, p_n) U_n(k, p_n) V_n^T e^{ip_n z} \right\} = 0, \tag{2.2.21}$$

where $k = (k_1, k_2)$ and V_n^∞ represents an amplitude associated with (2.2.15):

$$V_n^\infty = -U_n(k, p_n) / [\rho\omega(\partial\omega_n^2/\partial p)(k, p_n)]. \qquad (2.2.22)$$

We can introduce matrix notation, so that

$$W = [W_1, W_2, W_3], \qquad (2.2.23)$$

$$V^\infty = [V_1^\infty, V_2^\infty, V_3^\infty], \qquad (2.2.24)$$

$$D(p, x_3, x_3') = \text{diag}\left\{ e^{-ip_n(x_3 - x_3')} \right\} \qquad (2.2.25)$$

and

$$S(p) = [CU_1, CU_2, CU_3], \qquad (2.2.26)$$

where the C's and U's are evaluated at the appropriate p-root, or, correspondingly, r-root for $S(r)$. The entries in $D(p, x_3, x_3')$ define the phase lags associated with plane waves travelling between x_3' and x_3.

Equation (2.2.21) now takes the form

$$S(r)W^T + S(p)D(p, 0, z)V^{\infty T} = 0 \qquad (2.2.27)$$

and has solution

$$W^T = RD(p, 0, z)V^{\infty T}, \qquad (2.2.28)$$

where

$$R = - [S(r)]^{-1}S(p). \qquad (2.2.29)$$

Each component R_{mn} of the matrix R is a reflection coefficient, giving the amplitude of a reflected m^{th} type wave relative to

the amplitude of an incident wave of the nth type.

Formally, at least, the transform $\widetilde{G}$ is now determined. It can be written as the sum of the three direct waves associated with $\widetilde{G}^{\infty}$ and the nine reflected waves, each direct wave producing three reflected waves. That is

$$\widetilde{G} = \sum_{n=1}^{3} \widetilde{G}_n + \sum_{n=1}^{3} \sum_{m=1}^{3} \widetilde{G}_{mn}, \qquad (2.2.30)$$

where

$$\widetilde{G}_n = \frac{-u_n(k,p_n)U_n^T(k,p_n)e^{-ip_n(x_3-z)}}{\rho\omega(\partial\omega_n^2/\partial p)(k,p_n)} \quad , \quad x_3 > z \qquad (2.2.31)$$

$$\widetilde{G}_n = \frac{U_n(k,r_n)U_n^T(k,r_n)e^{-ir_n(x_3-z)}}{\rho\omega(\partial\omega_n^2/\partial p)(k,r_n)} \quad , \quad x_3 < z \qquad (2.2.32)$$

and

$$\widetilde{G}_{mn} = \frac{-U_m(k,r_m)R_{mn}U_n^T(k,p_n)e^{-i(r_m x_3 - p_n z)}}{\rho\omega(\partial\omega_n^2/\partial p)(k,p_n)}. \qquad (2.2.33)$$

The remainder of this section is devoted to the inversion of these transforms. The procedure will be illustrated for the reflected wave G_{mn}. We can abbreviate the notation by writing

$$\widetilde{G}_{mn} = F_{mn}(\omega,k)e^{-i(r_m x_3 - p_n z)}. \qquad (2.2.34)$$

The essential feature of (2.2.31), (2.2.32) or (2.2.33) is that the function multiplying the exponential is homogeneous of degree -2. As in the method of Willis (73) we proceed by setting

$$\Omega = \omega/|k| \quad \text{and} \quad \eta = k/|k|. \qquad (2.2.35)$$

In terms of these variables

$$\widetilde{G}_{mn} = \frac{1}{|k|^2} F_{mn}(\Omega,\eta)e^{-i|k|(r_m x_3 - p_n z)} , \qquad (2.2.36)$$

where r_m and p_n are now evaluated at (Ω,η). If polar coordinates are used in the (k_1,k_2) plane we can invert the transform $(2.2.36)$ to give

$$G_{mn}(t,x,z) = \frac{1}{8\pi^3} \lim_{\varepsilon \to 0} \oint_{|\eta|=1} ds \int_{-\infty+oi}^{\infty+oi} d\Omega\, F_{mn}(\Omega,\eta).$$

$$\int_0^\infty d|k|e^{-i|k|(\phi_{mn}(\Omega,t,x,z)-i\varepsilon)} , \qquad (2.2.37)$$

where

$$\phi_{mn}(\Omega,t,x,z) = \Omega t + \eta_1 x_1 + \eta_2 x_2 + r_m x_3 - p_n z \qquad (2.2.38)$$

and the convergence factor has been inserted to facilitate the integration. Performing the integration with respect to $|k|$ gives

$$G_{mn}(t,x,z) = \frac{1}{8\pi^3} \lim_{\varepsilon \to 0} \oint_{|\eta|=1} ds \int_{-\infty+oi}^{\infty+oi} \frac{d\Omega\, F_{mn}(\Omega,\eta)}{(\phi_{mn}(\Omega,t,x,z)-i\varepsilon)} . \qquad (2.2.39)$$

This expression has previously been obtained by Willis (73), who next evaluated the integral with respect to Ω by noting that F_{mn} was analytic in the upper half-plane so that by closing the contour in the upper half-plane and using Cauchy's theorem, the integral was reduced purely to a residue contribution from the point $\Omega = \Omega_{mn}$ at which

$$\phi_{mn}(\Omega,t,x,z) = 0i. \qquad (2.2.40)$$

Equation (2.2.40) has no solution in the upper half-plane when $t < 0$ since both r_m and $(-p_n)$ have positive imaginary parts and x_3 and z are both negative. Therefore, for $t < 0$, $G_{mn} = 0$ as required. Similarly, when $t > 0$ (2.2.40) has no solution in the lower half-plane. The p- and r-roots satisfy (2.2.17) which involves only ω^2, and so since only p-roots have negative imaginary parts,

$$p_n(-\Omega, k) = p_s(\Omega, k), \qquad\qquad (2.2.41)$$

for some s not necessarily equal to n. The r-roots have a similar property. Evaluation of $F_{mn}(\Omega, \eta)$ for Ω in the lower half-plane is therefore equivalent to evaluation of some $F_{rs}(-\Omega, \eta)$; thus F_{mn} is analytic in the lower half-plane also. Therefore, when $t > 0$ we can add to (2.2.39) the corresponding integral from $-\infty - 0i$ to $\infty - 0i$ since this is zero by Cauchy's theorem. The integral with respect to Ω in (2.2.39) can thus be replaced by one over a contour Γ which consists of circuits around the branch cuts, together with circuits around any poles that there may be on the real axis between the branch cuts. This contour is shown in figure 2.1 which shows explicitly poles at the origin and at $\Omega = \pm \gamma_R$, which correspond to Rayleigh waves. The point marked P corresponds to the solution of (2.2.40).

Thus, the basic representation is

$$G_{mn}(t, x, z) = \frac{1}{8\pi^3} \lim_{\varepsilon \to 0} \oint_{|\eta| = 1} ds \int_\Gamma \frac{d\Omega \, F_{mn}(\Omega, \eta)}{\phi_{mn}(\Omega, t, x, z) - i\varepsilon} . \qquad (2.2.42)$$

It involves a double integral, but this is around known contours and the integrand is explicit. The original method of Willis (73) required only the η-integration but the integrand had a very
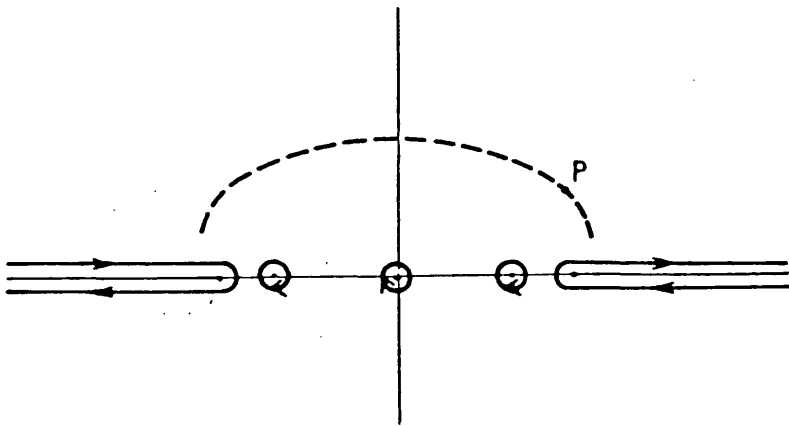
Figure 2.1. The contour Γ in the Ω -plane. It encloses branch cuts terminating at $\pm \gamma_n$, Rayleigh poles at $\pm \gamma_R$ and a pole at the origin. The locus of the point P as η varies is illustrated by the dashed line.

complicated dependence upon x and t, being evaluated at a solution of (2.2.40).

Similarly, for the two-dimensional problem the choice is between an explicit formula that requires the solution of equations like (2.2.40) and a formula, that contains the contour integral of a fairly straightforward function. The only significant differences between the two- and three- dimensional problems are that there is no η-integration in the two-dimensional case and, because this in effect loses a factor $|k|$, this is compensated for by use of a delta-function time dependence for the source which reinstates a factor $-i\Omega$. If the solution is to be computed at many points (x,t) the representation involving the contour integral is likely to display an advantage, because much of the integrand is independent of x and t, and can be stored and used repeatedly.

It is noted that this method of reducing the integrals has been used by Eason (66) who studied the special case of axisymmetric surface loading of an isotropic half-space using Laplace and Hankel transforms; but the general applicability of the method does not appear to have been demonstrated before.

Expressions corresponding to different types of source are easily obtainable from the present formulation since x and t appear in a simple fashion; in particular dipole sources are obtainable by differentiation with respect to x_1, x_2 and z.

For problems involving isotropic layers the representation simplifies, since we can reverse the order of integration. The integral around the unit circle is elementary and so the representation reduces to an integral around a contour that

is independent of x and t, of an integrand which is known

explicitly. This reduction, together with details for an

isotropic half-space, is given in the next section.

2.3 AN ISOTROPIC HALF-SPACE

For an isotropic half-space with Lamé moduli λ, μ the
matrix $K(\omega, \xi)$ has components

$$K_{ik}(\omega, \xi) = (\rho\omega^2 - \mu\xi_j\xi_j)\delta_{ik} - (\lambda + \mu)\xi_i\xi_k \qquad (2.3.1)$$

and has zero determinant when

$$\rho\omega^2 = (\lambda + 2\mu)\xi_j\xi_j \qquad \text{(once)} \qquad (2.3.2)$$

and

$$\rho\omega^2 = \mu\xi_j\xi_j \qquad \text{(twice)} \qquad (2.3.3)$$

Thus the condition (2.2.11) with $\xi = (k_1, k_2, p)$ gives

$$\omega_1^2 = a^2|\xi|^2, \quad \omega_2^2 = \omega_3^2 = \beta^2|\xi|^2, \qquad (2.3.4)$$

where $a = [(\lambda + 2\mu)/\rho]^{\frac{1}{2}}$ and $\beta = (\mu/\rho)^{\frac{1}{2}}$ represent the speeds
of longitudinal and shear waves respectively. Inverting
(2.3.4) produces

$$p_1 = -r_1 = -q_a, \quad p_2 = -r_2 = -q_\beta \text{ and } p_3 = -r_3 = -q_\beta, \qquad (2.3.5)$$

where

$$q_a = \left(\frac{\omega^2}{a^2} - |k|^2\right)^{\frac{1}{2}} \text{ and } q_\beta = \left(\frac{\omega^2}{\beta^2} - |k|^2\right)^{\frac{1}{2}}, \qquad (2.3.6)$$

the branches being chosen so that q_a and q_β have positive
imaginary part throughout the cut ω plane. Although the isotropic
case is degenerate to the extent that there is a double eigen-
value, we can still find an independent set of eigen-vectors
$U_n(\xi)$. With $\xi = (k_1, k_2, p)$ we may choose

$$U_1 = \begin{bmatrix} k_1 \\ k_2 \\ p \end{bmatrix} (|k|^2 + p^2)^{-\frac{1}{2}}, \qquad U_2 = \begin{bmatrix} k_1 p \\ k_2 p \\ -|k|^2 \end{bmatrix} (|k|^2 + p^2)^{-\frac{1}{2}}|k|^{-1},$$

$$U_3 = \begin{bmatrix} -k_2 \\ k_1 \\ 0 \end{bmatrix} |k|^{-1}. \tag{2.3.7}$$

U_1 corresponds to a P-wave and U_2, U_3 correspond to SV- and

SH- waves respectively.

The matrix $C(\xi)$ is given by

$$C(k_1, k_2, p) = \begin{bmatrix} \mu p & 0 & \mu k_1 \\ 0 & \mu p & \mu k_2 \\ \lambda k_1 & \lambda k_2 & (\lambda + 2\mu)p \end{bmatrix}. \tag{2.3.8}$$

From (2.3.7) and (2.3.8) using definition (2.2.26) we have

$$S(p) = \begin{bmatrix} -2\alpha k_1 p_1/\omega & \beta k_1 (p_2^2 - |k|^2)/(\omega |k|) & k_2 p_2/|k| \\ -2\alpha k_2 p_1/\omega & \beta k_2 (p_2^2 - |k|^2)/(\omega |k|) & -k_1 p_2/|k| \\ \alpha(p_2^2 - |k|^2)/\omega & 2\beta|k|p_2/\omega & 0 \end{bmatrix}. \tag{2.3.9}$$

The corresponding expression for $S(r)$ follows by replacing p

by $-r$. The calculation of the matrix of reflection coefficients,

R, requires the inversion of $S(r)$. The determinant of $S(r)$ is $\alpha\beta q_\beta D/\omega^2$, where

$$D = (q_\beta^2 - |k|^2)^2 + 4|k|^2 q_\alpha q_\beta \qquad (2.3.10)$$

and is zero when $\omega^2 = Y_R^2|k|^2$, Y_R denoting the Rayleigh wave speed. Full expressions for the components of the matrix R are given in the appendix.

As mentioned at the end of the preceding section we can perform the integration with respect to η for any of the terms G_n, G_{mn}. Any term has the form

$$I = \frac{1}{8\pi^3 ir} \int_\Gamma d\Omega \oint ds \frac{F(\Omega,\eta)}{\psi + \cos\theta} \quad , \qquad (2.3.11)$$

where $r = (x_1^2 + x_2^2)^{\frac{1}{2}}$ and $\eta_\alpha x_\alpha = r\cos\theta$. The function ψ depends upon Ω, t, x_3 and z, but since the p's and r's are independent of η, ψ does not depend upon η, nor does the contour Γ. Also, from equations (2.2.31), (2.2.32) and (2.2.33) it is clear that any one of the functions $F(\Omega,\eta)$ has the same η dependence as some $U_m U_n^T$ for some m and n. It is further noted that $m = 3$ if and only if $n = 3$ since SH- waves do not interact with SV- or P- waves. Thus, referring to (2.3.7), any $F(\Omega,\eta)$ has the form

$$F(\Omega,\eta) = \begin{bmatrix} a+b\eta_1^2 & b\eta_1\eta_2 & c\eta_1 \\ b\eta_1\eta_2 & a+b\eta_2^2 & c\eta_2 \\ d\eta_1 & d\eta_2 & e \end{bmatrix} \quad , \qquad (2.3.12)$$

where a,b,c,d,e are functions of Ω only. F is an isotropic tensor

valued function of (η_1, η_2) and, correspondingly G is an

isotropic function of (x_1, x_2). It suffices, therefore, to

evaluate the integral I for $x_1 = r$ and $x_2 = 0$. This requires the

calculation of the integrals

$$J_o = \int_o^{2\pi} \frac{d\theta}{\psi + \cos\theta} \quad , \quad J_\alpha = \int_o^{2\pi} \frac{\eta_\alpha d\theta}{\psi + \cos\theta} \quad , \quad J_{\alpha\beta} = \int_o^{2\pi} \frac{\eta_\alpha \eta_\beta d\theta}{\psi + \cos\theta} \quad ,$$

$$(2.3.13)$$

where $\eta = (\cos\theta, \sin\theta)$. As θ varies, the zero in the

denominator, which is at position P in the Ω plane, traces out

a curve, illustrated by the dashed line in figure 2.1. This

defines an additional cut in the Ω-plane across which the

integral with respect to η is not an analytic function of Ω.

However, for $t > 0$, this cut remains in the upper half-plane and

is separated from the contour Γ for any strictly positive value

of the parameter ε in (2.2.42). The complete expressions for

the integrals J, and the resulting representation for G, are

given in the Appendix.

2.4 ARRIVALS .

The arrivals, or wavefront singularities, associated with
the Green's tensor G have been discussed by Willis and Bedding
(75). However, in this section we describe how they are
generated by the representation developed here, since the
procedure for computing the integrals around Γ has been
designed to cope with singularities in the integrand which are,
associated with some of the arrivals. The case of an isotropic
half-space will be considered to facilitate the discussion
of the numerical results that follow. It is noted that the
arrivals have not been comprehensively summarized elsewhere.

We begin by considering the direct arrivals associated
with G_n. If γ_n represents the corresponding wave-speed (that
is $\gamma_1 = \alpha$, $\gamma_2 = \gamma_3 = \beta$), then when $x_3-z>0$ the ψ term, ψ_n say,
is given by

$$\psi_n = r^{-1}(\Omega t + p_n(x_3 - z) - 0i),\qquad (2.4.1)$$

where

$$p_n = -\left(\frac{\Omega^2}{\gamma_n^2} - 1\right)^{\frac{1}{2}}.\qquad (2.4.2)$$

The complex Ω-plane has cuts along the segments $(-\infty,-\gamma_n)$,
(γ_n,∞) of the real axis together with a cut along the curve
traced out by the zero of the function $\psi_n + \cos\theta$, as θ varies
from 0 to 2π. Although shown in a general way in figure 2.1 the
actual position of this curve depends upon the values of x,z
and t. If $t <(x_3-z)/\gamma_n$ it is easy to show that $\psi_n + \cos\theta$ has

no zeros at all in the Ω-plane cut along the segments of the

real axis as indicated. (The roots obtained from squaring and

solving the resulting quadratic both have negative imaginary

parts, hence $\psi_n + \cos\theta$ has a negative imaginary part and both

roots lie on Riemann sheets corresponding to r_n rather than

p_n). It follows by deforming the contour that $G_n = 0$, as

expected since a wave travelling with speed γ_n has had

insufficient time to travel from depth z to depth x_3 even at

$x_1 = x_2 = 0$. Zeros of $\psi_n + \cos\theta$ do however occur when

$t > (x_3-z)/\gamma_n$. If Ω lies just above the cut along the positive

real axis then p_n is real and negative but smaller in magnitude

than Ω/γ_n. ψ_n is therefore real and so $\psi_n + \cos\theta$ vanishes for

some θ provided that $|\psi_n| \leq 1$, that is if r is large enough.

For a given r, however, there is no real zero of $\psi_n + \cos\theta$ if

$|\cos\theta|$ is small enough. Thus the curve has a complex part and

may in addition have sections lying just above the real axis

for which $|\Omega| > \gamma_n$, if r is sufficiently large. The actual

behaviour of the zero of $\psi_n + \cos\theta$ as θ varies may be

established by considering the inverse of the mapping

$\cos\theta = -\psi_n(\Omega)$. This is singular when $d\psi_n/d\Omega = 0$, that is when

$$t + \frac{dp_n}{d\Omega}(x_3-z) = 0 \quad \text{and} \quad \psi_n(\Omega) + \cos\theta = 0. \tag{2.4.3}$$

These equations have explicit solution

$$t = (r^2\cos^2\theta + (x_3-z)^2)^{\frac{1}{2}}/\gamma_n. \tag{2.4.4}$$

For fixed t (2.4.4) gives the value of θ at which the zero of

$\psi_n(\Omega) + \cos\theta$ turns into the upper half of the Ω-plane. In

particular for $t > t_n$, where

$$t_n = (r^2 + (x_3 - z)^2)^{\frac{1}{2}}/\gamma_n ,$$ (2.4.5)

the zero of $\psi_n + \cos\theta$ is in the upper half-plane for all real

θ between 0 and 2π. Thus t_n defines a time at which the

character of the integrand changes and it will be shown that

t_n is the arrival time. It is useful to denote the zero of

$\psi_n \mp 1$ at time t_n by $\pm\Omega_n$. The cut Ω-plane is shown in figure

2.2a for $t < t_n$ and in figure 2.2b for $t > t_n$. In either case

the cut in the Ω-plane maps onto the segment $-1 \leq \psi_n \leq 1$ of the

real axis in the ψ_n-plane, and is a natural segment over which

to make a cut in the ψ_n-plane to define the branch of the

function $(\psi_n^2 - 1)^{\frac{1}{2}}$ that occurs in the integrand through the

integrals J. (see Appendix). It is helpful, in the analysis that

follows, to cut the ψ_n-plane along the segments $-\infty < \psi_n < -1$

and $1 < \psi_n < \infty$ of the real axis instead. The cuts shown in

figure 2.2a and 2.2b are then replaced by cuts produced by

the mapping of these new cuts into the Ω-plane. The new function

$(\psi_n^2 - 1)^{\frac{1}{2}}$ so defined takes the same values as the original one

everywhere on the contour Γ. The new cuts in the Ω-plane are

shown in figures 2.3a and 2.3b.

The integral may now be transformed by deforming the

contour so that it encloses the branch cuts in either figure

2.3a or 2.3b, depending on whether t is smaller than or

greater than t_n.

Examination of the integrand of G_n, given by equations

(A.5) to (A.7) of the appendix, reveals that when Ω is real and

$|\Omega| > \gamma_n$, ψ_n is real and the integrand of G_n evaluated at

(a) $t < t_n$
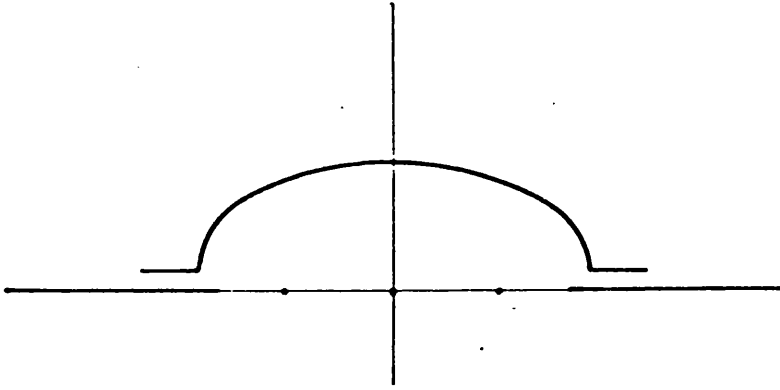
(b) $t \gtrsim t_n$
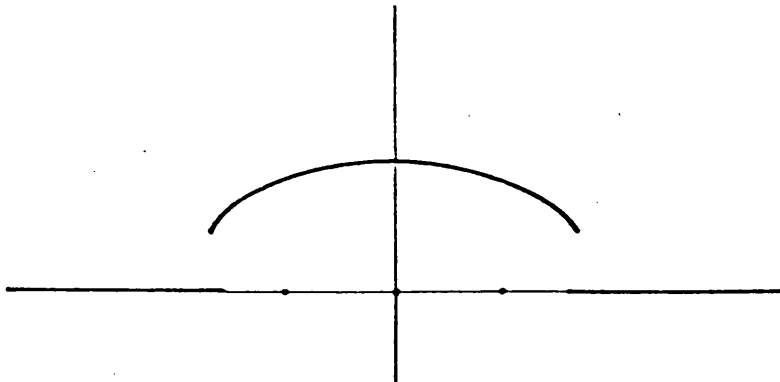
Figure 2.2. The branch cut (which is identical to the
locus of P shown schematically in figure
5.1) of the function $(\psi_n^2 - 1)^{\frac{1}{2}}$.

(a) $t < t_n$
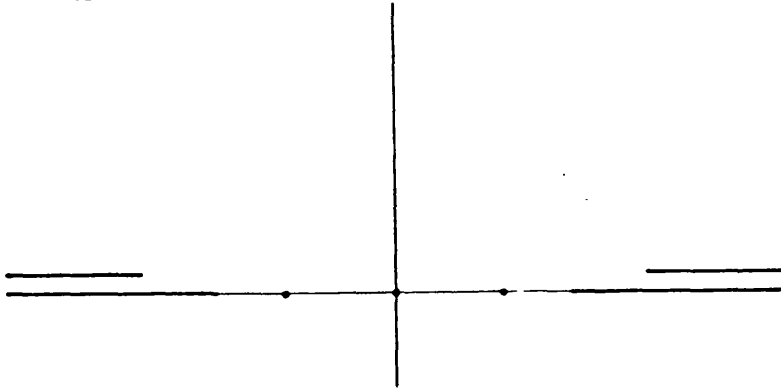
(b) $t > t_n$
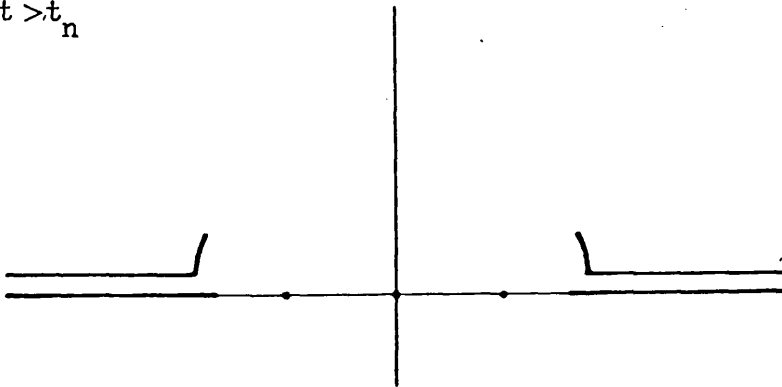
Figure 2.3. Complementary branch cuts for the function
$(\psi_n^2 - 1)^{\frac{1}{2}}$.

$-\Omega + 0i$ is minus its value at $\Omega + 0i$. It follows that the

integrals along the real arms of the branches cancel out. Thus,

when t is smaller than the time t_n, $G_n = 0$, and when t is

greater than t_n, G_n may be evaluated by integration around the

curved arcs in figure 2.3b only, and is non-zero. Thus t_n is the

arrival time. When t is just greater than the arrival time

these curved arcs are effectively short and straight, and the

term in the integrand that varies most rapidly is $(\psi_n^2-1)^{-\frac{1}{2}}$.

Asymptotically, therefore, G_n may be estimated by evaluating

every other term in the integrand at Ω_n, and approximating

ψ_n by its Taylor series about Ω_n, t_n. The other arc, near

$-\Omega_n$, can be treated similarly.

Near to Ω_n, t_n, since $\psi_n(\Omega_n,t_n) = 1$ and $\partial\psi_n(\Omega_n,t_n)/\partial\Omega = 0$,

we have

$$\psi_n(\Omega,t) \sim 1 + (t-t_n)\Omega_n/r + (\Omega-\Omega_n)(t-t_n)/r + (\Omega-\Omega_n)^2\psi_n''/2, \qquad (2.4.6)$$

where ψ_n'' denotes $\partial^2\psi_n/\partial\Omega^2$ evaluated at Ω_n, t_n. Asymptotically,

$(\psi_n^2-1)^{-\frac{1}{2}}$ takes the form

$$(\psi_n^2-1)^{-\frac{1}{2}} \sim (\psi_n'')^{-\frac{1}{2}} \left\{ (\Omega -\Omega_n)^2 + \frac{2(\Omega-\Omega_n)(t-t_n)}{r\psi_n''} + \frac{2\Omega_n(t-t_n)}{r\psi_n''} \right\}^{-\frac{1}{2}} .$$

$$(2.4.7)$$

The small complex section of the branch cut runs from Ω_n to the

value Ω_s of Ω at which (2.4.7) is singular, namely,

$$\Omega_s \sim \Omega_n + \left(\frac{2\Omega_n(t-t_n)}{r\psi_n''} \right)^{\frac{1}{2}} . \qquad (2.4.8)$$

Ω_s is complex, as required, since $r\,\psi_n''$ is positive.

The form of the arrival can now be determined by evaluating the integral

$$I = \oint (\psi_n^2-1)^{-\frac{1}{2}}\, d\Omega \qquad\qquad (2.4.9)$$

asymptotically, for t close to t_n, around a contour that encloses the complex arm of the branch cut. The result is

$$I = -i\pi(\psi_n'')^{-\frac{1}{2}}. \qquad\qquad (2.4.10)$$

The direct arrivals are now, in effect determined. They have step function time dependence and are given explicitly in the appendix.

The arrivals for reflected waves can be treated similarly. The ψ-function corresponding to G_{mn} is given by

$$\psi_{mn} = r^{-1}(\Omega t + r_m x_3 - p_n z - 0i). \qquad\qquad (2.4.11)$$

The integrand involving this term has a branch cut obtained from the inverse of the mapping $\cos\theta = -\psi_{mn}(\Omega)$. The branch cut moves into the upper half Ω-plane when Ω is such that $d\psi_{mn}/d\Omega = 0$. Correspondingly, the arrival time t_{mn}, and the corresponding value Ω_{mn} of Ω, are defined by the equations

$$\psi_{mn} = \pm 1, \quad d\psi_{mn}/d\Omega = 0. \qquad\qquad (2.4.12)$$

However, whereas for the direct waves $G_n = 0$ for $t < t_n$, we cannot make a corresponding statement for G_{mn}. The result depends upon the "odd" property of the integrand for the real Ω, and this property only holds for Ω large enough for all of the

p- and r- functions in the integrand to be real. There is no problem as long as the branch cut for $(\psi_{mn}^2-1)^{\frac{1}{2}}$ turns into the upper half-plane at a real value of Ω for which $|\Omega|>a$. G_{33} follows the pattern already established since it contains only q_β, but the other G_{mn} contain both q_α and q_β. Additionally, if ψ_{mn} contains q_α it is easy to show that there is no problem, so G_{11} (when x_3 and z not both zero), G_{12} (when $x_3 = 0$) and G_{21} (when z = 0) are all zero prior to their corresponding arrival times. However, G_{22}, together with G_{12} when $x_3 = 0$ and G_{21} when z = 0, have a more complicated behaviour, The function ψ_{22} contains only q_β, and so the branch cuts for $(\psi_{22}^2-1)^{\frac{1}{2}}$ may contain points on the real segments $\beta<|\Omega|< a$. The condition for this to occur may be investigated by considering the limiting case for which $|\Omega| = a$ is a solution of equations (2.4.12) with m = n = 2. This gives

$$r^{-1}(t_{22} + \frac{a}{\beta^2} \ (\frac{a^2}{\beta^2} - 1)^{-\frac{1}{2}}(x_3 + z)) = 0 \qquad (2.4.13)$$

and

$$r^{-1}(t_{22} + \frac{(a^2}{\beta^2} - 1)^{\frac{1}{2}}(x_3 + z)) = \overset{+}{-} 1. \qquad (2.4.14)$$

Eliminating t_{22} gives the condition

$$(x_3 + z) \overset{+}{-} r(a^2/\beta^2 - 1)^{\frac{1}{2}} = 0, \qquad (2.4.15)$$

which defines a cone, centred $x_3 = -z$, r = 0, outside which a head wave arrives before the reflected S-S wave. It can be shown that, if x lies within this cone, the real sections of the branch cut are outside the region $-a< \Omega <a$ and so G_{22} is zero

prior to the arrival time. This conclusion does not hold when x lies outside of the cone.

We can examine the form of the arrival in either case, by expanding the function in a Taylor series about the point t_{22}, Ω_{22} but in the head wave region it is necessary to evaluate the integral

$$I^1 = \int (\psi_{22}^2 - 1)^{-\frac{1}{2}} \, d\Omega \qquad (2.4.16)$$

around a closed contour that encloses a portion of the real arm of the branch as well as the end of the contour, whether or not the branch cut turns into the upper half plane. The result is, asymptotically for t close to t_{22},

$$I^1 = -(\psi_{22})^{-\frac{1}{2}} \left[\ln|t-t_{22}| + i\pi H(t-t_{22}) \right] , \qquad (2.4.17)$$

which is consistent with (2.4.10).

Thus, in the head wave region the wavefront singularity consists of both logarithmic and step function terms, while outside this region, it has just step function form. The full expressions for the arrivals for reflected waves are again given in the Appendix.

Finally, we consider the form of the head wave arrival itself. The arrival time t_H is the time at which the branch points for $(\psi_{22}^2 - 1)^{\frac{1}{2}}$ enter the segment $|\Omega| \leq a$, and is found, by substituting $\Omega = a$ into $\psi_{22}(\Omega) = \pm 1$, to be

$$t_H = (r - |x_3 + z|(a^2/\beta^2 - 1)^{\frac{1}{2}})/a . \qquad (2.4.18)$$

Expanding ψ_{22} in a Taylor series about $t = t_H$, $\Omega = a$ gives

- 32 -

$$\psi_{22} \sim 1 + a(t-t_H)/r + (\Omega - a)\psi_{22}'(a), \qquad\qquad (2.4.19)$$

so that at time t the branch point is given asymptotically by $\Omega = \Omega_b$ where

$$\Omega_b \sim a - a(t-t_H)[r\,\psi_{22}'\,(a)]^{-1} \ . \qquad\qquad (2.4.20)$$

We can now find the form of the head wave arrival by investigating the asymptotic behaviour of the integral defining G_{22}. The "odd" property is broken by the term q_a, which is small near to $\Omega = a$. The form of the arrival is found by expanding the integrand as far as the term linear in q_a, and is thus given by

$$I_H = \int_{\Omega_b}^{a} \left(\frac{\Omega^2}{a^2} - 1\right)^{\frac{1}{2}} (\psi_{22}^2 - 1)^{-\frac{1}{2}} \, d\Omega . \qquad\qquad (2.4.21)$$

Asymptotically, for t just greater than t_H, the result is

$$I_H = \frac{i\pi a^{\frac{1}{2}}(t-t_H)}{2r[\psi_{22}'(a)]^{3/2}} , \qquad\qquad (2.4.22)$$

which shows that the arrival is of the form of a linear ramp. The full expression for the head wave arrival is given in the Appendix.

2.5 THE SOLUTION AT r = 0

At a point directly above or below the source, the solution

takes a slightly different form from that given in section 3.

In particular, when r = 0, the integral in (2.3.11) may be

written as

$$I = \frac{1}{8\pi^3 i} \int_\Gamma d\Omega \oint \frac{ds F(\Omega,\eta)}{\Phi(\Omega,t,x_3,z)} \quad . \tag{2.5.1}$$

The evaluation of I requires the calculation of the integrals

$$J_0^1 = \int_0^{2\pi} d\theta \ , \ J_\alpha^1 = \int_0^{2\pi} \eta_\alpha \, d\theta \ , \ J_{\alpha\beta}^1 = \int_0^{2\pi} \eta_\alpha \eta_\beta \, d\theta \ , \tag{2.5.2}$$

which correspond to the integrals in (2.3.13), and where

$\eta = (\cos\theta, \sin\theta)$. The results are

$$J_0^1 = 2\pi \ , \ J^1 = 0 \ , \ J_{11}^1 = \pi \ ,$$

$$J_{12}^1 = J_{21}^1 = 2 \ , \ J_{22}^1 = \pi \ . \tag{2.5.3}$$

The terms G_n and G_{mn} are given by

$$G_n = \frac{1}{16\pi^3 i \rho} \int \frac{H_n^1(\Omega)}{\Phi(\Omega)} d\Omega \ , \ G_{mn} = \frac{1}{16\pi^3 i \rho} \int \frac{H_{mn}^1(\Omega)}{\Phi(\Omega)} d\Omega \ , \tag{2.5.4}$$

where H_n^1 and H_{mn}^1 are obtained from the corresponding H_n and H_{mn},

given in the Appendix, by replacing the J's by the corresponding

J^1's and the ψ's by the corresponding Φ's. The functions $H^1(\Omega)$

have no branch points in the upper half-plane, but may have poles

there. We consider G_n as an example; the corresponding Φ_n is, for $x_3 - z > 0$

$$\Phi_n(\Omega) = \Omega t + p_n(x_3 - z) - 0i. \tag{2.5.5}$$

It is easy to show that $\Phi_n(\Omega) = 0$ has no solutions for $t < (x_3 - z)/\gamma_n$, while for $t > (x_3 - z)/\gamma_n$ there are solutions at $\Omega = \pm\Omega_p$ where

$$\Omega_p = i(x_3 - z)(t^2 - (x_3 - z)^2/\gamma_n^2)^{-\frac{1}{2}} . \tag{2.5.6}$$

Thus, for $t > (x_3 - z)/\gamma_n$ we can deform the contour around the single pole in the upper half-plane to give by Cauchy's theorem

$$G_n = \frac{1}{8\pi^3 \rho} H_n^1(\Omega_p)/\Phi_n^1 , \tag{2.5.7}$$

where $\Phi_n^1 = d\Phi_n/d\Omega$ evaluated at $\Omega = \Omega_p$. That is

$$\Phi_n^1 = (t^2 - \frac{(x_3 - z)^2}{\gamma_n^2})/t. \tag{2.5.8}$$

We note that all of the denominators in H_n^1 and H_{mn}^1 are $0(\Omega_p^2)$ or higher for large Ω_p, so that near to the arrival time the corresponding G_n and G_{mn} are finite.

Thus, for $r = 0$, the closed solution for the Green's tensor can be obtained from the present representation, the terms G_n being given by (2.5.7) and (2.5.8) with corresponding expressions for the G_{mn} terms.

The solution at the epicentre, $r = 0$, $x_3 = 0$, has been

given previously by Sinclair (79). The solutions for $x_3 \neq 0$
do not appear to have been listed anywhere, probably because
they are of little practical importance in seismology or in
acoustic emission problems. We shall not list the solutions
here, but note that they are completely closed and can be
obtained, using simple algebra, from the solutions for
$r \neq 0$ given in the Appendix.

2.6 COMPUTATION

The Green's function G may be calculated by evaluating

the integrals in (A.4). However, there is no need to integrate

over the whole of the contour Γ, because the function $(\psi^2-1)^{\frac{1}{2}}$,

defined by the cuts in the Ω-plane shown in figures 3a,b, is

an even function and it is easy to verify that the integrands,

given by (A.5) to (A.12), each have the property

$$H(-\overline{\Omega}) = -\overline{H(\Omega)}, \qquad (2.6.1)$$

where the superposed bar denotes the complex conjugate. This

property guarantees that G is real, as it should be and, in

addition, allows the solution to be deduced from the imaginary

parts of the integrals of the functions $H(\Omega)$, over contours

in the right half of the complex Ω-plane. In addition, there

are other simplifications. The term G_n is known, from section

4, to be zero for $t < t_n$, where t_n is the arrival time

$(r^2 + (x_3-z)^2)^{\frac{1}{2}}/\gamma_n$. When $t > t_n$, the function $(\psi_n^2 -1)^{\frac{1}{2}}$ is real

when $|\Omega| > \gamma_n$ and Ω lies just above or below the real axis. For

such values of Ω, $\psi_n^2 - 1$ is real and single-signed, because

a sign change can only occur at one of the branch points of

$(\psi_n^2-1)^{\frac{1}{2}}$, which are complex. The sign is positive since ψ_n^2-1 is

positive when Ω is real and large. It follows, therefore, that

when $t > t_n$, $H(\Omega)$ is real at any point just above or below the

branch cuts for the functions p_n, r_n and the symmetry property

(5.1) shows that the branch integrals cancel. Therefore, since

the terms H_n have no Rayleigh poles, when $t > t_n$ the term G_n

may be calculated from the contribution from the pole at the origin alone. This result is not wholly surprising, since the infinite-body Green's tensor could also be obtained explicitly by elementary methods (see for example, Love (44)). Similar reasoning applies to the term G_{33}, which involves only q_β. The integrals for the remaining terms G_{mn} can also be simplified.

When t is greater than t_{mn} (or t_H if a head wave exists for the term in question), similar reasoning to the above shows that $H_{mn}(\Omega)$ is real when $|\Omega| > a$ and Ω lies just above or below the real axis. The branch points for $(\psi_{mn}^2 - 1)^{\frac{1}{2}}$ are either complex (for $t > t_{mn}$) or else are real and lie between $\Omega = \beta$ and $\Omega = a$ (for $t_{mn} > t > t_H$). It follows therefore, that the branch cuts contribute nothing for $|\Omega| > a$ and the terms G_{mn} may be evaluated from the integration around the section of the branch cut $\beta < \Omega < a$, together with the pole contributions from the origin and the Rayleigh pole. These pole contributions are found as follows

$$I = \oint_C H(\Omega) d\Omega , \qquad (2.6.2)$$

over a contour C enclosing a pole of $H(\Omega)$ at $\Omega = \Omega_p$. If this pole is of order n, then $H(\Omega)$ can be expanded in the Laurent series

$$H(\Omega) = \sum_{k=-n}^{\infty} a_k (\Omega - \Omega_p)^k . \qquad (2.6.3)$$

We evaluate the integral I numerically by choosing C to be a circle with radius r and centre at Ω_p and using the trapezium rule over N points. Thus, putting $\Omega = re^{i\zeta}$,

$$I = \int_0^{2\pi} H(\Omega_p + re^{i\zeta})ire^{i\zeta}d\zeta = \int_0^{2\pi} \sum_{R=-n}^{\infty} ia_k(re^{i\zeta})^{k+1}d\zeta , \qquad (2.6.4)$$

which we approximate by

$$I \simeq \frac{2\pi}{N} \sum_{j=1}^{N} \sum_{k=-n}^{\infty} ia_k \left\{ re^{2\pi i(N-j)/N} \right\}^{k+1} . \qquad (2.6.5)$$

Interchanging the order of summation gives

$$I \simeq \frac{2\pi i}{N} \sum_{k=-n}^{\infty} a_k r^{k+1} \sum_{j=1}^{N} e^{2\pi i(N-j)(k+1)/N} . \qquad (2.6.6)$$

It is clear that whenever N is a multiple of $2(k+1)$ the second

sum in (2.6.6) is zero apart from rounding errors. Further, if

N is a multiple of twice the prime factors of m, where m is

greater than the order of the pole, n, then

$$I \simeq 2\pi ia_{-1} + \frac{2\pi i}{N} \sum_{k=m-1}^{\infty} a_k r^{k+1} \sum_{j=1}^{N} e^{2\pi i(N-j)(k+1)/N} . \qquad (2.6.7)$$

From Cauchy's theorem we know that $I = 2\pi ia_{-1}$ and so the second

term in (2.6.7) is an error term. Thus, we can choose $r < 1$ to

give the required accuracy. Inspection of equations (A.5) to

(A.12) shows that $H(\Omega)$ can have poles at the origin up to order

5. For such poles, choice of a very small radius r would cause

loss of significant figures, while choice of a larger r would

require an increase in the number of integration points to cut

out more terms in the Laurent series. It was found in practice

that a radius of 0.05 was suitable, which with double precision

arithmetic guaranteed six figure accuracy.

The branch cut integrals may be simply evaluated using

the trapezium rule. The terms that contain no head-wave contributions have (at most) square root singularities at the ends $\Omega = \beta, a$ of the range of integration, which can be dealt with by use of variable transformations ($\Omega = \beta + u^2$ or $\Omega = a - r^2$). In practice, high accuracy was not sought and results were usually correct to 4 figures. The terms that contribute to the head wave require slightly more elaborate treatment because their integrands have a singularity at $\Omega = \Omega_s$ (defined approximately by equation (2.4.8) with the suffix n replaced by the double suffix 22), which depends on x and t and lies on the branch line when $t_{22} < t < t_H$. This singularity can also be handled by using a change of variables, but to avoid the need to calculate the whole integrand at different values of Ω for each x and t, the "smooth" part (namely, $(\psi_{22}^2 - 1)^{\frac{1}{2}} H(\Omega)$) can be evaluated at equal intervals and intermediate points estimated by linear interpolation. Thus, only the term $(\psi_{22}^2 - 1)^{-\frac{1}{2}}$ has to be evaluated at different points for each x and t. The results in practice were correct to at least 3 figures.

Finally, it is recalled that much of the integrand $H(\Omega)$ is independent of x and t, and may be tabulated for use in evaluating the Green's tensor at different x and t.

2.7 FLUID-LOADED STRUCTURES

The analysis presented here for a half-space may be extended to apply to the reflection and transmission of waves at an interface between different media. The basic relations, for the two-dimensional problem, are given in section 2 of Bedding and Willis (80). For the special case of an isotropic fluid-loaded half-space (the fluid occupying $x_3 > 0$), if the density of the fluid is ρ' and c denotes its wave speed, it can be shown that the reflection coefficients, for waves within the solid, take the form

$$R_{11} = - \left\{ \left[(q_\beta^2 - |k|^2)^2 - 4|k|^2 q_\alpha q_\beta \right] + \frac{\rho' q_\alpha \omega^4}{\rho q_c \beta^4} \right\} / D,$$

$$R_{22} = R_{11} ,$$

$$R_{12} = -4\beta |k| q_\beta (q_\beta^2 - |k|^2)/(\alpha D),$$

$$R_{21} = 4\alpha |k| q_\alpha (q_\beta^2 - |k|^2)/(\beta D),$$

$$R_{33} = 1, \tag{2.7.1}$$

where

$$D = (q_\beta^2 - |k|^2)^2 + 4|k|^2 q_\alpha q_\beta + \rho' q_\alpha \omega^4/(\rho q_c \beta^4) \tag{2.7.2}$$

and

$$q_c = (\omega^2/c^2 - |k|^2)^{\frac{1}{2}} . \tag{2.7.3}$$

Equations (2.7.1) reduce to (A.1) when $\rho' \to 0$. Within the solid, the representation (A.4) for G still applies, except

that the reflection coefficients that appear in equations (A.8) to (A.12) are now given by (2.7.1). Pole contributions come from the origin, $\Omega = 0$ and the zeros $\pm \gamma_s$ of (2.7.2), which correspond to Stoneley waves. There are additional branch points at $\Omega = \pm c$ but no new wave fronts are introduced in the solid if $c < \beta$.

In the next section some results are given for the response within a fluid-loaded half-space.

Finally, it is remarked that transmission coefficients may also be found and the response in the fluid due to a source in the solid, or vice versa, may be found. In addition, the transient response of a fluid-loaded plate, (or layered plate) could be found, using the generalized ray method together with the inversion technique described in this chapter.

2.8 RESULTS

Figures 2.4, 2.5 and 2.6 show the non-zero components of the Green's tensor as functions of time. Poisson's ratio is taken as 0.25, and the (31) and (13) components of G have been plotted with their signs reversed, to facilitate comparison with corresponding plots given by Johnson (74), who considered the half-space $x_3 > 0$. Figure 2.4 shows the response at the surface, at a horizontal distance equal to five times the depth $|z|$ of the source and figures 2.5, 2.6 show the response at the same horizontal distance but at depths equal to $0.5|z|$ and $2|z|$, respectively. The plots agree with those of Johnson, except that his figure 6, which corresponds to the present figure 2.6, shows no jumps at the time of arrival of the S-P reflected wave (corresponding to m=1, n=2). Figure 2.6 does contain such jumps and their amplitudes are consistent with the asymptotic formula (A.20). The various arrivals are indicated in the figures.

The dashed curves in figures 2.4, 2.5, 2.6 show the corresponding responses for the case when the solid half-space is overlaid by a fluid half-space. The fluid is specified by the ratios

$$\rho'/\rho = 0.382, \quad c/\beta = 0.564, \tag{2.8.1}$$

which correspond roughly to granite under water. With these values, the Stoneley wave has speed $Y_s = .5598\beta = .9925c$. The results show that the fluid affects the details of the wave amplitudes but does not produce any major qualitative change.

Figure 2.4. The non-zero components of the Green's tensor evaluated at the point $(5|z|,0,0)$ on the surface of a half-space, where $|z|$ denotes the depth of the source.

————— free half-space   -------- fluid-loaded half-space

G_{11}

S

HW

P

$\beta t/|z|$

3   4   5   6

ONE DIVISION = $1/(200\rho\beta^2|z|)$

$-G_{31}$

3   4   5   6

G_{22}

3   4   5   6

3   4   5   6

$-G_{13}$

G_{33}

3   4   5   6

- 44 -

Figure 2.5. The non-zero components of the Green's tensor evaluated at the point $(5|z|,0, .5|z|)$ on the surface of a half-space where $|z|$ denotes the depth of the source.

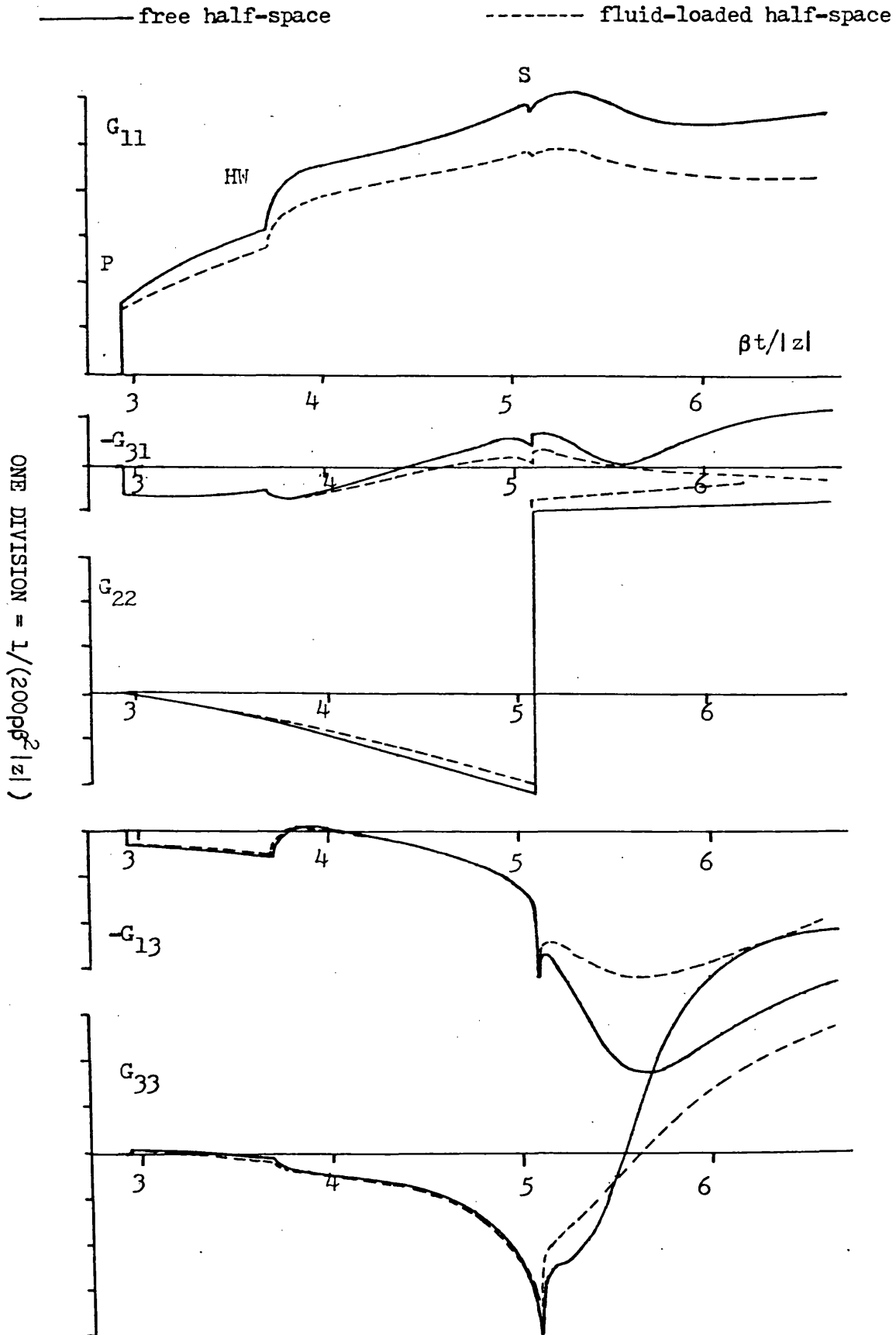——— free half-space   —————— fluid-loaded half-space
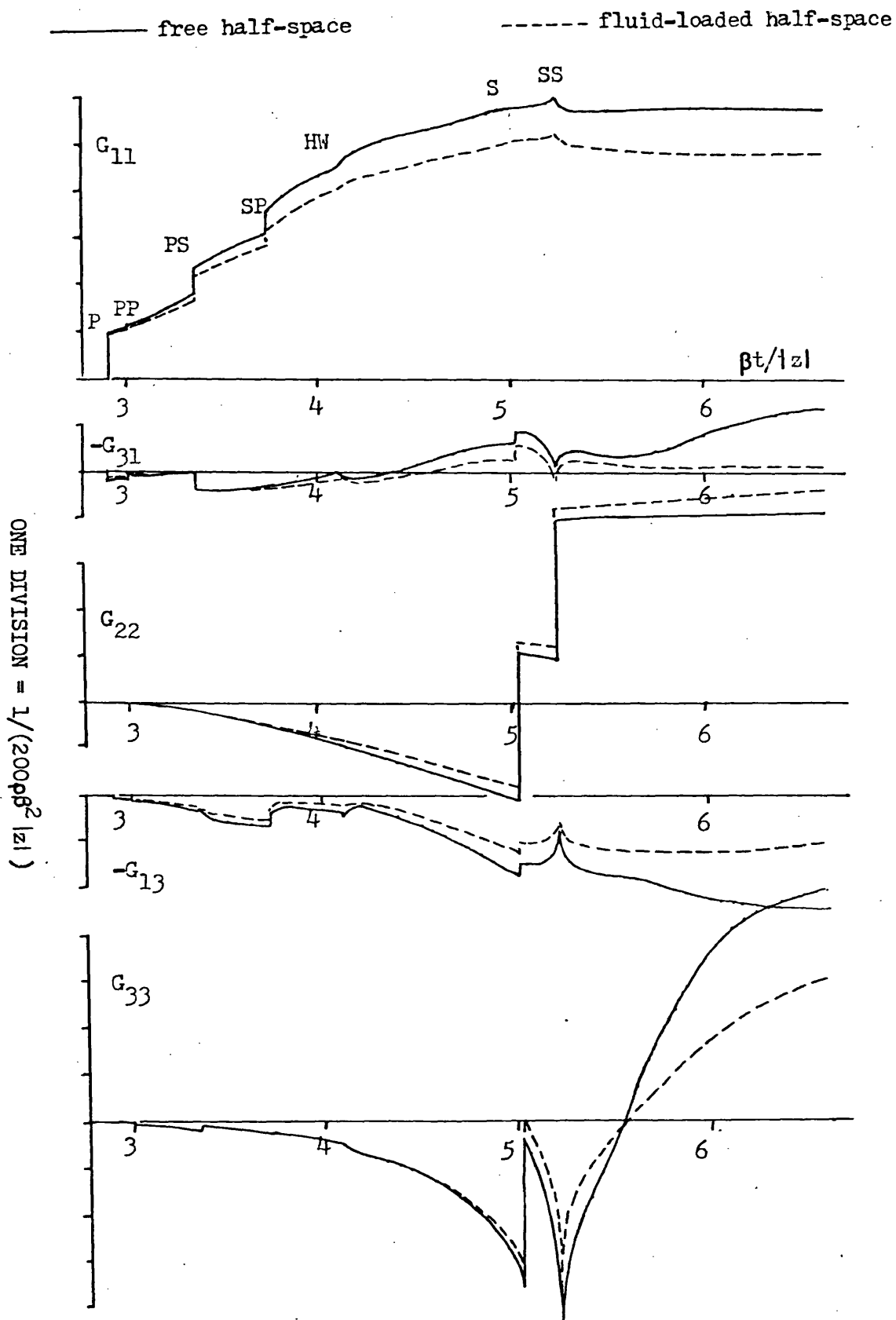
Figure 2.6. The non-zero components of the Green's tensor

evaluated at the point $(5|z|,0,2|z|)$ on the surface of a half-

space, where $|z|$ denotes the depth of the source.

——————free half-space   - - - - - - fluid-loaded half-space

ONE DIVISION = $1/(200\rho\beta^2|z|)$
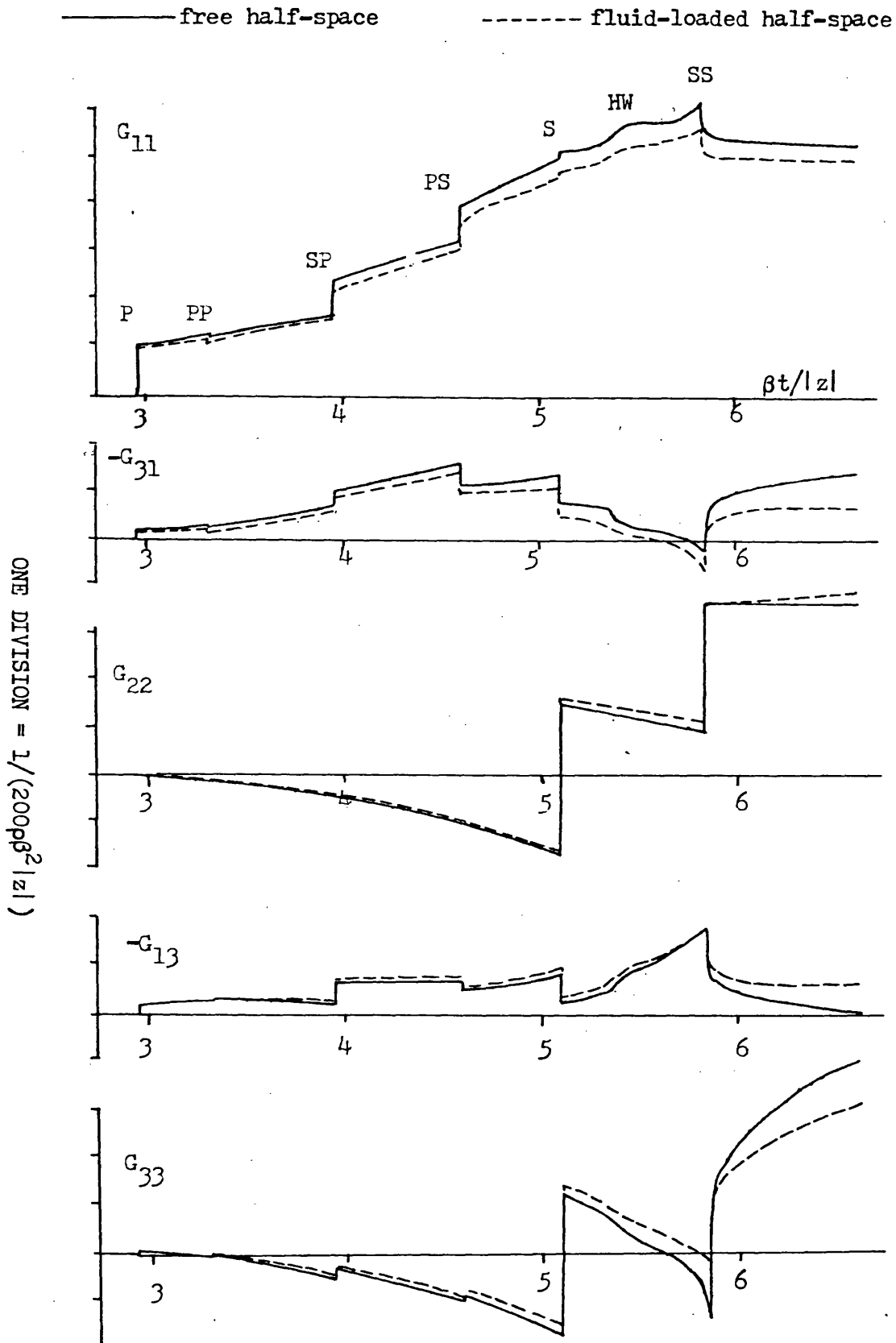
2.9 CONCLUSIONS

In this chapter a new method is presented for reducing the terms in a "generalized ray " expansion of the dynamic Green's tensor for an elastic half-space or layered medium. For isotropic media the final representation involves the integral around a contour, which is independent of both time (t), and position, (x), of a fairly simple explicit function. Much of the integrand is independent of x and t and may be tabulated to save computational time when evaluating the Green's tensor for a range of values of x and t. Thus, the method is likely to be more efficient than the established method of Cagniard (39), which involves the explicit discussion of algebraic functions, and the method of Willis (73), which requires the solution of algebraic equations for each position x and time t. Although the solution for a half-space has been described, each term in a "generalized ray " series could be handled in the same way.

$$G = \sum_{n=1}^{3} G_n + \sum_{m=1}^{3} \sum_{n=1}^{3} G_{mn}, \qquad (A.3)$$

where G_n, $n=1,2,3$ are associated with direct waves and their sum yields G^{∞} and G_{mn}, $m,n=1,2,3$ are associated with reflected waves. The reasoning that led to (2.2.39), with the path of integration replaced by the contour Γ, gives when $x_1 = r$ and $x_2 = 0$,

$$G_n = \frac{1}{16\pi^3 i \rho r} \int_\Gamma H_n(\Omega) d\Omega \; , \; G_{mn} = \frac{1}{16\pi^3 i \rho r} \int_\Gamma H_{mn}(\Omega) d\Omega, \qquad (A.4)$$

where $H_n(\Omega)$, $H_{mn}(\Omega)$ are as listed.

$$H_1(\Omega) = \begin{bmatrix} -J_{11}(\Psi_1)/(q_\alpha \Omega^3) & 0 & J_1(\Psi_1)/\Omega^3 \\[2ex] 0 & -J_{22}(\Psi_1)/(q_\alpha \Omega^3) & 0 \\[2ex] J_1(\Psi_1)/\Omega^3 & 0 & -J_0(\Psi_1) q_\alpha/\Omega^3 \end{bmatrix} , \quad (A.5)$$

$$H_2(\Omega) = \begin{bmatrix} -J_{11}(\Psi_2) q_\beta/\Omega^3 & 0 & -J_1(\Psi_2)/\Omega^3 \\[2ex] 0 & -J_{22}(\Psi_2) q_\beta/\Omega^3 & 0 \\[2ex] -J_1(\Psi_2)/\Omega^3 & 0 & -J_0(\Psi_2)/(q_\beta \Omega^3) \end{bmatrix} , \quad (A.6)$$

$$H_3(\Omega) = \begin{bmatrix} -J_{22}(\Psi_3)/(\beta^2 q_\beta \Omega) & 0 & 0 \\[2ex] & -J_{11}(\Psi_3)/(\beta^2 q_\beta \Omega) & 0 \\[2ex] 0 & 0 & 0 \end{bmatrix} \quad , \quad (A.7)$$

$$H_{11}(\Omega) = \begin{bmatrix} -R_{11}J_{11}(\psi_{11})/(q_\alpha\Omega^3) & 0 & R_{11}J_1(\psi_{11})/\Omega^3 \\\\ 0 & -R_{11}J_{22}(\psi_{11})/(q_\alpha\Omega^3) & 0 \\\\ -R_{11}J_1(\psi_{11})/\Omega^3 & 0 & R_{11}J_0(\psi_{11})q_\alpha/\Omega^3 \end{bmatrix},$$

$$(A.8)$$

$$H_{12}(\Omega) = \begin{bmatrix} R_{12}\alpha J_{11}(\psi_{12})/(\beta\Omega^3) & 0 & R_{12}\alpha J_1(\psi_{12})/(\beta q_\beta\Omega^3) \\\\ 0 & R_{12}\alpha J_{22}(\psi_{12})/(\beta\Omega^3) & 0 \\\\ R_{12}\alpha q_\alpha J_1(\psi_{12})/(\beta\Omega^3) & 0 & R_{12}\alpha q_\alpha J_0(\psi_{12})/(\beta q_\beta\Omega^3) \end{bmatrix}$$

$$(A.9)$$

$$H_{21}(\Omega) = \begin{bmatrix} -R_{21}\beta q_\beta J_{11}(\psi_{21})/(\alpha q_\alpha\Omega^3) & 0 & R_{21}\beta q_\beta J_1(\psi_{21})/(\alpha\Omega^3) \\\\ 0 & -R_{21}\beta q_\beta J_{22}(\psi_{21})/(\alpha q_\alpha\Omega^3) & 0 \\\\ R_{21}\beta J_1(\psi_{21})/(\alpha q_\alpha\Omega^3) & 0 & -R_{21}\beta J_0(\psi_{21})/(\alpha\Omega^3) \end{bmatrix}$$

$$(A.10)$$

$$H_{22}(\Omega) = \begin{bmatrix} R_{22}J_{11}(\psi_{22})q_\beta/\Omega^3 & 0 & R_{22}J_1(\psi_{22})/\Omega^3 \\\\ 0 & R_{22}J_{22}(\psi_{22})q_\beta/\Omega^3 & 0 \\\\ -R_{22}J_1(\psi_{22})/\Omega^3 & 0 & -R_{22}J_0(\psi_{22})/(q_\beta\Omega^3) \end{bmatrix}$$

$$(A.11)$$

$$H_{33}(\Omega) = \begin{bmatrix} -J_{22}(\psi_{33})/(\beta^2 q_\beta \Omega) & 0 & 0 \\ 0 & -J_{11}(\psi_{33})/(\beta^2 q_\beta \Omega) & 0 \\ 0 & 0 & 0 \end{bmatrix}$$

(A.12)

$$H_{13}(\Omega) = H_{31}(\Omega) = H_{23}(\Omega) = H_{32}(\Omega) = 0.$$ (A.13)

In these equations, ψ_n is given by (2.4.1) when $x_3 - z > 0$; a small modification, indicated in the text, is needed when $x_3 - z < 0$. ψ_{mn} is defined by (2.4.12), for any (x_3, z).

The direct arrivals are obtained, as outlined in section 2.4, by employing the preceding formulae in conjunction with (2.4.10) and (2.4.17); they are listed below.

(a) Direct rays

$$G_1 \backsim \frac{H(t-t_1)}{4\pi\rho\alpha^2 R^3} \begin{bmatrix} r^2 & 0 & r(x_3-z) \\ 0 & 0 & 0 \\ r(x_3-z) & 0 & (x_3-z)^2 \end{bmatrix} ,$$ (A.14)

$$G_2 \backsim \frac{H(t-t_2)}{4\pi\rho\beta^2 R^3} \begin{bmatrix} (x_3-z)^2 & 0 & -r(x_3-z) \\ 0 & 0 & 0 \\ -r(x_3-z) & 0 & r^2 \end{bmatrix} ,$$ (A.15)

$$G_3 \sim \frac{H(t-t_3)}{4\pi\rho\beta^2 R} \begin{bmatrix} 0 & 0 & 0 \\ 0 & 1 & 0 \\ 0 & 0 & 0 \end{bmatrix} . \tag{A.16}$$

In these expressions,

$$R^2 = r^2 + (x_3 - z)^2 \tag{A.17}$$

and

$$t_1 = R/a, \quad t_2 = t_3 = R/\beta . \tag{A.18}$$

(b) **Reflected rays:**

$$G_{11} \sim \frac{H(t-t_{11})R_{11}}{4\pi\rho a^2 S^3} \begin{bmatrix} r^2 & 0 & r|x_3+z| \\ 0 & 0 & 0 \\ -r|x_3+z| & 0 & -(x_3+z)^2 \end{bmatrix} , \tag{A.19}$$

$$G_{12} \sim \frac{H(t-t_{12})R_{12}a}{4\pi\rho r(\psi''_{12})^{\frac{1}{2}}\beta\Omega_{12}^3} \begin{bmatrix} -1 & 0 & -1/q_\beta \\ 0 & 0 & 0 \\ q_a & 0 & q_a/q_\beta \end{bmatrix} , \tag{A.20}$$

$$G_{21} \sim \frac{H(t-t_{21})R_{21}\beta}{4\pi\rho r(\psi''_{21})^{\frac{1}{2}}aq_a\Omega^3_{21}} \begin{bmatrix} q_\beta & 0 & q_a q_\beta \\ 0 & 0 & 0 \\ 1 & 0 & q_a \end{bmatrix} \quad , \qquad (A.21)$$

$$G_{33} \sim \frac{H(t-t_{33})}{4\pi\rho\beta^2 s} \begin{bmatrix} 0 & 0 & 0 \\ 0 & 1 & 0 \\ 0 & 0 & 0 \end{bmatrix} \quad , \qquad (A.22)$$

In these expressions,

$$s^2 = r^2 + (x_3 + z)^2 \quad , \qquad (A.23)$$

$$t_{11} = s/a \quad , \quad t_{33} = s/\beta \qquad (A.24)$$

and terms such as R_{mn} are evaluated at the corresponding root Ω_{mn} of (2.4.12). The roots Ω_{12}, Ω_{21} cannot be given explicitly but

$$\Omega_{11} = as/r \quad , \quad \Omega_{33} = \beta s/r \quad . \qquad (A.25)$$

For the remaining term, G_{22}, $t_{22} = t_{33}$ and $\Omega_{22} = \Omega_{33}$. When $\Omega_{22} > a$, that is, when

$$s > ar/\beta \quad , \qquad (A.26)$$

the point x lies within the cone defined by (2.4.13) and it follows that

$$G_{22} \sim \frac{-H(t-t_{22})R_{22}}{4\pi\rho\beta^2 S^3}
\begin{bmatrix}
(x_3+z)^2 & 0 & -r|x_3+z| \\
0 & 0 & 0 \\
r|x_3+z| & 0 & -r^2
\end{bmatrix} . \tag{A.27}$$

When $S < ar/\beta$, however,

$$G_{22} \sim \frac{[\cos\theta\, H(t-t_{22}) - \pi^{-1}\sin\theta \ln|t-t_{22}|]}{4\pi_\rho \beta^2 S^3}
\begin{bmatrix}
(x_3+z)^2 & 0 & -r|x_3+z| \\
0 & 0 & 0 \\
r|x_3+z| & 0 & -r^2
\end{bmatrix} ,$$

$$\tag{A.28}$$

where

$$\cos\theta = \frac{[(x_3+z)^2-r^2]^2 - 16(x_3+z)^2(r^2-\beta^2 S^2/a^2)}{[(x_3+z)^2-r^2]^2 + 16(x_3+z)^2(r^2-\beta^2 S^2/a^2)} , \tag{A.29}$$

so that

$$R_{22} = -\cos\theta + i\sin\theta . \tag{A.30}$$

(c) <u>Head-wave arrivals</u>

Finally, the head-wave arrival time t_H is given by substituting $\Omega = a$ into $\psi_{22}(\Omega,x,t) = +1$; thus

$$at_H = r + |x_3+z|(a^2/\beta^2-1)^{\frac{1}{2}} . \tag{A.31}$$

When t is close to t_H, it is obtained that

$$G_{22} \sim \frac{2(t-t_H)H(t-t_H)(a^2/\beta^2-1)^{\frac{1}{2}}}{\pi\rho a(a^2/\beta^2-2)^2 r^{\frac{1}{2}}(\Theta)^{3/2}} \begin{bmatrix} (a^2/\beta^2-1)^{\frac{1}{2}} & 0 & -1 \\ 0 & 0 & 0 \\ 1 & 0 & -(a^2/\beta^2-1)^{\frac{1}{2}} \end{bmatrix},$$

(A.32)

where $\Theta = r - |x_3 + z|(a^2/\beta^2 - 1)^{-\frac{1}{2}}$.

Similar forms can be derived for G_{12} when $x_3 = 0$ and for G_{21} when $z = 0$.

CHAPTER 3   THE RESPONSE OF A FLUID-LOADED PLATE STIFFENED BY A

FINITE NUMBER OF BEAMS.

3.1   INTRODUCTION

This chapter and the two chapters following it deal with the

vibration of, and radiation from, fluid-loaded plates with attached

stiffening beams.

A thin elastic plate is commonly used as a model for aircraft

and marine structures but such structures are highly complex and no

single model is valid at all frequencies.To examine the range of

validity for the fluid-loaded thin plate model it is necessary to

consider the characteristic wavelength of vibrations in the plate.

Structural damping causes a flexural wave in the plate to decay

exponentially with distance, so that after travelling several

wavelengths its amplitude is negligible. Thus, if the characteristic

wavelength, λ, is short enough the effects of boundaries and of the

curvature of the structure can be neglected. In particular, therefore,

λ must be shorter than the radius of curvature of the structure.

This gives a low frequency limit for the validity of the model.

Below this limit a model such as a cylindrical shell might be more

suitable.

For thin plate theory to be valid the characteristic

wavelength, λ, must be larger than the thickness of the plate to

justify the "plane strain" assumption. λ must also be larger than any

beam cross-section if the beams are to be modelled as line attachments.

This gives an upper limit to the range of frequencies for which the

model is valid, above which the finite thickness of the beams and

the plate become significant.

In this chapter and in chapters 4 and 5 the plate is modelled

using the classical thin plate equation and the beams are modelled

as line discontinuities in the stiffness and mass of the plate. In the simplest realization of this model the beams are replaced by equivalent line forces. The general solutions however, are obtained using Green's functions whose exact form is not specified. In this chapter and in chapter 4 the beams are considered more generally as line attachments capable of exerting moments as well as forces.

This chapter looks at the excitation of an infinite thin elastic plate, fluid-loaded on one side and stiffened by a finite number of parallel attached beams.

The vibration of plates with structural discontinuities has been examined by Heckl (61) who looked at the transmission of plate flexural waves across beams attached to the plate and by Lamb (61) who examined the input impedance of a beam attached to a plate, although neither study included the effects of fluid-loading.

Kovinskaya and Nikiforov (73) also looked at the vibration of plates without fluid-loading but with one or more attached beams and analysed the spatial directivity of the flexural wave fields produced by a point excitation.

Romanov (71) examined the sound radiated from a fluid-loaded plate with two attached beams when the excitation took the form of random forces between the two beams. The sound radiated by a point excited plate has been studied by Lin and Hayek (77) for one reinforcing beam and by Romanov (77) for several beams and is the subject of a letter by Garrelick and Lin (75).

Finally, the scattering of a plane acoustic wave by a beam reinforced plate has been studied by Stepanishen (78) and by Leppington (78).

In the study of fluid-loaded plates with a finite number of beams, authors have concentrated exclusively on the sound radiated into the fluid. For applications to structures such as a ship's hull, however, the vibrations of the hull are also of interest.

In this chapter we shall examine the vibration of the plate and the radiated sound for a general excitation, although calculations are performed only for a point excitation.

3.2   THE GENERAL SOLUTION

Consider an infinite thin elastic plate lying in the plane $z = 0$ and driven by a time harmonic force distribution $f(x,y)e^{-i\omega t}$ applied normal to the plate surface. The plate is stiffened by parallel beams attached along the lines $x = x_n$, $n = 1,\ldots, N$, which exert forces $F_n(y)\delta(x-x_n)e^{-i\omega t}$ and moments $M_n(y)\delta'(x-x_n)e^{-i\omega t}$ on the plate.

Compressible fluid occupies the half-space $z > 0$, and the plate is backed by an effective vacuum (a light fluid whose interaction with the plate can be neglected).

The vertical (positive z direction) motion of the plate, $u(x,y)e^{-i\omega t}$ satisfies

$$u(x,y) = \int\int_{-\infty}^{\infty} dx'dy'\ G(x-x',y-y') \cdot \left\{ f(x',y') - \sum_{n=1}^{N} F_n(y')\delta(x'-x_n) \right.$$

$$\left. - \sum_{n=1}^{N} M_n(y')\delta'(x'-x_n) \right\}, \tag{3.2.1}$$

where $G(x-x',y-y')$ is the plate Green's function and represents the displacement at a point (x,y) due to a unit point force at (x',y'). The harmonic time dependence is suppressed in all that follows.

We can take an ordinary Fourier transform in the y-direction, defined by

$$\tilde{A}(x,k_y) = \int_{-\infty}^{\infty} A(x,y)e^{ik_y y}dy, \tag{3.2.2}$$

which reduces (3.2.1) to

$$\tilde{u}(x,k_y) = \tilde{G}(x,k_y) * \left\{ \tilde{f}(x,k_y) - \sum_{n=1}^{N} \tilde{F}_n(k_y)\delta(x-x_n) - \sum_{n=1}^{N} \tilde{M}_n(k_y)\delta'(x-x_n) \right\},$$

(3.2.3)

where $*$ denotes convolution w.r.t. x.

The forces $F_n(y)$ are related to the plate displacements at the beams by

$$\tilde{F}_n(k_y) = \tilde{Z}_n(k_y)\tilde{u}(x_n,k_y),$$

(3.2.4)

where $i\tilde{Z}_n(k_y)/\omega$ is the spectral bending impedance of the nth beam.

The moments $M_n(y)$ are related to the angular displacements of the plate by

$$\tilde{M}_n(k_y) = \tilde{Y}_n(k_y)\frac{\partial\tilde{u}}{\partial x}(x_n,k_y),$$

(3.2.5)

where $i\tilde{Y}_n(k_y)/\omega$ is the rotational impedance of the nth beam.

Substituting for F_n and M_n in (3.2.3) gives

$$\tilde{u}(x,k_y) = \tilde{G}(x,k_y) * \left\{ \tilde{f}(x,k_y) - \sum_{n=1}^{N} \tilde{Z}_n(k_y)\tilde{u}(x_n,k_y)\delta(x-x_n) \right.$$

$$\left. - \sum_{n=1}^{N} \tilde{Y}_n(k_y)\frac{\partial\tilde{u}}{\partial x}(x_n,k_y)\delta'(x-x_n) \right\}.$$

(3.2.6)

Equation (3.2.6) can be simplified by noting that

$$\tilde{G}(x,k_y)*\delta(x-x_n) = \tilde{G}(x-x_n,k_y)$$

and

$$\tilde{G}(x,k_y)*\delta'(x-x_n) = \frac{\partial\tilde{G}}{\partial x}(x-x_n,k_y).$$

The notation can be simplified by writing $\widetilde{A}(x,k_y) = A(x)$, since the transform variable k_y occurs merely as a parameter. Finally, writing $\psi(x) = G(x)*f(x)$ yields

$$u(x) = \psi(x) - \sum_{n=1}^{N} Z_n G(x-x_n) u(x_n) - \sum_{n=1}^{N} Y_n G'(x-x_n) u'(x_n). \qquad (3.2.7)$$

Differentiation of (3.2.7) w.r.t. x produces

$$u'(x) = \psi'(x) - \sum_{n=1}^{N} Z_n G'(x-x_n) u(x_n) - \sum_{n=1}^{N} Y_n G''(x-x_n) u'(x_n). \qquad (3.2.8)$$

Equations (3.2.7) and (3.2.8) are true for all x, and in particular putting $x = x_m$, $m = 1,\ldots, N$ gives

$$u(x_m) = \psi(x_m) - \sum_{n=1}^{N} Z_n G(x_m-x_n) u(x_n) - \sum_{n=1}^{N} Y_n G'(x_m-x_n) u'(x_n) \qquad (3.2.9)$$

and

$$u'(x_m) = \psi'(x_m) - \sum_{n=1}^{N} Z_n G'(x_m-x_n) u(x_n) - \sum_{n=1}^{N} G''(x_m-x_n) u'(x_n). \qquad (3.2.10)$$

The coupled equations (3.2.9) and (3.2.10) represent a system of 2N simultaneous equations for the transformed translational and rotational displacements at the N beams.

$G(x_m-x_n) = \widetilde{G}(x_m-x_n,k_y)$ is a measure of the interaction between

the beams at x_m and x_n. In particular, $\widetilde{G}(x_m-x_n,0)$ is the displacement at $x = x_m$ due to a unit line source at $x = x_n$, and $\frac{\partial \widetilde{G}}{\partial x}(x_m-x_n,0)$ is the angular displacement at $x = x_m$ due to a unit line moment at $x = x_n$.

The solutions of (3.2.9) and (3.2.10) for $u(x_n)$ and $u'(x_n)$ can be substituted into (3.2.7) to give $u(x)$, and $u(x,y)$ can then be found by Fourier inversion.

If the moments on the plate produced by the beams are neglected, i.e. $\widetilde{Y}_n(k_y) = 0$, then (3.2.7) becomes

$$u(x) = \Psi(x) - \sum_{n=1}^{N} Z_n G(x-x_n)u(x_n), \qquad (3.2.11)$$

and (3.2.9) becomes

$$\sum_{n=1}^{N} L_{mn}u(x_n) = \Psi(x_n), \quad m = 1,\ldots, N \qquad (3.2.12)$$

where

$$L_{mn} = \delta_{mn} + G(x_m-x_n)Z_n \qquad (3.2.13)$$

and δ_{mn} is the Kronecker delta.

(3.2.12) is then a system of N simultaneous equations whose solution may be substituted into (3.2.11) to give $u(x)$. Fourier inversion can then be used to find $u(x,y)$.

In the remainder of this chapter the moments produced by the beams are neglected, although their inclusion would not introduce any extra difficulties in principle. The plate is modelled using the classical thin plate equation.

If the beams are modelled as line discontinuities in
the mass and stiffness of the plate then they can be replaced
by equivalent line attachments capable of exerting forces on the
plate.

3.3 THE GREEN'S FUNCTION FOR A FLUID-LOADED PLATE

In order to solve equations (3.2.12) for a given plate-beam system we need to know the Green's function for the fluid-loaded plate and the spectral impedances of the beams.

If the fluid has sound speed c and density ρ_0, then its displacement potential $\Phi(x,y,z)e^{-i\omega t}$ satisfies;

$$\nabla^2\Phi + k_0^2\Phi = 0, \quad z > 0, \qquad (3.3.1)$$

where k_0 is the acoustic wavenumber ω/c.

The Green's function for a fluid-loaded plate, with bending stiffness D and mass per unit area m, satisfies;

$$D\nabla^4 G(x,y) - \omega^2 m G(x,y) - \rho_0\omega^2\Phi\Big|_{z=0} = \delta(x)\delta(y). \qquad (3.3.2)$$

Continuity of displacement at the fluid-plate boundary gives

$$G(x,y) = -\frac{\partial\Phi(x,y,z)}{\partial z}\Big|_{z=0}. \qquad (3.3.3)$$

Standard Fourier transform techniques can be used to find $G(x,y)$ as follows.

We define the Fourier transform for two dimensions by;

$$\tilde{f}(k_x,k_y) = \int\int_{-\infty}^{\infty} f(x,y)e^{ik_x x}e^{ik_y y}dxdy, \qquad (3.3.4)$$

with the corresponding inverse given by

$$f(x,y) = \frac{1}{4\pi^2} \int\int\limits_{-\infty}^{\infty} \bar{f}(k_x,k_y)e^{-ik_x x}e^{-ik_y y}dk_x dk_y. \qquad (3.3.5)$$

Transforming (3.3.1) gives

$$\frac{d^2\bar{\Phi}}{dz^2} + (k_o^2 - k_x^2 - k_y^2)\,\bar{\Phi} = 0, \qquad (3.3.6)$$

which has solution

$$\bar{\Phi}(k_x,k_y,z) = A(k_x,k_y)e^{ik_z z}, \qquad (3.3.7)$$

where $k_z = (k_o^2 - k_x^2 - k_y^2)^{\frac{1}{2}}$ and imag $(k_z) \geq 0$.

Therefore, on the surface of the plate

$$\bar{\Phi}(k_x,k_y,0) = A(k_x,k_y) \qquad (3.3.8)$$

and hence, from (3.3.4)

$$\bar{G}(k_x,k_y) = -ik_z A(k_x,k_y). \qquad (3.3.9)$$

Transforming (3.3.2) and substituting for $\bar{\Phi}(k_x,k_y,0)$ using (3.3.8) and (3.3.9) yields;

$$\left\{ D(k_x^2 + k_y^2)^2 - \omega^2 m - i\rho_o \omega^2/k_z \right\}\bar{G}(k_x,k_y) = 1$$

from which

$$\bar{G}(k_x,k_y) = \left\{ D(k_x^2 + k_y^2)^2 - \omega^2 m - i\rho_o \omega^2/k_z \right\}^{-1}, \qquad (3.3.10)$$

and

$$\widetilde{G}(x_m - x_n, k_y) = \frac{1}{2\pi} \int_{-\infty}^{\infty} \overline{G}(k_x, k_y) e^{-ik_x(x_m - x_n)} dk_x \qquad (3.3.11)$$

The occurrence of the term $k_z = (k_0^2 - k_x^2 - k_y^2)^{\frac{1}{2}}$ in the integrand produces branch cuts in the complex k_x plane which prevent us from evaluating (3.3.11) analytically. For problems where the fluid-loading is very light, that is $\rho_0 \to 0$, the term $i\rho_0 \omega^2 / k_z$ can be neglected and the integral evaluated by residues. Romanov (77) argues that at high enough frequencies the integral in (3.3.11) can be approximated by the contribution from the pole of the integrand near to the real axis, which corresponds physically to assuming that the beams only interact through flexural waves in the plate.

We do not wish to make any restrictions here and so we retain the integral representation for $\widetilde{G}(x_m - x_n, k_y)$ given in (3.3.11).

If the nth beam has bending stiffness B_n and mass per unit length M_n, then the force due to the nth beam is given by

$$F_n(y) = B_n \frac{\partial^4}{\partial y^4} u(x_n, y) - \omega^2 M_n u(x_n, y). \qquad (3.3.12)$$

Fourier transforming in the y direction gives;

$$\widetilde{F}_n(k_y) = \left[B_n k_y^4 - \omega^2 M_n \right] \cdot u(x_n, k_y)$$

which implies that

$$\widetilde{Z}_n(k_y) = \widetilde{F}_n(k_y) / \widetilde{u}(x_n, k_y) = B_n k_y^4 - \omega^2 m. \qquad (3.3.13)$$

It should be noted that the solution in section 3.2 does

not depend on the specific form of the Green's function or the
beam impedance. A simpler model using a membrane with attached
line masses could have been studied, as could the algebraically
more complicated model using Timoshenko beams and the
Timoshenko-Mindlin plate, and including the moments on the
plate due to the beams.

$\tilde{L}_{mn}(k_y)$ in (3.2.8) can now be found from (3.3.11) and
(3.3.13) and so we have a formal method of solution. The
transformed displacement $\tilde{u}(x,k_y)$ can then be found from (3.2.6).

The solution $u(x,y)$ can be found by performing the inverse
transform;

$$u(x,y) = \frac{1}{2\pi} \int_{-\infty}^{\infty} \tilde{u}(x,k_y)e^{-ik_y y}dk_y. \qquad (3.3.14)$$

The computation however, is lengthy because the evaluation
of the integrand at each point requires the calculation of the
integrals (3.3.11) and the solution of the set of simultaneous
equations. If, however, the excitation is of the form

$$f(x,y) = F(x)e^{ik_y y}, \qquad (3.3.15)$$

then

$$u(x,y) = \tilde{u}(x,k_y)e^{ik_y y}, \qquad (3.3.16)$$

so $u(x,y)$ can be found directly from (3.2.6). It should be noted
that a line excitation parallel to the beams takes the form of
(3.3.15) with $k_y = 0$.

The calculation of the fluid pressure from $u(x,y)$ requires

the evaluation of two convolution integrals, or equivalently the calculation from $\bar{u}(k_x, k_y)$ requires the evaluation of two inverse transforms. Either computation is lengthy, unless the excitation is of the special harmonic form

$$f(x,y) = Ae^{i(k_x x + k_y y)}, \qquad\qquad (3.3.17)$$

in which case the pressure $p(x,y,z)$ can be obtained directly from $\bar{u}(k_x, k_y)$.

The following two sections, 3.4 and 3.5 are devoted to finding asymptotic approximations to the plate displacement and fluid pressure, respectively, for problems where the excitation is not of the form (3.3.15) or (3.3.17).

3.4 ASYMPTOTIC EVALUATION OF THE FARFIELD FLUID PRESSURE

The Fourier transform of (3.2.5) is

$$\bar{u}(k_x,k_y) = \bar{G}(k_x,k_y).\bar{f}(k_x,k_y) + \bar{G}(k_x,k_y)$$

$$\cdot \sum_{n=1}^{N} \tilde{z}_n(k_y)e^{ik_x x_n}\tilde{u}(x_n,k_y),$$

(3.4.1)

which can be written as

$$\bar{u}(k_x,k_y) = \bar{G}(k_x,k_y).\bar{f}(k_x,k_y).C_{ms}(k_x,k_y),$$

(3.4.2)

where

$$C_{ms}(k_x,k_y) = 1 - \left[\sum_{n=1}^{N}\tilde{z}_n(k_y)e^{ik_x x_n}\tilde{u}(x_n,k_y)\right]/\bar{f}(k_x,k_y).$$

(3.4.3)

If no beams are present then $C_{ms} = 1$, so C_{ms} is a "correction factor" corresponding to the mass and stiffness discontinuities at the beams. It was introduced by Lin and Hayek (77), who studied the case $N = 1$.

The fluid pressure $p(x,y,z)$ is related to the displacement gradient by

$$p(x,y,z) = -\omega^2\rho_0\Phi.$$

(3.4.4)

Hence

$$\bar{p}(k_x,k_y,z) = -\omega^2\rho_0\Phi = -\omega^2\rho_0 A(k_x,k_y)e^{ik_z z}.$$

(3.4.5)

We can use (3.3.3) and invert to give;

$$p(x,y,z) = \frac{-i\omega^2\rho_0}{4\pi^2}\int\int_{-\infty}^{\infty}\left\{\bar{u}(k_x,k_y)exp\left[-i(k_x x + k_y y + k_z z)\right]/k_z\right\}dk_x dk_y,$$

(3.4.6)

where $\bar{u}(k_x, k_y)$ is given by (3.4.2).

Introducing spherical polar coordinates;

$$x = R \sin\phi \cos\theta \, , \quad y = R \sin\phi \sin\theta \, , \quad z = R \cos\theta \qquad (3.4.7)$$

and writing

$$k_x = k_o \sin\alpha \cos\beta \, , \quad k_y = k_o \sin\alpha \sin\beta \, , \quad k_z = k_o \cos\alpha, \qquad (3.4.8)$$

enables us to write (3.4.6) as

$$p(R,\theta,\phi,) = -i\omega^2 \rho_o \frac{}{4\pi^2} \int_0^{\pi/2-i\infty} d\alpha \int_0^{2\pi} d\beta \left\{ k_o \sin\alpha . \exp\left[-ik_o Rg(\alpha, \beta, \theta, \phi)\right] \bar{u}(\alpha,\beta) \right\}, \qquad (3.4.9)$$

where

$$g(\alpha,\beta,\theta,\phi) = \cos\phi\cos\alpha + \sin\alpha\cos\phi \cos(\beta - \theta). \qquad (3.4.10)$$

The contour for the α integral consists of the straight lines from the origin to $\alpha = \pi/2$ and from $\alpha = \pi/2$ to $\alpha = \pi/2 - i\alpha$.

We now seek an asympototic expansion of (3.4.9) for large values of R. For large values of $k_o R$ the integrand is rapidly oscillating except at points of stationary phase, that is where

$$\frac{\partial g}{\partial \alpha} = \frac{\partial g}{\partial \beta} = 0 \, . \qquad (3.4.11)$$

Now

$$\frac{\partial g}{\partial \alpha} = -\sin\alpha\sin\phi\sin(\beta - \theta),$$

and

$$\frac{\partial g}{\partial \beta} = -\cos\phi \sin\alpha + \cos\alpha \cos\phi \cos(\beta - \theta),$$

so the stationary phase point is at

$$\alpha = \phi, \beta = \theta \, (\phi \neq 0).$$

Approximating $g(\alpha, \beta)$ by its Taylor expansion about the stationary phase point and neglecting terms of higher order than quadratic in $(\alpha - \phi)$ and $(\beta - \theta)$ allows us to obtain an approximation to $p(R, \theta, \phi)$. Details of a similar approximation are given in section 4.7.

The result is that for sufficiently large $k_0 R$,

$$p(R, \theta, \phi) \simeq -\omega^2 \rho_0 \frac{e^{ik_0 R}}{2\pi R} \bar{u}(\alpha = \phi, \beta = \theta) \qquad (3.4.12)$$

which is a spherically spreading, travelling acoustic wave. Physically the pressure can be thought of as a summation of plane waves, and the approximation used here corresponds to taking account only of those travelling towards or almost towards the receiver.

For a given position and frequency we need only calculate the terms $\widetilde{G}(x_m - x_n, k_0 \sin\theta \sin\phi)$ and solve the set of simultaneous equations once to find the farfield fluid pressure.

3.5 ASYMPTOTIC EVALUATION OF THE FARFIELD PLATE DISPLACEMENT

The plate displacement $u(x,y)$ is given by inverse transforming equation (3.4.2), namely;

$$u(x,y) = \frac{1}{4\pi^2} \int\!\!\int_{-\infty}^{\infty} \bar{G}(k_x,k_y)\bar{F}(k_x,k_y)C_{ms}(k_x,k_y).$$

$$\exp\left[-i(k_x x + k_y y)\right]dk_x dk_y. \qquad (3.5.1)$$

To evaluate (3.5.1) we make the following substitutions;

$$x = r\cos\theta, \ y = r\sin\theta$$

and

$$k_x = k_1\cos\theta - k_2\sin\theta, \ k_y = k_1\sin\theta + k_2\cos\theta. \qquad (3.5.2)$$

(3.5.1) then becomes

$$u(r,\theta) = \frac{1}{4\pi^2} \int\!\!\int_{-\infty}^{\infty} \bar{G}(k_1,k_2)\bar{F}(k_1,k_2,\theta)C_{ms}(k_1,k_2,\theta)e^{-ik_1 r}dk_1 dk_2. \qquad (3.5.3)$$

Now let $k_1 = k\sin\gamma$, $k_2 = k\cos\gamma$, so that

$$u(r,\theta) = \frac{1}{4\pi^2} \int_{-\infty}^{\infty}\!\int_0^{\pi} \bar{G}(k,\gamma)\bar{F}(k,\gamma,\theta)C_{ms}(k,\gamma,\theta)e^{-ikr\,\sin\gamma}k\,d\gamma dk. \qquad (3.5.4)$$

For large values of kr the integrand is rapidly oscillating except at the stationary phase point which is given by

$$\frac{\partial}{\partial\gamma}(\sin\gamma) = 0, \text{ i.e. } \gamma = \pi/2. \qquad (3.5.5)$$

The contour in the complex γ plane can be written as a sum of a

contour which passes through this point in such a way that

$re(\sin \gamma)$ = constant (its value at $\gamma = \pi/2$ and $im(\sin \gamma) < 0$,

plus the two lines from $\gamma = 0$ to $\gamma = -i\infty$ and $\gamma = \pi$ to

$\gamma = \pi + i\infty$. The integrals along these last two contours cancel

to give

$$u(r,\theta) \simeq \frac{1}{4\pi^2} \cdot \int_{-\infty}^{\infty} \left(\frac{2\pi i k}{r}\right)^{\frac{1}{2}} \bar{G}(k,\pi/2)\bar{f}(k,\pi/2,\theta)C_{ms}(k,\pi/2,\theta)e^{-ikr}dk. \qquad (3.5.6)$$

If the plate bending stiffness D is real, that is, if damping

in the plate is neglected, then $\bar{G}(k,\pi/2)$ has poles on the real

axis at $k = \pm K$, (see Crighton (79)). The contour can be closed

in the lower half plane and the Riemann-Lebesgue lemma used to

show that the major contribution to the integral comes from the

residue contribution at $k = -K$. Hence,

$$u(r,\theta) \simeq \left(\frac{ik}{2\pi r}\right)^{\frac{1}{2}} \bar{f}(-K,\pi/2,\theta)C_{ms}(-K,\pi/2,\theta)e^{iKr} \bigg/ \frac{\partial Q(k)}{\partial k} \bigg|_{k=-K,} \qquad (3.5.7)$$

where

$$Q(k) = 1/\bar{G}(k) = Dk^4 - \omega^2 m - i\rho_0 \omega^2 \bigg/ (k_0^2 - k^2)^{\frac{1}{2}}.$$

The displacement (3.5.7) has the form of a plane flexural wave

in the plate travelling towards the receiver.

If plate damping is included then K has a small imaginary

part, and (3.5.7) corresponds physically to assuming that damped

flexural waves in the plate are the predominant motion in the

plate farfield.

3.6 COMPUTATION FOR A POINT FORCE EXCITATION

For a time - harmonic point force excitation

$$f(x,y) = F_0 \delta(x)\delta(y) \tag{3.6.1}$$

and

$$\tilde{f}(k_x,k_y) = F_0. \tag{3.6.2}$$

For a plate stiffened with an odd number of equally spaced,

identical beams and excited by a point force on the middle beam,

(3.4.3) becomes;

$$C_{ms}(k_x,k_y) = 1 - \tilde{z}(k_y)\sum_{n=-M}^{M} e^{ik_x nd}u(nd,k_y), \tag{3.6.3}$$

where $M = \frac{N-1}{2}$, $\tilde{z}(k_y)$ is the spectral impedance of each beam,

and d is the beam spacing. From (3.4.12) and the definition of

C_{ms} we have

$$\frac{p_N(R,\theta,\phi)}{p_0(R,\theta,\phi)} = C_{ms}(k_x = k_0\sin\phi\cos\theta, \ k_y = k_0\sin\phi\sin\theta), \tag{3.6.4}$$

where $p_N(R,\theta,\phi)$ is the pressure radiated from a plate stiffened

with N beams and $p_0(R,\theta,\phi)$ the pressure radiated from an unstiffened

plate.

Similarly from (3.5.7)

$$\frac{u_N(r,\theta)}{u_0(r,\theta)} = C_{ms}(k_x = - K\cos\theta, \ k_y = -K\sin\theta), \tag{3.6.5}$$

where $u_N(r,\theta)$ is the displacement at r,θ of a plate stiffened

by N beams and $u_o(r,\theta)$ the displacement of an unstiffened plate.

The calculation of C_{ms} requires finding $\tilde{u}(nd,k_y)$, and it is worth noting that the line input impedance I_L of the stiffened plate is given by

$$I_L = \frac{iF_o}{\omega \tilde{u}(0,0)} \; ; \qquad (3.6.7)$$

and so is easily calculated.

The point input impedance I_p is harder to find, since it requires the evaluation of an integral. It is given by

$$I_p = \frac{iF_o}{2\pi\omega} \int_{-\infty}^{\infty} \frac{e^{-ik_y y}}{\tilde{u}(0,k_y)} \, dy. \qquad (3.6.8)$$

The evaluation of the integral in (3.3.11) is complicated by the poles on or near to the real axis. Contour integration can be used to simplify the calculation as follows;

From (3.3.11) and (3.3.10) we have

$$\tilde{G}(x_m-x_n,k_y) = \frac{1}{2\pi} \int_{-\infty}^{\infty} \frac{e^{-ik_x(x_m-x_n)} \, dk_x}{D(k_x^2 + k_y^2)^2 - \omega^2 m - i\rho_o \omega^2/k_z} \qquad (3.6.9)$$

where $k_z = (k_o^2 - k_x^2 - k_y^2)^{\frac{1}{2}}$.

To ensure that $\text{im}(k_z) > 0$ we can introduce branch cuts as follows.

(i)   if $k_y^2 < k_o^2$ then we have an 'L' shaped branch cut in the upper half plane from $(k_o^2 - k_y^2)^{\frac{1}{2}}$ on the real axis to the origin and then along the imaginary axis to $+ i\infty$; we also have a corresponding branch cut in the lower half plane.

(ii) if $k_y^2 > k_0^2$ then the cut is from $i(k_y^2 - k_0^2)^{\frac{1}{2}}$ to $+ i\infty$ on the

imaginary axis and from $-i(k_y^2 - k_0^2)^{\frac{1}{2}}$ to $-i\infty$.

These branch cuts are shown in figure 3.1. Writing $k_y = k_0 q$

and $k_x = k_0 \eta$ reduces (3.6.9) to

$$\tilde{G}(x_m - x_n, k_0 q) = \frac{i}{2\pi \rho_0 c^2} I_{mn}. \qquad (3.6.10)$$

where

$$I_{mn} = \int_{-\infty}^{\infty} \frac{\exp[-ik_0 \eta (x_m - x_n)](1 - q^2 - \eta^2)^{\frac{1}{2}} \, d\eta}{1 + ia(1 - q^2 - \eta^2)^{\frac{1}{2}}[(q^2 + \eta^2)^2 \Omega^2 - 1]} \qquad (3.6.11)$$

and

$$a = \frac{mk_0}{\rho_0}, \quad \Omega^2 = \frac{\omega^2}{\omega_0^2} \quad \text{and} \quad \omega_0 = c^2 \sqrt{\frac{m}{D}}.$$

ω_0 is the classical coincidence frequency for the fluid and plate.

For $(x_m - x_n) < 0$ we can close the contour in the upper half

plane around the branch cut and the poles, η_p, of the integrand.

These poles satisfy

$$Q(\eta) = 1 + ia(1 - q^2 - \eta^2)^{\frac{1}{2}}\left[(q^2 + \eta^2)^2 \Omega^2 - 1\right] = 0. \qquad (3.6.12)$$

Terms not involving $(1 - q^2 - \eta^2)^{\frac{1}{2}}$ cancel across the branch cut to

give

$$I_{mn} = -2\int_{i\beta}^{i\infty} \frac{(1 - q^2 - \eta^2)^{\frac{1}{2}} \exp(-ik_0 \eta (x_m - x_n))}{1 + a^2(1 - q^2 - \eta^2)\left[\Omega^2(q^2 + \eta^2)^2 - 1\right]^2} \, d\eta$$

Figure 3.1. The branch cuts for $k_z = (k_o^2 - k_y^2 - k_x^2)^{\frac{1}{2}}$ in the complex k_x plane. The branch points are at $k_x = \pm (k_o^2 - k_y^2)^{\frac{1}{2}}$.

(a) $k_o^2 > k_y^2$

$(k_o^2 - k_y^2)^{\frac{1}{2}}$

(b) $k_o^2 < k_y^2$

$(k_o^2 - k_y^2)^{\frac{1}{2}}$

$$+ 2\int_0^a \frac{(1-q^2-\eta^2)^{\frac{1}{2}}\exp(-ik_o\eta(x_m-x_n))}{1 + a^2(1-q^2-\eta^2)\left[\Omega^2(q^2+\eta^2)^2-1\right]^2} \, d\eta + 2\pi i\sum_1^3 res \quad,$$

(3.6.13)

where $a =$ real part $(1-q^2)^{\frac{1}{2}}$

$\beta =$ imaginary part $(1-q^2)^{\frac{1}{2}}$

and res denotes the residue contribution from the three poles

η_p in the upper half plane. Note that if $k_y^2 > k_o^2$ then $q^2 > 1$ and

$a = 0$. The second integral in (3.6.13) is then not included.

For $x_m-x_n > 0$ we can close the contour in the lower half

plane and obtain a result similar to (3.6.13).

In general we can write

$$I_{mn} = -2i\int_\beta^\infty \frac{(1-q^2+\eta^2)^{\frac{1}{2}}\exp(-k_o\eta\lceil x_m-x_n\rvert)}{1 + a^2(1-q^2+\eta^2)[\Omega^2(q^2-\eta^2)^2-1]^2} \, d\eta$$

$$+ 2\int_0^a \frac{(1-q^2-\eta^2)^{\frac{1}{2}}\exp(ik_o\eta\mid x_m-x_n\mid)}{1 + a^2(1-q^2-\eta^2)\left[\Omega^2(q^2+\eta^2)^2-1\right]^2} \, d\eta$$

$$+ 2\pi i\sum_{p=1}^3 \frac{\exp(ik_o\eta_p\mid x_m-x_n\mid)(1-q^2-\eta_p^2)}{ia\eta_p\left[\Omega^2(q^2+\eta_p^2)(4-5q^2-5\eta_p^2) + 1\right]} \quad,$$

(3.6.14)

where η_p are the roots of $Q(\eta) = 0$ which lie in the upper half

plane.

At high frequencies, i.e., large values of $k_o\mid x_m-x_n\mid$, the

major contribution to (3.6.14) is from the residue contribution

at the real root of $Q(\eta) = 0$, but for the results described in this

section the full expression (3.6.14) is used.

$\widetilde{G}(x_m-x_n,k_y)$ is a measure of the effect of the mth beam on

the nth beam. The first integral in (3.6.14) represents the

portion of that effect due to excited evanescent (decaying)

nearfield motion of the fluid, and the second integral, the

effect due to excited acoustic (non-decaying) motion of the fluid.

The residue terms represent the effect as transmitted through the

plate, and in particular the residue term from the real pole

represents the effect on the nth beam of flexural waves produced

in the plate by the mth beam.

For computation a change of variable was used to reduce the

range of integration in the first integral to a finite range,

then the integrals were calculated numerically using a standard

Gauss - Legendre quadrature routine.

3.7 RESULTS

The model developed in this chapter can be used to examine the effects of the various structural and material parameters. The results presented here are intended only to demonstrate some of the general features of the model.

The calculations are for a steel plate, of thickness h meters, in water for the following physical constants:

ρ_o = 1000 kg m^{-3}

c = 1432 m s^{-1}

m = 7897.5h kg m^{-2}

M = 40.34 mh kg m^{-1}

Young's Modulus for steel, E = 2.03×10^{11} kg m^{-1} s^{-2}

Second Moment of Area of Beam, I = 926.3 h^4

Poisson's Ratio, ν = 0.3.

The bending stiffness of the plate is given by

$$D = \frac{Eh^3}{12(1-\nu^2)} \quad , \qquad\qquad\qquad (3.7.1)$$

and the bending stiffness of a beam by

$$B = EI. \qquad\qquad\qquad\qquad (3.7.2)$$

The classical coincidence frequency ω_o is

$$\omega_o = 1337/h \text{ radians per second.}$$

The N beams attached to the plate are assumed to be equally spaced and separated by a distance d = 192h.

For example, if h = 0.00635 m (i.e. 6.35 mm) then the beam spacing is 1.22m and Ω = 0.025 corresponds to a frequency of 838 Hz.

We have calculated the 'correction factor' C_{ms} which occurs in equations (3.6.4) and (3.6.5). It should be noted that the farfield pressure, p_o, radiated from a plate with no stiffening beams varies with R, the distance from the point of excitation, with ϕ , the angle of observation from the plate normal, and with frequency. The displacement of the unstiffened plate varies only with R and with frequency. All of the figures shown here show the pressure or displacement relative to that obtained for the unstiffened plate.

Although equations (3.6.4) and (3.6.5) have been derived for harmonic point excitation of the middle beam, for the special case $\theta = 0^o$ they are identical to the expressions obtained for a line excitation, since the asymptotic methods used correspond to plane wave approximations, and the R dependence has been removed by the normalization.

Figure 3.2 shows the variation of the correction factor for the farfield plate displacement (or velocity) with normalized frequency. The vertical scale is 20 log $(|u_N|/|u_o|)$ where u_N is the displacement with N attached beams and u_o is the displacement of an unstiffened plate. The receiver is at an angle $\theta = 0^o$ to the normal to the beams, so the results are for a point or line force excitation. Plots are shown for N = 1, 3 and 9.

At very low frequencies the system is dominated by the fluid loading, so the addition of any number of beams has little effect.

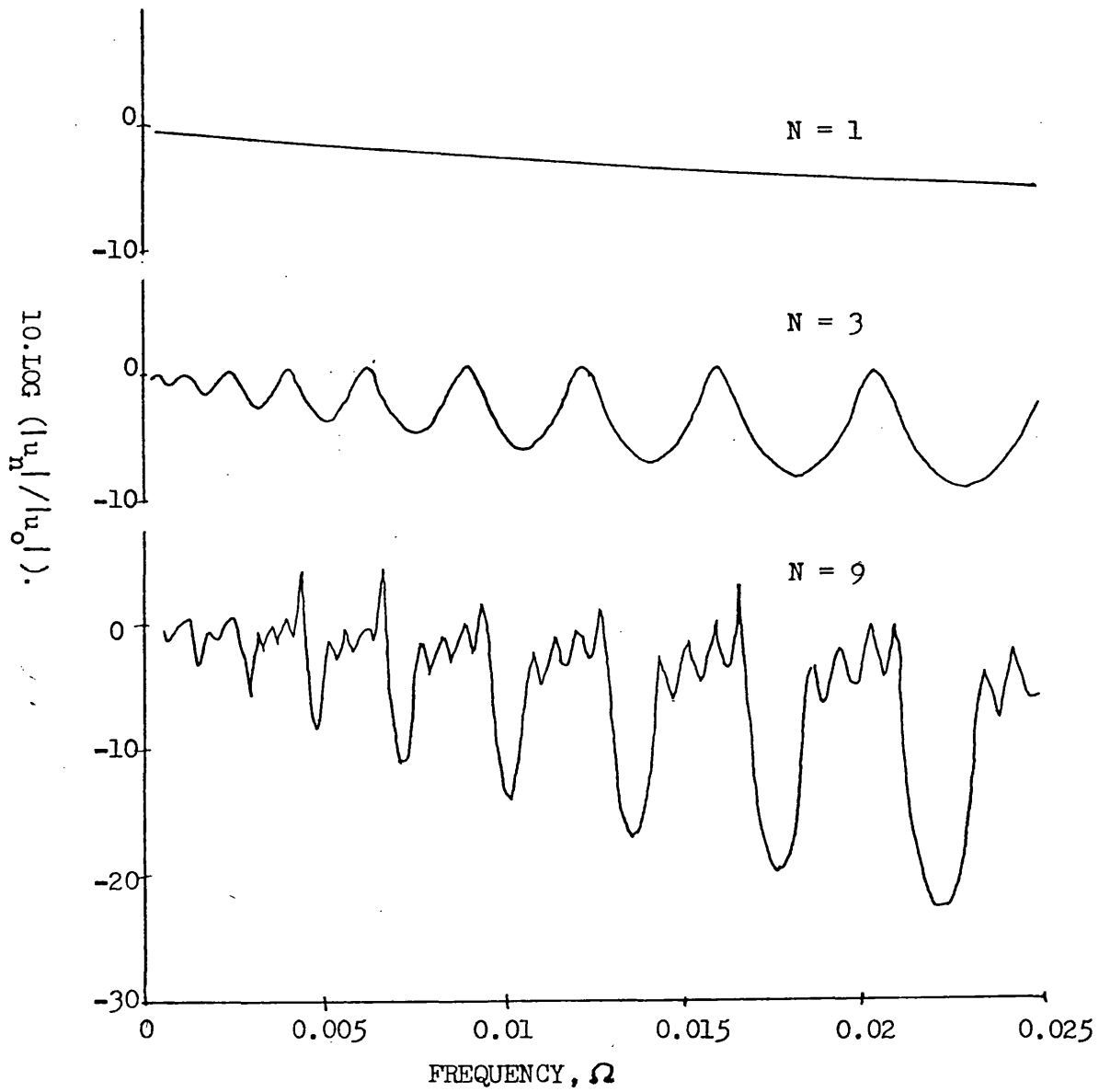The displacement of a plate with a single beam decreases in.

Figure 3.2. The "Correction Factor" for the plate

displacement against normalized frequency

for $\theta = 0^{\circ}$ and $N = 1,3$ and 9.

amplitude, relative to the unstiffened plate, with frequency. The stiffness of the beam has no effect for $\theta = 0^{\circ}$, but the inertia of the beam becomes increasingly more significant.

The decrease in displacement is due to the increase in the line input impedance of the stiffened plate relative to the unstiffened plate. The ratio of the moduli of these impedances is shown in figure 3.3.

Introducing two additional beams (N = 3) produces resonances in the system. The maxima are related to the line input impedance of the system. The ratio of the impedance of the stiffened plate (N = 3) to that of the unstiffened plate is shown in figure 3.4.

The impedance minima (and displacement maxima) occur when the beam spacing is an odd multiple of $\lambda/4$, where λ is the free wavelength in the unstiffened plate. At these frequencies a standing wave could be set up in the plate with an anode at the middle (driven) beam and nodes at the other two beams.

The displacement minima (figure 3.2) occur at frequencies for which the beam spacing is a multiple of $\lambda/2$. At these frequencies we could have a standing wave in the plate with nodes at each beam. For more than three beams a different pattern emerges; the case N = 9 in figure 3.2 is shown as an example. The response can be split into alternate frequency bands, which either give a much smaller response than the unstiffened plate, or a response of about the same level, but containing resonances which can be attributed to wavelength - beam spacing matching.

The formation of these bands, termed stop and pass bands respectively, is a result of the equal spacing of the beams, and will be discussed in more detail in the next chapter. We note here, however, that the start of each stop band corresponds to

a minimum in the line input impedance, and the end to an impedance maximum. The line input impedance of a plate with 9 beams relative to that of an unstiffened plate is shown in figure 3.5.

Figure 3.6 shows the variation with frequency of the correction factor for the farfield fluid at a point $\theta = \phi = 0$ directly above the point of excitation. The vertical scale is $20 \log (|P_N|/|P_o|)$ and plots are shown for N = 1, 3 and 9.

For point (or line) excitation of the stiffened plate at low frequencies the system is dominated by the fluid loading and the beams have little effect on the radiated pressure.

As in figure 3.3 the only effect of a single beam is to increase the input impedance of the system, and the radiated pressure is correspondingly decreased.

For the case N = 3 the minima and maxima all occur at minima in the input impedance (figure 3.4), the minima occuring when the outer beams are moving in counter phase to the applied force. The phase difference between the outer beams and the applied force is shown in figure 3.7.

The remaining plot in figure 3.6 is for the case N = 9. The peaks in the radiated pressure occur at impedance minima (figure 3.5) for which adjacent beams are moving in phase. Each peak is followed by a trough at frequencies for which the beam spacing is a multiple of the free wavelength in the unstiffened plate. At these frequencies, if we consider only flexural waves in the plate, all of the beams are moving in phase, but a 'free mode' for the system is a standing wave with nodes at the beams. It is noted that the maxima and minima occur at the bounding frequencies of stopping bands. The phase difference between adjacent beams (at x = 0 and x = d) is shown in figure 3.8.
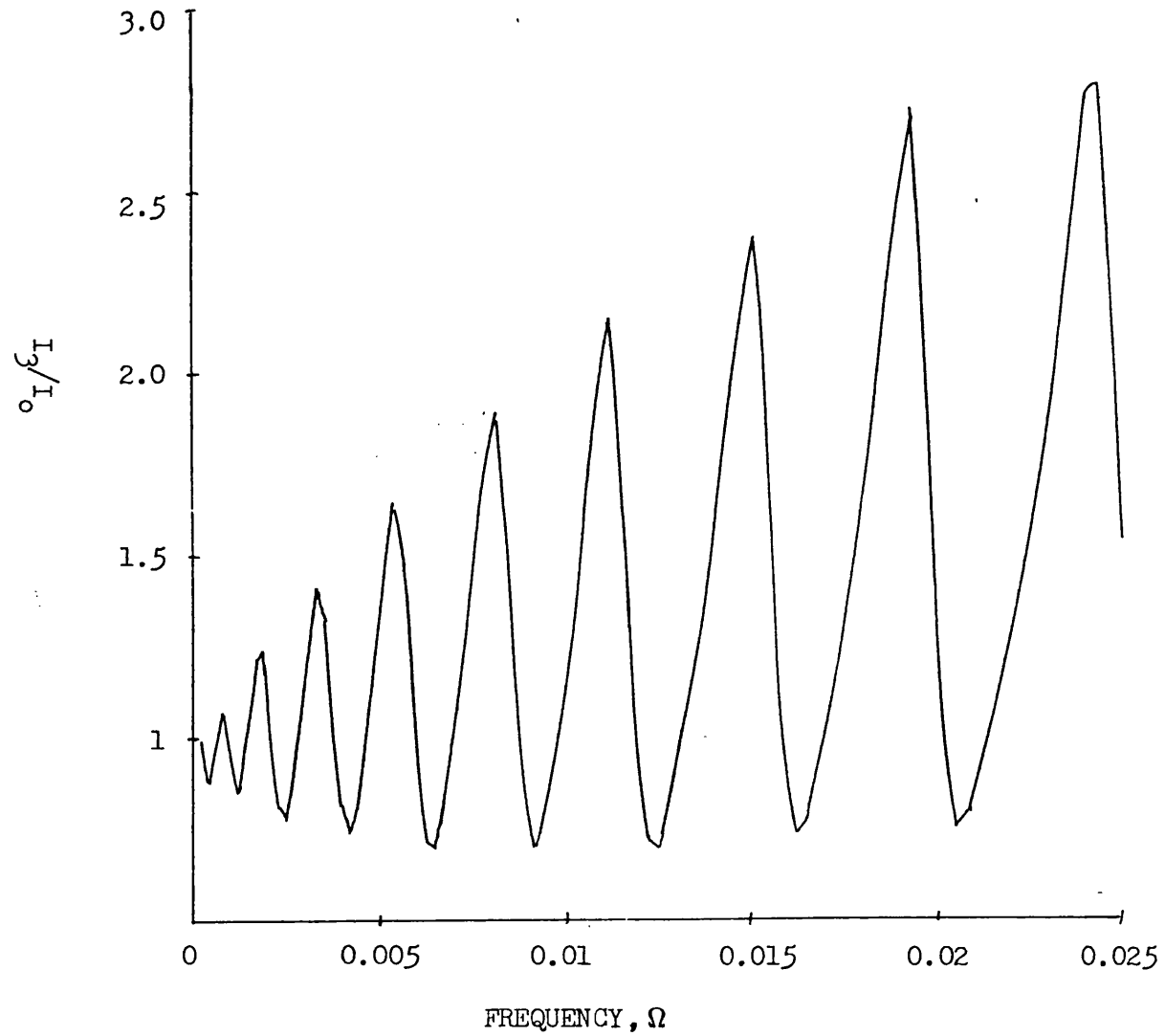
Figure 3.4. The line input impedance against frequency
of a plate stiffened with three beams. I_3 is
the impedance of the stiffened plate, I_0 that
of the unstiffened plate.
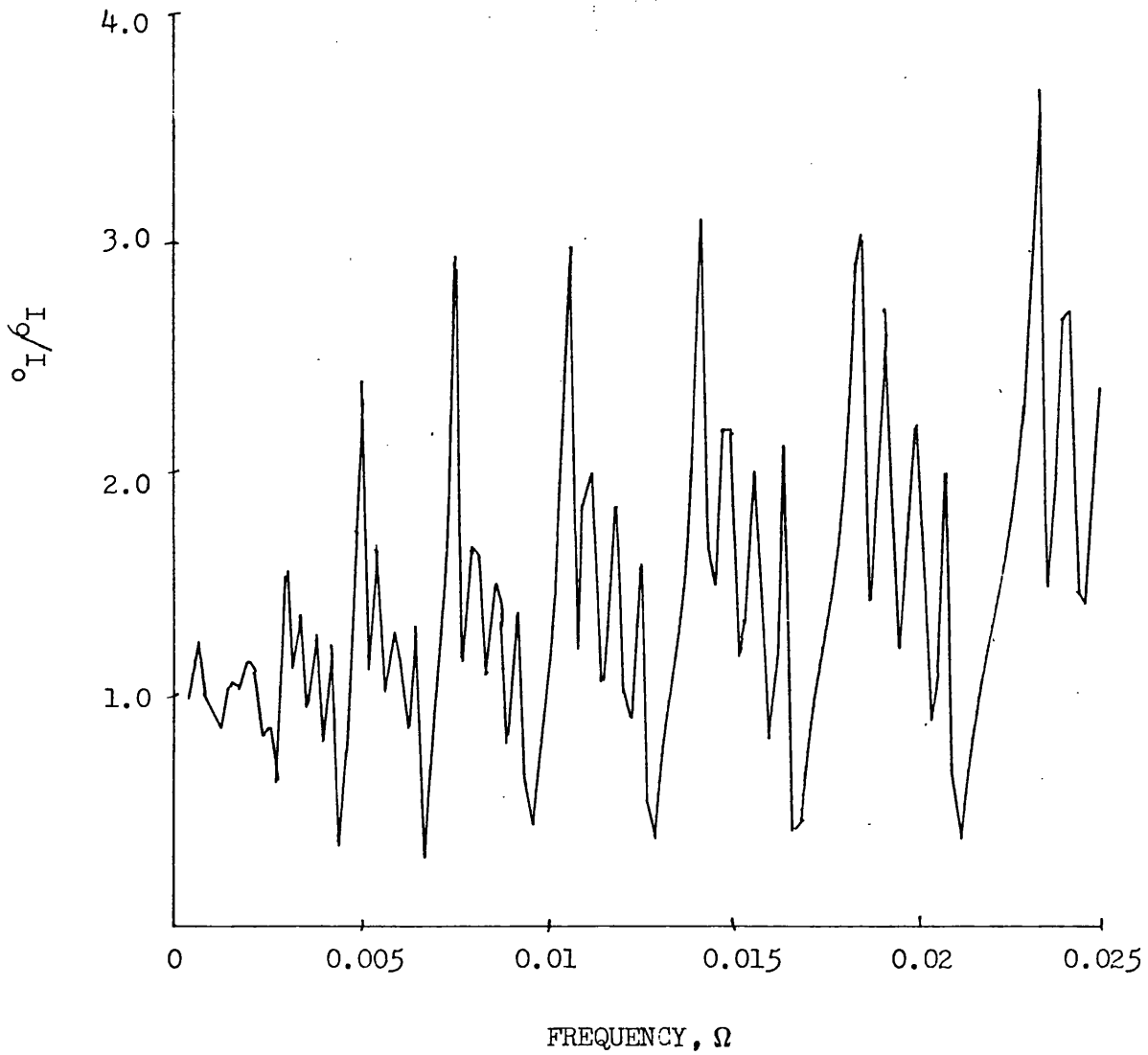
Figure 3.5. The line input impedance against frequency of a plate stiffened with nine beams. I_9 is the impedance of the stiffened plate, I_o that of the unstiffened plate.
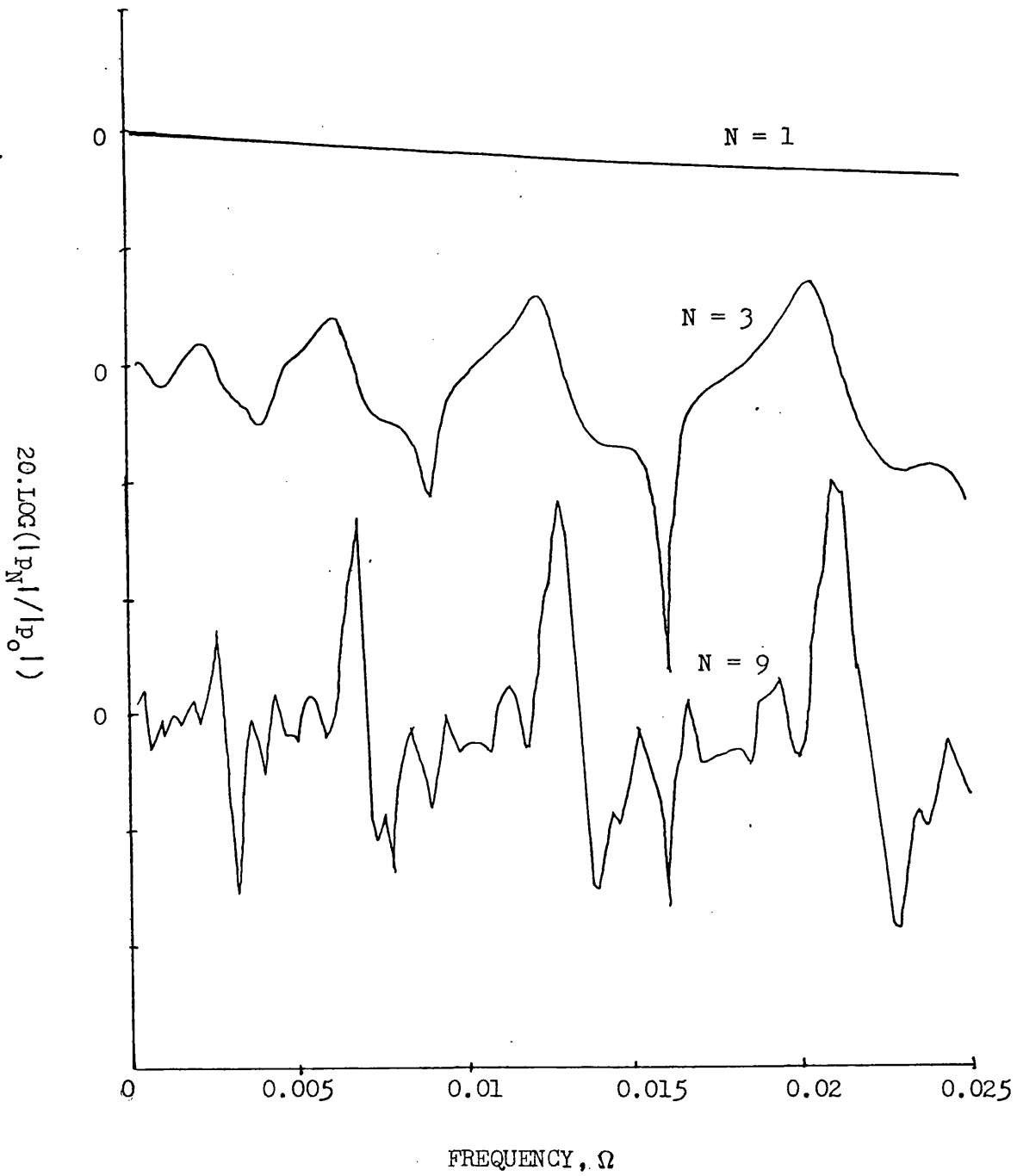
Figure 3.6. The "Correction Factor" for the fluid pressure against normalized frequency, for $\theta = \phi = 0^{\circ}$ and N = 1,3 and 9. One division on the vertical scale is equal to 5 units (dBs).
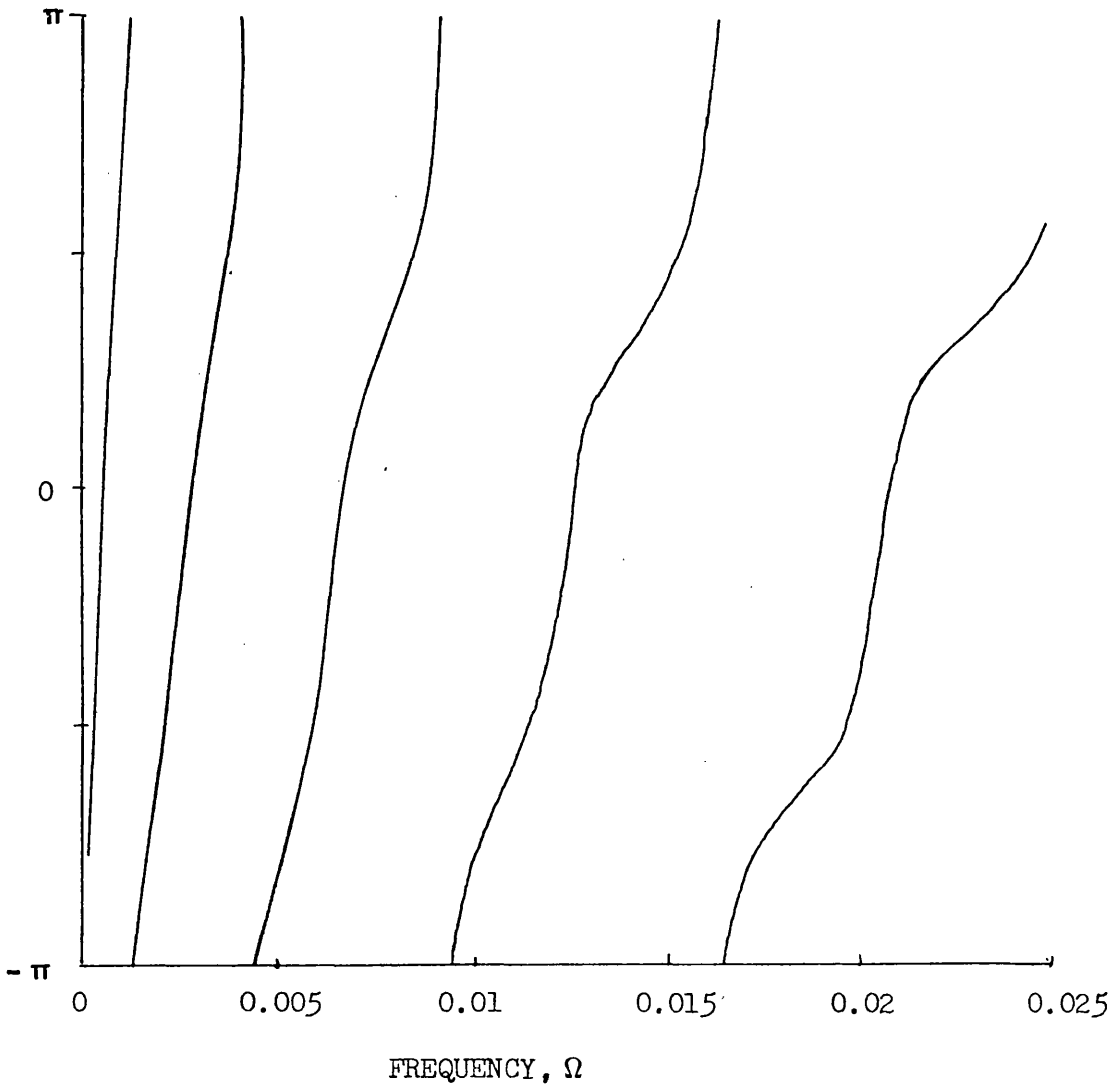
Figure 3.7. The phase difference between the beams at

x = 0 and x = d against frequency for the

line excitation at x = 0 of a plate with

3 beams.
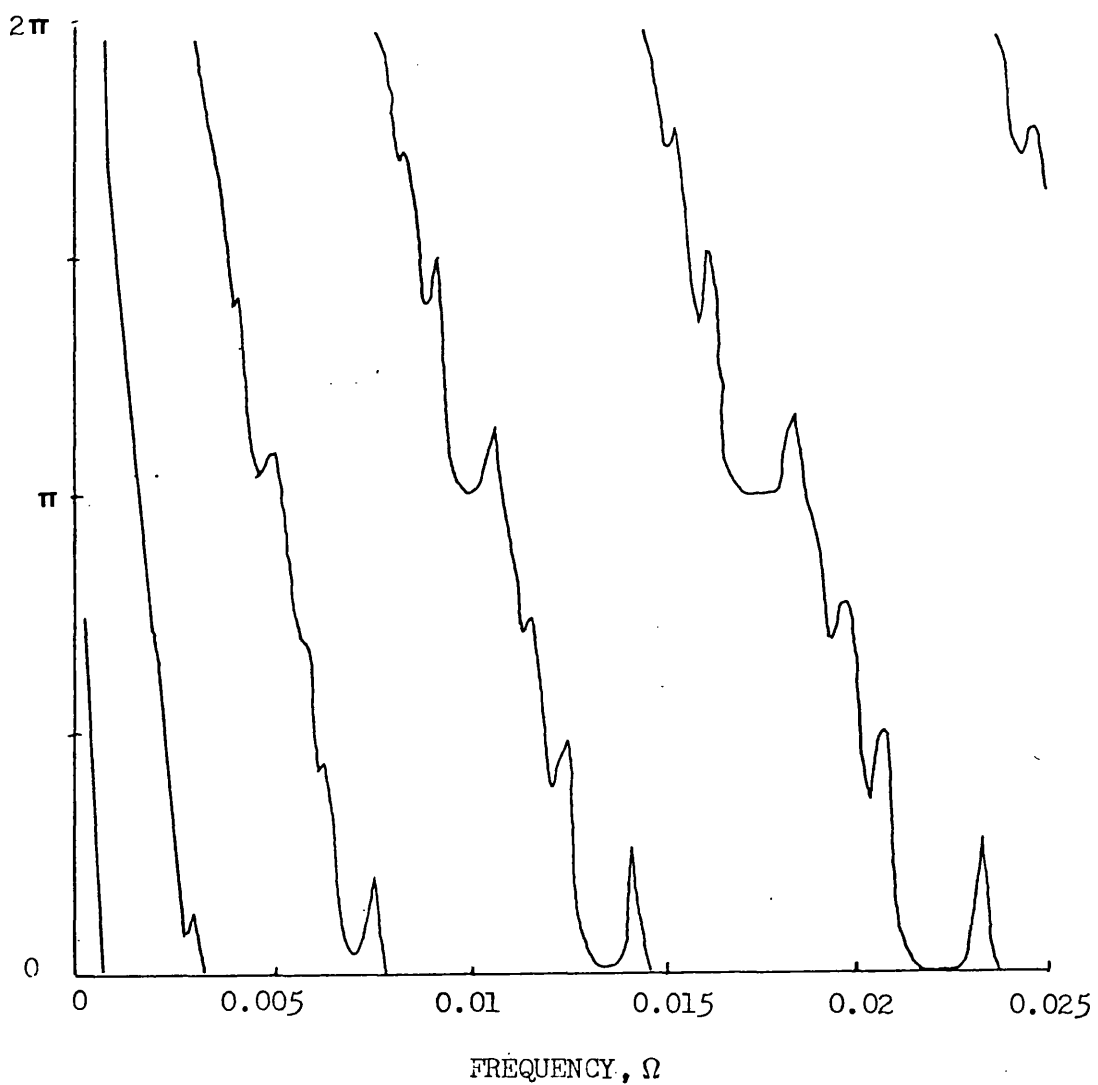
Figure 3.8.   The phase difference between the beams at

x = 0 and x = d against frequency for the

line excitation at x = 0 of a plate with

9 beams.

In the stopping bands the beams are either in phase or in counter phase.

Figures 3.9 and 3.10 show the variation of the farfield pressure as a function of the angle ϕ from the plate normal. θ is fixed at 0° so the plots are for a point or a line force. The vertical scale is $|P_N|/|P_0|$ and again plots are for $N = 1$, 3 and 9. Figure 3.9 is for a frequency $\Omega = 0.0025$ which corresponds to a pressure maximum in figure 3.6, while figure 3.10 is for $\Omega = 0.005$ which corresponds to an impedance maximum in figure 3.5. Neither figure shows much variation with the angle ϕ, which supports the explanation of figure 3.6 already given.

Figures 3.11.a and 3.11.b show the variation of the plate displacement (relative to the displacement of the unstiffened plate) as a function of the angle from the normal to the beams, θ . The vertical scale is $|u_N|/|u_0|$ and the normalized frequency of excitation $\Omega = 0.0025$. The results are for a point excitation. The case $N = 1$ shows a peak at about $\theta = 15^{\circ}$. At this angle the trace wavelength along the beam of a free wave in the plate matches the wavelength of a free wave in the beam. Thus, this is the preferred direction for plane waves to propagate. Waves travelling in this direction pass through additional identical beams with the same ease and so the curves for $N = 3$ and 9 exhibit peaks at the same angle. The beams are stiffer than the plate at all frequencies so this peak will always be present.

We have already shown in figure 3.2 the formation of pass and stop bands as the number of beams is increased. From figure 3.2 we can see that $\Omega = 0.0025$ is at the end of a pass band for $\theta = 0^{\circ}$, but whether or not we are in a pass band for a given plane

Figure 3.9.   The "Correction Factor" for the fluid pressure

against ϕ, the angle from the normal to the

plate, for $\Omega = 0.0025$, $\theta = 0$ and $N = 1,3,9$.

Figure 3.10.   The "Correction Factor" for the fluid pressure

against ϕ , the angle from the normal to the

plate, for Ω = 0.005, θ = 0 and N = 1,3,9.
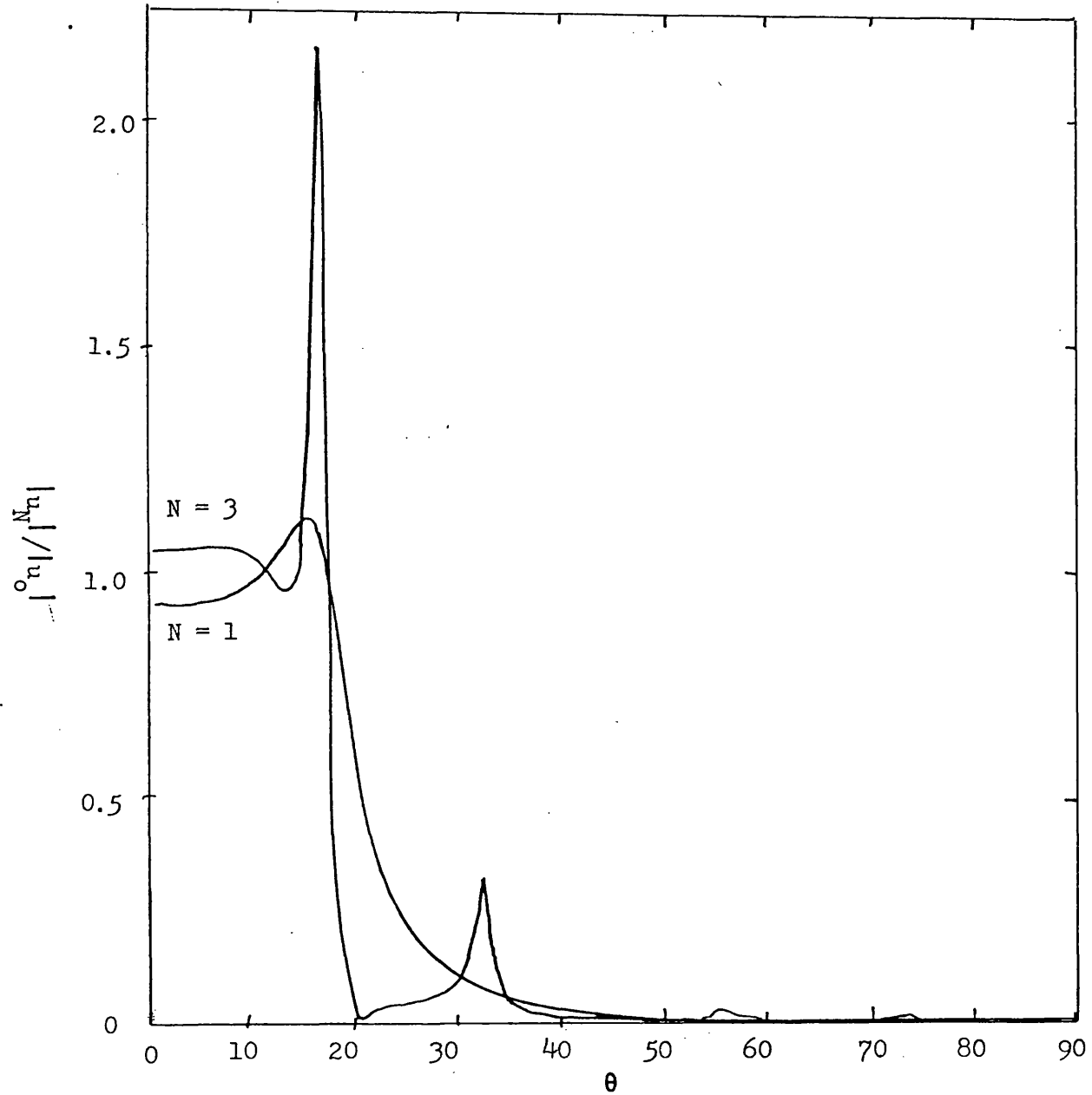
Figure 3.11a   The "Correction Factor" for the plate

displacement against θ, the angle from the

normal to the beams, for $\Omega = 0.0025$, $N = 1,3$.
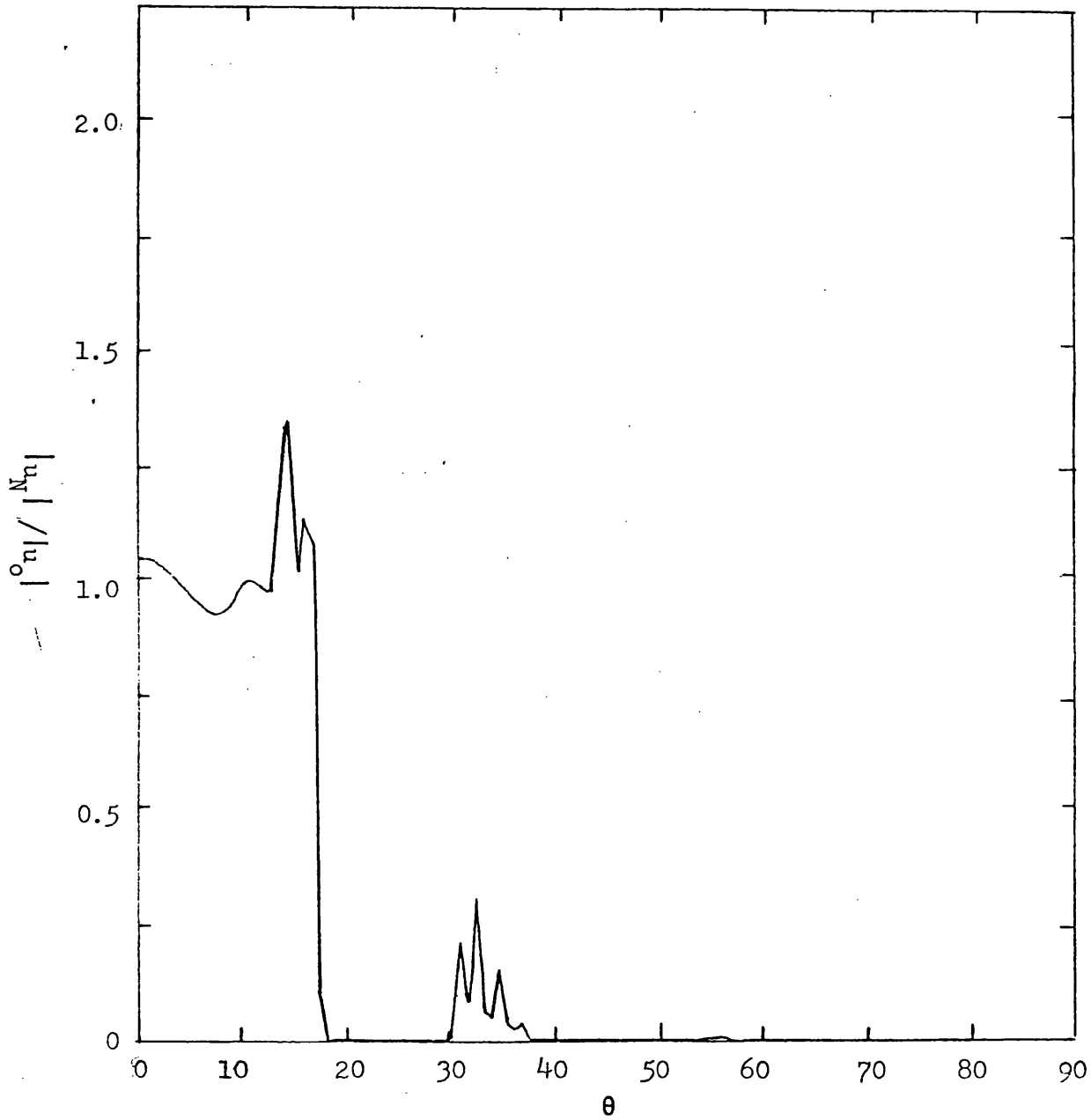
Figure 3.11b   The "Correction Factor" for the plate

displacement against θ , the angle from the

normal to the beams, for Ω = 0.0025, N = 9.

wave depends not only on the frequency but also on the direction

of propagation, θ . From figure 3.11b we can see that for

Ω = 0.0025 there are clear pass bands forming between θ = 0° and

θ = 18° and between θ = 30° and θ = 38°.

Plots for angles outside the range θ = 0° to 90° can be obtained

by symmetry.

The final figure, 3.12 shows the variation of the farfield

fluid pressure as a function of the angle θ . The angle ϕ is fixed

at 45° and the frequency Ω at 0.0025. Once again there is little

spatial variation in the fluid pressure, supporting the
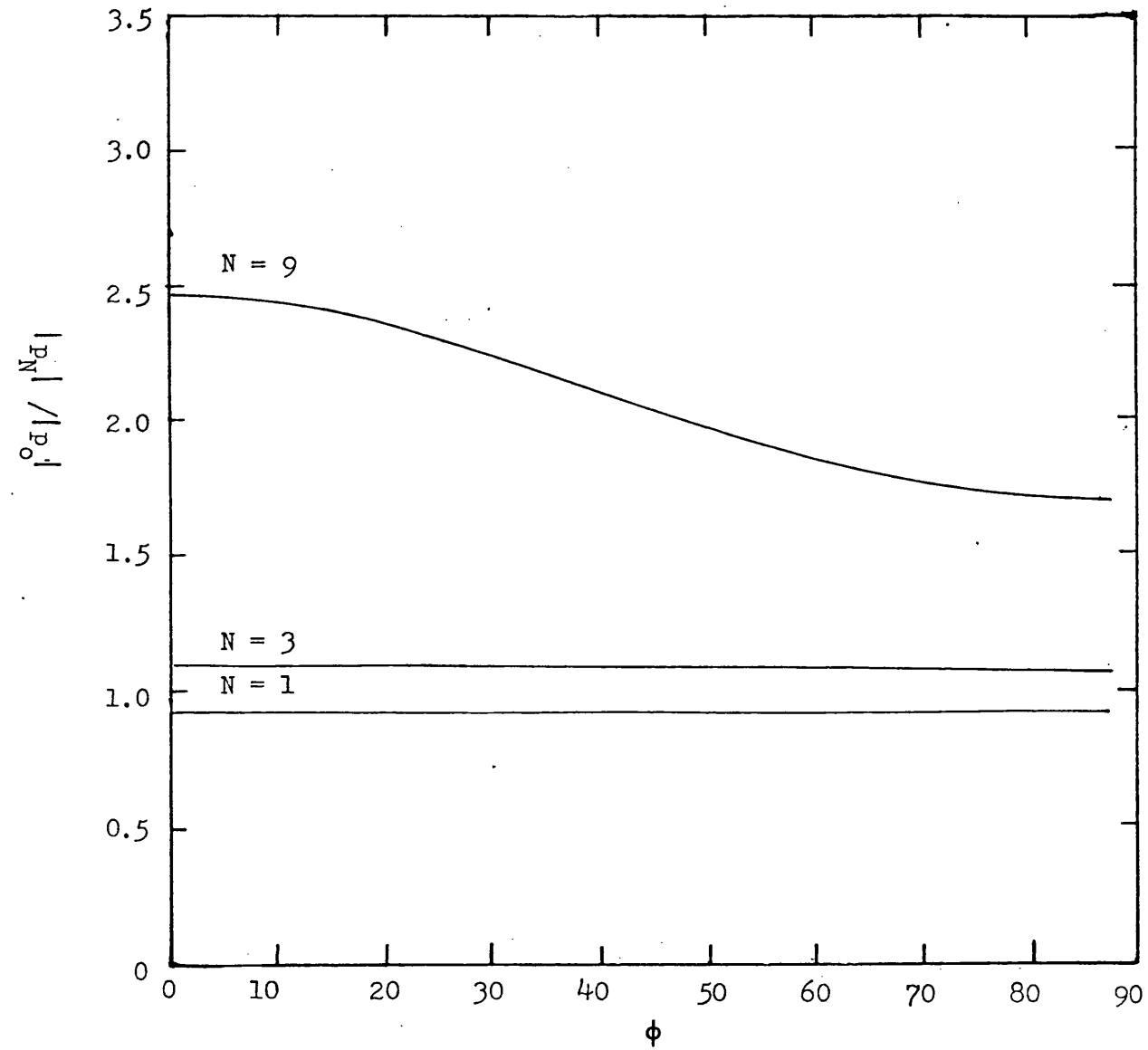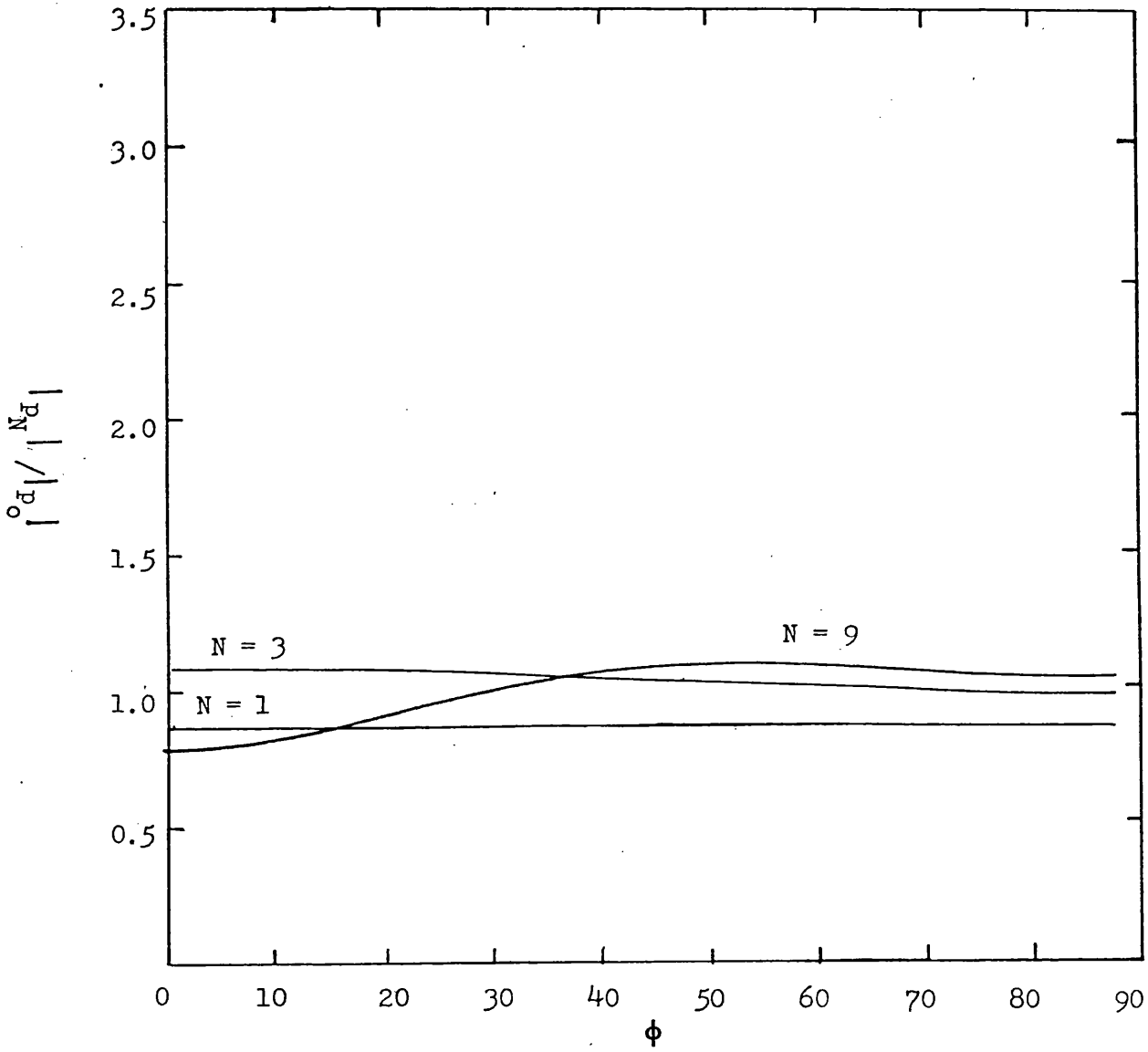
interpretation of figure 3.6.
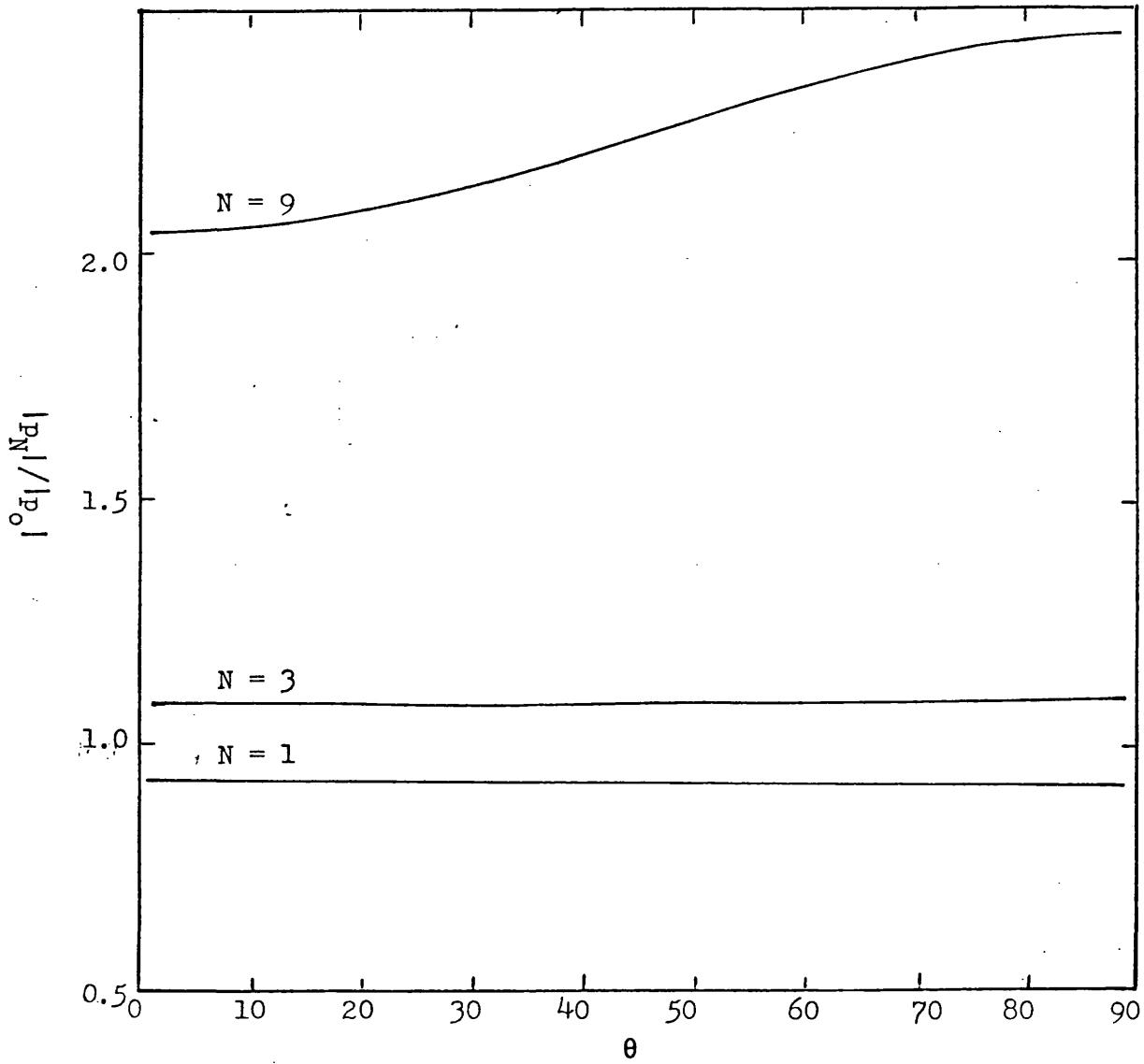
Figure 3.12.   The "Correction Factor" for the fluid pressure

against θ, the angle from the normal to the

beams, for Ω = 0.0025, ϕ = $45°$ and N = 1,3,9.

3.8 CONCLUSIONS

In this chapter expressions have been obtained for the response of a fluid-loaded plate to a general force distribution. These expressions have been reduced by asymptotic expansions to forms more amenable to computation, and results presented for the response of a point excited plate with equally spaced stiffening beams.

The farfield approximations used correspond physically to taking account only of plane waves travelling in the direction from source to receiver, and so the results presented in the previous section can be explained by. considering such waves and the ease with which they can propagate through the system.

It has been shown that a plate stiffened with equally spaced beams tends to produce pass and stop bands, dependent on frequency Ω and angle θ. This tendency is a direct result of the equal spacing chosen here, and results for unequally spaced beams would not demonstrate such structure and would be more difficult to interpret.

The farfield pressure has been shown to depend upon the input impedance of the structure and on the phase of the displacement at adjacent beams.

Finally, a "preferred direction" for plane waves to propagate across a beam attached to a plate has been demonstrated, a property first noted by Heckl (61) for an unloaded plate.

The model developed here has been used to demonstrate some of the general features of the structure. The interpretation of these features and their dependence on the structural and material parameters has been checked by performing the calculations for a different system, although the results are not included here. Thus, some qualitative predictions can be made as to the response of any given system, without detailed calculation.

CHAPTER 4   THE RESPONSE OF A FLUID-LOADED PLATE STIFFENED BY A

PERIODIC ARRAY OF BEAMS.

4.1   INTRODUCTION

In chapter 3 results were given for the response of a fluid-
loaded plate stiffened by a finite array of equally spaced beams.
As a natural extension this chapter studies the analogous problem
for a plate stiffened by an infinite periodic array of identical
beams.

The radiated sound from such structures has been studied by
Evseev (73), Rumerman (75), Leppington (78) and most recently by
Mace (80a), although Mead (73, 75, 76) has made general studies
of periodic systems without fluid loading.

This chapter gives an alternative, though ultimately
equivalent method of solution, which exhibits clearly the structure
of the problem.

For comparison with the results of chapter 3 the same thin
plate model is used, and solutions are obtained for the plate
displacement and the fluid pressure. Apart from calculations of
the input mobility by Mace (80a) previous authors have confined
their results to the fluid pressure.

In this chapter the problem is formulated in terms of
discrete convolutions and the solution is obtained using a
transform related to the Z - transform.

4.2 THE FORMAL SOLUTION

Consider a plate periodically stiffened with beams attached along the lines $x = nd$. Analogously to (3.2.7) and using the notation of chapter 3, the displacement $u(x)$ is given by

$$u(x) = \psi(x) - \sum_{n=-\infty}^{\infty} Z_n G(x-nd) u(nd) - \sum_{n=-\infty}^{\infty} Y_n G'(x-nd) u'(nd). \qquad (4.2.1)$$

Since the beams are assumed to be identical we have $Z_n = Z$ and $Y_n = Y$. In the sequel we assume that the variables have been non-dimensionalized so that the beams lie along the lines $x = n$.

We define the discrete convolution '□' of two functions by

$$(A \,\square\, B)(x) = \sum_{n=-\infty}^{\infty} A(x-n) B(n). \qquad (4.2.2)$$

We note in passing that in general

$$(A \,\square\, B)(x) \neq (B \,\square\, A)(x),$$

although

$$(A \,\square\, B)(n) = (B \,\square\, A)(n). \qquad (4.2.3)$$

Introducing this notation into (4.2.1) gives

$$u(x) = \psi(x) - Z(G \,\square\, u)(x) - Y(G' \,\square\, u')(x), \qquad (4.2.4)$$

which differentiated with respect to x yields

$$u'(x) = \psi'(x) - Z(G' \,\square\, u)(x) - Y(G'' \,\square\, u')(x). \qquad (4.2.5)$$

In particular, substituting $x = n$ into (4.2.4) and (4.2.5) produces a pair of coupled convolution equations for the

translational and rotational displacements, u(n) and u'(n), at the beams, namely:

$$(L^B \square \ddot{u})(n) + Y(G' \square u')(n) = \psi(n) \qquad (4.2.6a)$$

$$Z(G' \square u)(n) + (L^T \square u')(n) = \psi'(n) \qquad (4.2.6b)$$

where

$$L^B(n) = \delta_{no} + ZG(n), \qquad (4.2.7)$$

and

$$L^T(n) = \delta_{no} + YG''(n). \qquad (4.2.8)$$

Equations (4.2.6) are true for any n so we can operate on them with the discrete convolution operators $L^T \square$ and $YG' \square$ respectively. Subtracting the resulting equations yields;

$$\left(\left[L^T \square L^B - YZG' \square G'\right] \square u\right)(n) = (L^T \square \psi)(n) - Y(G' \square \psi')(n), \qquad (4.2.9)$$

where we have used the linearity of the operator $\square$ together with (4.2.3).

Writing

$$L(n) = \left[L^T \square L^B - YZG' \square G'\right](n) \qquad (4.2.10)$$

it is clear that we can formally solve (4.2.9) if we can find the inverse M(n) such that

$$(M \square L)(n) = \delta_{no}. \qquad (4.2.11)$$

Hence we can find u'(n) from (4.2.6a) provided that we can find the inverse of G'(n).

As in chapter 3 we shall now confine our attention to the case where the beams exert no moments on the plate, i.e. we set Y = 0.

(4.2.6a) then reduces to

$$(L \square u)(n) = \Psi(n),$$ (4.2.12)

where $L(n) = \delta_{no} + ZG(n)$, and the problem is reduced to finding

the inverse $M(n)$ such that

$$(M \square L)(n) = \delta_{no}.$$ (4.2.13)

(4.2.12) has the solution

$$u(n) = (M \square \Psi)(n),$$ (4.2.14)

and from (4.2.4) with $Y = 0$,

$$u(x) = \Psi(x) - Z(G \square (M \square \Psi))(x).$$ (4.2.15)

This is a formal solution for the displacement $u(x)$.

The next section is devoted to a transform technique for solving equations involving discrete convolutions.

4.3 THE DISCRETE FOURIER TRANSFORM

We define the discrete Fourier transform of a function F(n) by

$$\widetilde{F}(\alpha) = \sum_{n=-\infty}^{\infty} e^{i\alpha n} F(n),$$

(4.3.1)

with corresponding inverse given by

$$F(n) = \frac{1}{2\pi} \int_{-\pi}^{\pi} e^{-i\alpha n} \widetilde{F}(\alpha) d\alpha.$$

(4.3.2)

The transform is related to the Z-transform Z(x) since

$$Z(x) = \sum_{n=-\infty}^{\infty} x^{-n} F(n) = \sum_{n=-\infty}^{\infty} e^{-n\ln x} F(n) = \widetilde{F}(i\ln x).$$

(4.3.3)

The discrete Fourier transform has the following three properties:

(i) Application of the transform reduces a discrete convolution of two functions $(F \square G)(n)$ to the product of their individual transforms. This is easily shown as follows;

$$\widetilde{(F \square G)}(\alpha) = \sum_{n} e^{i\alpha n} \left\{ \sum_{m} F(n-m) G(m) \right\}$$

$$= \sum_{n} \sum_{m} e^{i\alpha m} G(m) e^{i\alpha(n-m)} F(n-m)$$

$$= \sum_{m} e^{i\alpha m} G(m) \sum_{n} e^{i\alpha n} F(n)$$

where $\sum_{r}$ denotes a sum over all r. Hence

$$\widetilde{(F \square G)}(\alpha) = \widetilde{F}(\alpha) \cdot \widetilde{G}(\alpha).$$

(4.3.4)

(ii) Clearly from the definition (4.3.1) $\widetilde{F}(\alpha)$ is periodic in α with period 2π, that is

$$\widetilde{F}(a) = \widetilde{F}(a + 2\pi), \text{ for all } a.\tag{4.3.5}$$

(iii) The transform can be obtained from the ordinary Fourier transform as follows;

$$\widetilde{F}(a) = \sum_n e^{ian} F(n) = \frac{1}{2\pi} \sum_n e^{ian} \int_{-\infty}^{\infty} \bar{F}(k) e^{-ikn} dk,$$

where $\bar{F}(k)$ denotes the ordinary Fourier transform of F.
Interchanging the order of summation and integration and using the Poisson summation formula,(see Lighthill (58)),

$$\sum_n e^{ixn} = 2\pi \sum_n \delta(x - 2n\pi),\tag{4.3.6}$$

gives

$$\widetilde{F}(a) = \int_{-\infty}^{\infty} \bar{F}(k) \sum_n \delta(a - k - 2n\pi) dk,$$

hence

$$\widetilde{F}(a) = \sum_n \bar{F}(a - 2n\pi).\tag{4.3.7}$$

Thus the discrete Fourier transform can be obtained from a sum of ordinary Fourier transforms.

Application of the discrete Fourier transform to the equation

$$(M \Box L)(n) = \delta_{no}\tag{4.3.8}$$

produces

$$\widetilde{M}(a) . \widetilde{L}(a) = 1$$

from which, using (4.3.2) we have

$$M(n) = \frac{1}{2\pi} \int_{-\pi}^{\pi} \frac{e^{-ian}}{\widetilde{L}(a)} da.\tag{4.3.9}$$

Thus the discrete Fourier transform provides the required technique

for finding inverse convolution operators.

Application of the transform to equations (4.2.6a) and (4.2.6b) reduces them to a pair of linear algebraic equations for $\tilde{u}(a)$ and $\tilde{u}'(a)$.

The displacements and rotation at the beams can be found from $\tilde{u}(a)$ and $\tilde{u}'(a)$ using (4.3.2), but we must revert to (4.2.4) to find the displacement at any x. An ordinary Fourier transform of (4.2.4) gives

$$\bar{u}(k) = \bar{\Psi}(k) - Z\bar{G}(k)\tilde{u}(k) - YK\bar{G}(k)\tilde{u}'(k). \qquad (4.3.10)$$

Inversion of this equation to find $u(x)$ is likely to be quicker than finding $u(x)$ directly from (4.2.4) by evaluating the convolutions, since we usually have a simple expression for $\bar{G}(k)$. In particular, for the case when the beams exert no moments on the plate, from (4.2.12)

$$(L \square u)(n) = \psi(n),$$

that is

$$\tilde{u}(a) = \tilde{\Psi}(a)/\tilde{L}(a), \qquad (4.3.11)$$

and from (4.3.10)

$$\bar{u}(k) = \bar{\Psi}(k) - Z\bar{G}(k)\tilde{\Psi}(k)/\tilde{L}(k), \qquad (4.3.12)$$

where

$$\tilde{L}(k) = 1 + Z\tilde{G}(k) = 1 + Z\sum_{n}\bar{G}(k-2n\pi)$$

and

$$\tilde{\Psi}(k) = \sum_{n}\bar{\Psi}(k-2n\pi) = \sum_{n}\bar{G}(k-2n\pi)\bar{f}(k-2n\pi). \qquad (4.3.13)$$

Equation (4.3.12) can be inverted to give $u(x)(= \tilde{u}(x,k_y))$ and

inverted again to give the solution $u(x,y)$.

This completes the formal solution. The remainder of this section is devoted to a slightly more sophisticated transform which can be used to find $u(x)$ directly from (4.2.4).

We define the modified discrete Fourier transform of a function $F(x)$ by

$$\widetilde{F}(x,a) = \sum_n e^{ian} F(n+x), \qquad (4.3.14)$$

with corresponding inverse

$$F(x) = \frac{1}{2\pi} \int_{-\pi}^{\pi} \widetilde{F}(x,a) da. \qquad (4.3.15)$$

We note that $\widetilde{F}(0,a) = \bar{F}(a)$, the discrete Fourier transform of $F(x)$. Thus $\widetilde{F}(0,a)$ has the same properties as $\bar{F}(a)$, whilst in general $\widetilde{F}(x,a)$ has the following properties;

(i) Application of the transform reduces the more general convolution $(F \square G)(x)$ to a product of their transforms, namely

$$\widetilde{(F \square G)}(x,a) = \widetilde{F}(x,a)\widetilde{G}(0,a) \qquad (4.3.16)$$

(ii) The transform can be obtained from the ordinary Fourier transform as follows:

$$\widetilde{F}(x,a) = \sum_n e^{ian} F(n+x),$$

hence,

$$\widetilde{F}(x,a) = \frac{1}{2\pi} \sum_n e^{ian} \int_{-\infty}^{\infty} \bar{F}(k) e^{-ik(n+x)} dk.$$

Interchanging the order of summation and integration as before and using the Poisson summation formula gives

$$\widetilde{F}(x,a) = \int_{-\infty}^{\infty} \bar{F}(k) \sum_n \delta(a-k-2\pi m) e^{-ikx} dk,$$

hence,

$$\widetilde{F}(x,a) = e^{-iax} \sum_n e^{i2\pi mx} \widetilde{F}(a-2\pi m). \qquad (4.3.17)$$

It is interesting to note that $\widetilde{F}(x,a)$ is of the form

$$\widetilde{F}(x,a) = e^{-iax} A(x,a), \qquad (4.3.18)$$

where $A(x,a)$ is a periodic function of x with period equal to the

beam spacing (which is normalized to unity here). Thus, $\widetilde{F}(x,a)$ has the

form of a Floquet wave with propagation constant a. Such waves

are well known from the study of periodic structures and will

be discussed in the next section.

The relation (4.3.15) thus shows that any function $F(x)$ can

be represented as a superposition of Floquet waves.

For the case $Y = 0$ (4.2.4) reduces to

$$u(x) = \psi(x) - Z(G \square u)(x). \qquad (4.3.19)$$

Application of the modified transform gives

$$\widetilde{u}(x,a) = \widetilde{\psi}(x,a) - Z\widetilde{G}(x,a)\widetilde{u}(0,a). \qquad (4.3.20)$$

We can put $x = 0$ to give

$$\widetilde{L}(0,a)\widetilde{u}(0,a) = \widetilde{\psi}(0,a), \qquad (4.3.21)$$

where $\widetilde{L}(0,a) = 1 + Z\widetilde{G}(0,a)$. $\qquad (4.3.22)$

Hence,

$$\widetilde{u}(0,a) = \widetilde{\psi}(0,a)/\widetilde{L}(0,a),$$

and from (4.3.20)

$$\widetilde{u}(x,a) = \widetilde{\psi}(x,a) - \frac{Z\widetilde{G}(x,a)\widetilde{\psi}(0,a)}{1+Z\widetilde{G}(0,a)}. \qquad (4.3.23)$$

$u(x)$ can then be found using the inversion formula (4.3.15), that is

$$u(x) = \frac{1}{2\pi} \int_{-\pi}^{\pi} \tilde{u}(x,a)da. \qquad\qquad (4.3.24)$$

The more general problem for $Y \neq 0$ can be solved similarly.

4.4 FREE WAVE PROPAGATION

To examine the free wave motion, if any, of the periodically
stiffened plate, we set the external force f(x) to zero. Hence,
$\psi(x)$ and $\widetilde{\psi}(x,a)$ are both zero. The transformed equation (4.3.21)
reduces to

$$\widetilde{L}(0,a)\widetilde{u}(0,a) = 0. \tag{4.4.1}$$

If $\widetilde{u}(0,a)$ is non-zero, that is, the displacement at the beams is
non-zero then we must have

$$\widetilde{L}(0,a) = 0. \tag{4.4.2}$$

Let $a = k_f$ be a root of (4.4.2), then (4.4.1) is satisfied if

$$\widetilde{u}(0,a) = A.\delta(a-k_f). \tag{4.4.3}$$

and from (4.3.20)

$$\widetilde{u}(x,a) = -\widetilde{ZG}(x,a).A\delta(a-k_f). \tag{4.4.4}$$

$\widetilde{L}(0,a)$ is periodic in a with period 2π, and so $k_f + 2n\pi$ is also
a root of (4.4.2).

Assuming the $-\pi < Re(k_f) \leq \pi$ we can invert (4.4.4) to give

$$u(x) = -\frac{ZA}{2\pi} \widetilde{G}(x,k_f), \tag{4.4.5}$$

which, using (4.3.17), can be written as

$$u(x) = g(x).e^{-ik_f x}, \tag{4.4.6}$$

where $g(x)$ is periodic in x with period 1. Thus the free waves
in the stiffened plate are Floquet waves.

If the so called Floquet wavenumber, k_f, is real then u(x) given
by (4.4.6) represents a non-decaying propagating wave, if k_f has
a non-zero imaginary part then u(x) is either exponentially
growing or decaying depending upon the sign of $Im(k_f)$ and the

direction considered.

It remains to consider the case $\tilde{u}(0,a) = 0$. If $\tilde{u}(o,a) = 0$ then clearly $u(n) = 0$ for all n, that is, there is no displacement at any of the beams, and therefore no forces on the plate due to the beams. The free waves are thus the same as for the unstiffened plate, but with the extra restriction that $u(n) = 0$.

For the unstiffened plate we have

$$\bar{Z}_p(k).\bar{u}(k) = 0, \tag{4.4.7}$$

where $\bar{Z}_p(k) = 1/\bar{G}(k)$ is the spectral impedance of the plate, and the bar denotes the ordinary Fourier transform.

For non-zero $\bar{u}(k)$ we must have

$$\bar{Z}_p(k) = 1/\bar{G}(k) = 0. \tag{4.4.8}$$

If $k = \pm k_p$ are the real roots of the equation (see Crighton(79)), then

$$\bar{u}(k) = A\delta(k-k_p) + B\delta(k + k_p) \tag{4.4.9}$$

and

$$u(x) = \frac{A}{2\pi} e^{-ik_p x} + \frac{B}{2\pi} e^{ik_p x}, \tag{4.4.10}$$

The condition $u(n) = 0$ gives $k_p = n\pi$ and $B = -A$, and

$$u(x) = A(e^{ik_p x} - e^{-ik_p x}). \tag{4.4.11}$$

Thus if $k_p = n\pi$, that is, if the beam spacing is a multiple of the half-wavelength in the unstiffened plate, we can have a free standing wave in the periodic structure with nodes at the beam positions.

The solutions of $\tilde{L}(0,a) = 0$ cannot be found analytically for the fluid-loaded structure, but if we assume that the fluid loading is light enough to be neglected then we can obtain an analytic expression for the solutions, as explained in section 4.6.

4.5 THE NORMALIZED EQUATIONS

To evaluate $\tilde{u}(x,a)$ given in (4.3.23) for a given structure we need to know $\bar{Z}(k_y)$ and $\tilde{G}(x,a)$, (which can be found from $\bar{G}(k_x,k_y)$) for a system of variables normalized to the beam spacing.

The unnormalized equations for the fluid displacement potential $\Phi'(x',y',z')e^{-i\omega t}$ and the plate displacement $u'(x',y')e^{-i\omega t}$, where the primed variables are unnormalized, are as follows;

In the fluid:

$$\nabla^2\Phi'(x',y',z') + \frac{\omega^2}{c^2}\Phi'(x',y',z') = 0, \quad z' > 0, \tag{4.5.1}$$

On the plate:

$$D\nabla^4 u'(x',y') + \sum_{n=-\infty}^{\infty}\left\{\delta(x'-nd)\left[B\frac{\partial^4 u'}{\partial y'^4} - \omega^2 M u'\right]\right\}$$

$$- \omega^2 m u'(x',y') - \rho_0\omega^2\Phi'(x',y',z') = F'(x',y'). \tag{4.5.2}$$

and at the interface

$$u'(x',y') = -\frac{\partial}{\partial z'}\Phi'(x',y',z')\bigg|_{z'=0}, \tag{4.5.3}$$

where

D is the plate bending stiffness,

B is the beam bending stiffness,

M is the mass per unit length of a beam,

m is the mass per unit area of the plate,

ρ_0 is the fluid density,

c is the fluid wave speed,

and d is the beam spacing.

We introduce the following dimensionless variables;

$$x = x'/d, \quad y = y'/d, \quad z = z'/d, \quad u = u'/d \quad \text{and} \quad \phi = \phi'/d^2,$$

together with

$$\Omega^2 = \frac{\omega^2 M d^3}{D}, \quad \lambda^2 = \frac{md}{M}, \quad \beta^2 = \frac{\rho_0 d^2}{M}, \quad \gamma^2 = \frac{D}{Mc^2 d},$$

$$S = \frac{B}{Dd}, \quad k_0 = \frac{\omega d}{c} \quad \text{and} \quad f = \frac{F' d^2}{D}. \tag{4.5.4}$$

The normalized system of equations is

$$\nabla^2 \phi(x,y,z) + k_0^2 \phi(x,y,z) = 0, \quad z > 0 \tag{4.5.5}$$

$$\nabla^4 u(x,y) - \Omega^2 \lambda^2 u(x,y) + \sum_{n=-\infty}^{\infty} \delta(x-n) \left[S \frac{\partial^4 u}{\partial y^4} - \Omega^2 u \right] - \Omega^2 \beta^2 \phi(x,y,0) = f(x,y), \tag{4.5.6}$$

$$u(x,y) = -\frac{\partial}{\partial z} \phi(x,y,z) \Big|_{z=0}. \tag{4.5.7}$$

Taking ordinary Fourier transforms in x and y of (4.5.5) yields

$$\left[\frac{\partial^2}{\partial z^2} - (k_x^2 + k_y^2) + k_0^2 \right] \bar{\phi}(k_x, k_y, z) = 0, \tag{4.5.8}$$

which has the solution for outgoing waves

$$\bar{\phi}(k_x, k_y, z) = A(k_x, k_y) e^{ik_z z}, \tag{4.5.9}$$

where

$$k_z = (k_0^2 - k_x^2 - k_y^2)^{\frac{1}{2}} \quad \text{with imag} \ (k_z) \geq 0.$$

The transform of (4.5.7) gives

$$\bar{u}(k_x, k_y) = -\frac{\partial}{\partial z} \bar{\phi}(k_x, k_y, z) \Big|_{z=0} = - ik_z A(k_x, k_y). \tag{4.5.10}$$

From (4.5.10) we obtain

$$A(k_x, k_y) = \bar{\Phi}(k_x, k_y, 0) = \frac{-\bar{u}(k_x, k_y)}{ik_z} \cdot \tag{4.5.11}$$

Finally, transforming (4.5.6) and using (4.5.11) gives

$$\bar{Z}_p(k_x, k_y)\bar{u}(k_x, k_y) + \bar{Z}_B(k_y)\widetilde{u}(k_x) = \bar{f}(k_x, k_y), \tag{4.5.12}$$

where

$$\bar{Z}_p(k_x, k_y) = (k_x^2 + k_y^2)^2 - \Omega^2(\lambda^2 - \frac{\beta^2}{ik_z}) \tag{4.5.13}$$

and

$$\bar{Z}_B(k_y) = Sk_y^4 - \Omega^2. \tag{4.5.14}$$

$\bar{Z}_p$ and $\bar{Z}_B$ are related to the plate and beam spectral impedances, respectively. Hence the transform of the plate Green's function is

$$\bar{G}(k_x, k_y) = \frac{1}{\bar{Z}_p(k_x, k_y)} \cdot \tag{4.5.15}$$

4.6. THE SOLUTION NEGLECTING FLUID - LOADING

Neglecting fluid-loading simplifies the problem significantly. In the physical system the fluid couples each region of the plate to every other region. In the absence of fluid-loading, coupling between regions is only through their mutual boundaries, and this physical simplification is reflected in the mathematics of the problem.

For simplicity we shall consider motion independent of the y direction. For this problem the displacement is

$$u(x,y) = \tilde{u}(x,k_y=0) = u(x)\Big|_{k_y=0} . \tag{4.6.1}$$

The required modified transforms are obtained from the known ordinary Fourier transforms as follows:

$$\tilde{L}(0,a) = 1 + z \cdot \tilde{G}(0,a) = 1 + z \cdot \sum_n \bar{G}(a-2\pi m,0) \tag{4.6.2}$$

where

$$z = \bar{Z}_B(k_y = 0)$$

and from (4.5.15) and (4.5.13) with $B^2 = 0$ and $k_y = 0$

$$\bar{G}(k,0) = 1/(k^4 - \Omega^2 \lambda^2). \tag{4.6.3}$$

The infinite sum in (4.6.2) can be written as

$$\sum_n \bar{G}(a - 2\pi m,0) = \frac{1}{4\pi i} \oint_\Gamma \frac{\cot (z/2)dz}{(a- z)^4 - \Omega^2 \lambda^2} , \tag{4.6.4}$$

where Γ is a positively oriented contour enclosing the poles of cot $(z/2)$.

The circular contour at infinity can be added and Cauchy's theorem invoked to evaluate the integral as a sum of residue contributions from the four zeros z_r of the denominator. Thus,

$$\sum_n {}' \bar{G}(a - 2\pi m, 0) = \frac{1}{2} \sum_{r=1}^{4} \frac{\cot (z_r/2)}{4(a - z_r)^3} \, , \qquad (4.6.5)$$

where

$$z_r = k_p e^{\frac{i\pi r}{2}} + a$$

and

$$k_p = \Omega^{\frac{1}{2}} \lambda^{\frac{1}{2}} . \qquad (4.6.6)$$

Hence

$$\sum_n {}' \bar{G}(a - 2\pi m, 0) = \frac{-1}{4k_p^3} \left\{ \frac{\sin k_p}{\cos a - \cos k_p} - \frac{\sinh k_p}{\cos a - \cosh k_p} \right\} . \qquad (4.6.7)$$

Therefore, for the unloaded plate, $\tilde{L}(0, a)$ can be written in the closed form;

$$\tilde{L}(o, a) = 1 - \frac{Z}{4k_p^3} \left\{ \frac{\sin k_p}{\cos a - \cos k_p} - \frac{\sinh k_p}{\cos a - \cosh k_p} \right\} . \qquad (4.6.8)$$

The Floquet wavenumbers, k_f, are given by the zeros of $\tilde{L}(0, a)$ and so satisfy

$$\cos^2 k_f - A \cos k_f + B = 0, \qquad (4.6.9)$$

where

$$A = \cos k_p + \cosh k_p + \frac{Z}{4k_p^3} (\sin k_p - \sinh k_p)$$

and

$$B = \cos k_p \cosh k_p - \frac{Z}{4k_p^3} (\sinh k_p \cos k_p - \sin k_p \cosh k_p).$$

The discriminant for (4.6.9) can be written as

$$A^2 - 4B = (\cos k_p - \cosh k_p)^2 + \left(\frac{Z}{4k_p^3}\right)^2 (\sin k_p - \sinh k_p)^2 -$$

$$\frac{Z}{2k_p^3} (\sinh k_p + \sin k_p)(\cosh k_p - \cos k_p) \qquad (4.6.10)$$

which is clearly positive for non-zero k_p. Hence we have two

real roots for $\cos k_f$ from (4.5.8).

If $k_p = n\pi$ then $\sin k_p = 0$ and clearly one root for $\cos k_f$

is $\cos k_p$, that is, $k_f = \pm k_p + 2n\pi$, $n = 0, \pm 1, \pm 2, \ldots$

Generally, for $k_p > 0$, we have

$$A > \cos k_p + \cosh k_p > 2, \qquad (4.6.11)$$

and the roots of (4.6.9) are

$$\cos k_f = A/2 \pm (A^2/4 - B)^{\frac{1}{2}}. \qquad (4.6.12)$$

The "plus" sign gives $\cos k_f > A/2 > 1$ and hence yields complex

(imaginary) values of k_f, whilst the "minus" sign gives real

values of k_f if $-1 \leq \cos k_f \leq 1$ and complex values for k_f

otherwise.

Thus, for a stiffened plate without fluid loading (4.6.12)

leads to a closed expression for the Floquet wavenumbers, namely

$$k_f^{\pm} = \cos^{-1}(A/2 \pm (A^2/4 - B)^{\frac{1}{2}}). \qquad (4.6.13)$$

The corresponding free waves are of the form (4.4.4). The

Floquet waves corresponding to $\overset{+}{-} k_f^+$ are exponentially growing

in one direction and so are likely to be prohibited by

boundary conditions, as are the waves corresponding to $\overset{+}{-}k_f^-$ if

imag $(k_f^-) \neq 0$. The real solutions for k_f give propagating Floquet

waves. It has already been noted that for frequencies at which

$k_p = n\pi$, $k_f = n\pi$ is a solution, and it can be shown that at these

frequencies k_f changes from being complex to being real as follows;

Consider $\mathcal{L}(0,a) = F(\cos a , k_p) = F(x,k_p)$. From (4.6.9) we have

$$F(x,k_p) = x^2 - A(k_p)x + B(k_p). \qquad (4.6.14)$$

If $x = (-1)^n + \delta x$ and $k_p = n\pi + \delta k_p$ then to first order in δx

and δk_p

$$F(x,k_p) = \delta x(2 \cdot (-1)^n - A(n\pi)) + \delta k_p(-(-1)^n A'(k_p) + B'(k_p))\Big|_{k_p = n\pi} . \qquad (4.6.15)$$

We note that $Z = -\Omega^2 = -k_p^4/\lambda^2$ and so

$$A'(n\pi) = \sinh(n\pi)\left(1 + \frac{1}{4\lambda^2}\right) + \frac{n\pi}{4\lambda^2} (\cosh n\pi - (-1)^n)$$

and

$$B'(n\pi) = (-1)^n \sinh (n\pi)\left(1 + \frac{1}{4\lambda^2}\right). \qquad (4.6.16)$$

The condition $F(x,k_p) = 0$ thus requires that

$$\delta x = \frac{-\delta k_p(1 - (-1)^n \cosh n\pi)n\pi}{(2(-1)^n - A(n\pi))4\lambda^2} , \qquad (4.6.17)$$

but $\cosh n\pi > 1$ and $A(n\pi) > 2$ $(n > 0)$ so

$$\delta x = - K\delta k_p(-1)^n, \text{ where } K > 0. \qquad (4.6.18)$$

Thus, if $\delta k_p > 0$ then $|x| = |(-1)^n + \delta x| < 1$ and hence $k_f = \cos^{-1} x$

is real. If $\delta k_p < 0$ then $|x| > 1$ and k_f is complex. Thus,

frequencies for which $k_p = n\pi$ mark the boundary between a stop

band (k_f complex) and a pass band (k_f real).

The bounding frequencies of the pass and stop bands have

been matched by Mead (75) to the natural frequencies of a single

"element" of the periodic structure. $k_p(\Omega) = n\pi$ clearly corresponds

to the resonant frequencies of a single element with fixed ends,

i.e. with the boundary condition $u(n) = 0$. The other bounding

frequency corresponds to the resonant frequency with free ends,

that is, a frequency for which the system

$$\frac{\partial^4 u}{\partial x^4} - k_p^4 u = 0,$$

with $\quad \left.\dfrac{\partial u}{\partial x}\right|_{x=n} = 0$ (4.6.19)

and $\quad \left.\dfrac{\partial^3 u}{\partial x^3}\right|_{x=n} = \dfrac{Z}{2} u(n)$

has a non-trivial solution. The required condition is easily shown

to be

$$\tilde{L}(0, n\pi) = 0, \tag{4.6.20}$$

where odd or even n correspond respectively to odd or even solutions

of (4.6.19).

If $\tilde{L}(0, a) = 0$, then for a stiffened plate with or without

fluid-loading, the displacement satisfies

$$u(m + 1) = e^{-ia} u(m) \tag{4.6.21}$$

and so we need only study a single element of the system to

determine the free nodes of the whole structure. The presence of

fluid-loading however, prevents us from finding simple analytic

solutions.

4.7. ASYMPTOTIC EVALUATION OF THE PLATE DISPLACEMENT AND

THE FLUID PRESSURE

The evaluation of the plate displacement, $u(x,y)$, requires the inversion of either (4.3.12) or (4.3.23), that is, it requires the evaluation of a double integral, the integrand for which involves an infinite sum. In order to simplify the computation and to produce results for comparison with those obtained in chapter 3, this section is devoted to the finding of asymptotic expressions for the plate displacement and the fluid pressure. The assumptions are that the receiver is either in the fluid a long way from the plate, or is on the plate far from any point of excitation.

The farfield fluid pressure can be obtained from the ordinary Fourier transform of the plate displacement (4.3.12) using equations (4.5.9) and (4.5.11). The resulting expression for the normalized displacement potential is

$$\Phi(x,y,z) = \frac{-1}{4\pi^2} \int\int_{-\infty}^{\infty} \frac{\bar{u}(k_x,k_y)e^{ik_z z}}{ik_z} e^{-i(k_x x + k_y y)} dk_x dk_y. \qquad (4.7.1)$$

The unnormalized fluid pressure is

$$p(x',y',z') = -\rho_0 \omega^2 d^2 \Phi(x'/d, y'/d, z'/d). \qquad (4.7.2)$$

To evaluate the integral in (4.7.1) we make the following substitutions;

$x = R\sin\mu\cos\theta$, $y = R\sin\mu\sin\theta$, $z = R\cos\mu$, $k_x = k_0\sin\alpha\cos\beta$, $k_y = k_0\sin\alpha\sin\beta$. $\qquad (4.7.3)$

Thus $k_z = (k_0^2 - k_x^2 - k_y^2)^{\frac{1}{2}} = k_0\cos\alpha$ and $dk_x dk_y = k_0^2 \sin\alpha\cos\alpha\, d\alpha d\beta$.

(4.7.1) becomes

$$\Phi(R,\theta,\mu) = \frac{ik_o}{4\pi^2} \int_{-\pi/2+i\infty}^{\pi/2-i\infty} d\alpha \int_0^\pi d\beta \, \sin\alpha \, \bar{u}(k_o,\alpha,\beta) \cdot \exp\left\{ik_o Rg(\alpha,\beta,\mu,\theta)\right\} \qquad (4.7.4)$$

where

$$g(\alpha,\beta,\mu,\theta) = \cos\alpha\cos\mu - \sin\alpha\sin\mu\cos(\beta-\theta). \qquad (4.7.5)$$

For large values of $k_o R$ the integrand is rapidly oscillating except at the stationary points of $g(\alpha,\beta,\mu,\theta)$ and the integral can be asymptotically evaluated using the stationary phase method.

The stationary phase points are given by

$$\frac{\partial g}{\partial \alpha} = \frac{\partial g}{\partial \beta} = 0. \qquad (4.7.6)$$

$$\frac{\partial g}{\partial \beta} = 0 \Rightarrow \sin\alpha\sin\mu\sin(\beta-\theta) = 0, \qquad (4.7.7)$$

which gives $\beta = \theta$.

$$\frac{\partial g}{\partial \alpha} = 0 \Rightarrow -\sin\alpha\cos\mu - \cos\alpha\sin\mu\cos(\beta-\theta) = 0. \qquad (4.7.8)$$

Substituting $\beta = \theta$ gives

$$-\sin(\alpha+\mu) = 0, \text{ i.e. } \alpha = -\mu.$$

Thus the stationary phase point is at $\alpha = -\mu$, $\beta = \theta$.

Near to the stationary phase point we can expand $g(\alpha,\beta)$ in a Taylor series

$$g(\alpha,\beta) = g(-\mu,\theta) + \frac{(\alpha+\mu)^2}{2} g_{\alpha\alpha} + (\alpha+\mu)(\beta-\theta)g_{\alpha\beta} + \frac{(\beta-\theta)^2}{2} g_{\beta\beta} +$$

higher order terms, $\qquad (4.7.9)$

where $g_{\alpha\alpha} = \frac{\partial^2 g}{\partial \alpha^2}(\alpha,\beta)\Big|_{\alpha=-\mu, \beta=\theta}$ etc.

Hence

$$g(\alpha,\beta) \simeq 1 - \frac{(\alpha+\mu)^2}{2} - \frac{(\beta-\theta)^2}{2} \sin^2\mu. \qquad (4.7.10)$$

If we assume that the major contribution to the integral is from the region around the stationary phase point then substituting (4.7.10) into (4.7.4) gives

$$\Phi(R,\theta,\mu) \simeq \frac{-ik_o}{4\pi^2} \sin\mu\, \bar{u}(k_o,-\mu,\theta).e^{ik_oR}$$

$$\iint \exp\left[\frac{-ik_oR}{2}\left((\alpha+\mu)^2 + (\beta-\theta)^2\sin^2\mu\right)\right] d\beta d\alpha. \qquad (4.7.11)$$

If we change variables to h_1 and h_2 where

$$h_1^2 = i(\alpha+\mu)^2 \quad \text{and} \quad h_2^2 = i(\beta-\theta)^2\sin^2\mu$$

i.e. $h_1 = \dfrac{(1+i)}{\sqrt{2}}(\alpha+\mu)$ and $h_2 = \dfrac{(1+i)}{\sqrt{2}}(\beta-\theta)\sin\mu$

then (4.7.11) becomes

$$\Phi(R,\theta,\mu) \simeq \frac{-k_o e^{ik_oR}}{4\pi^2} \bar{u}(k_o,-\mu,\theta) \iint \exp(-k_oR(h_1^2+h_2^2))dh_1dh_2. \qquad (4.7.12)$$

Hence

$$\Phi(R,\theta,\mu) \simeq \frac{-e^{ik_oR}}{2\pi R} \bar{u}(k_o,-\mu,\theta) \qquad (4.7.13)$$

This expression for the displacement potential corresponds to a spherically spreading acoustic wave in the fluid. At certain frequencies however, the plate wavenumber $K = N\pi$ for some integer N, and at such a frequency, Ω_o say, $\tilde{L}(K-2n\pi) = 0$, for any n. If $k_o > \pi$ then at least one of these zeros of $\tilde{L}$, k_f say, is less than k_o. The residue contribution from the pole of the integrand in

(4.7.1) at k_f would appear to be $O(1)$, (since $k_y = 0$ and therefore k_z is real), and to dominate the contribution from the stationary phase point, but it can be shown that this is not the case.

Near to $k = K = N\pi$ and $\Omega = \Omega_0$ we have from (4.5.13)

$$Q(k,\Omega) = \bar{Z}_p(k_x = k, \; k_y = 0)$$

$$= k^4 - \Omega^2(\lambda^2 + \beta^2(k^2-k_0^2)^{-\frac{1}{2}}), \qquad (4.7.14)$$

where k_y has been set to zero merely to simplify the following expressions. Writing $k = K + \delta k$, $\Omega = \Omega_0 + \delta\Omega$ gives

$$Q(k,\Omega) = A\delta k + B\delta\Omega + C\delta k^2 + D\delta\Omega\delta k + E\delta\Omega^2 \qquad (4.7.15)$$

where

$$A(K,\Omega_0) = K(4K^2 + \Omega_0^2\beta^2\gamma^3),$$

$$B(K,\Omega_0) = -2\Omega_0(\lambda^2 + \beta^2\gamma),$$

$$C(K,\Omega_0) = 6K^2 - \tfrac{1}{2}\Omega_0^2\beta^2\gamma^5(2K^2 + k_0^2),$$

$$D(K,\Omega_0) = 2\Omega_0 K\beta^2\gamma^3,$$

$$E(k,\Omega_0) = -\lambda^2 - \beta^2\gamma$$

and $\gamma = (K - k_0^2)^{-\frac{1}{2}}$.

We can write $\tilde{L}(k,\Omega)$ as

$$\tilde{L}(k,\Omega) = 1 + Z\left[\frac{1}{Q(k,\Omega)} + \frac{1}{Q(k-2N\pi,\Omega)}\right] + Z\sum_{n\neq 0,N}\frac{1}{Q(k-2n\pi,\Omega)}, \qquad (4.7.16)$$

and substitute for $Q(k,\Omega)$ and $Q(k-2N\pi,\Omega)$, noting that A and D are odd functions of K while B, C and E are even functions, to give

$$\widetilde{L}(k,\Omega) = 1 + \frac{2Z(B\delta\Omega + C\delta k^2 + E\delta^2\Omega)}{\delta k^2(A+D\delta\Omega)^2 - (B\delta\Omega + C\delta k^2 + E\delta^2\Omega)^2} + Z\sum_{n\neq 0,N}\frac{1}{Q(k-2n\pi,\Omega)}.$$

If k,Ω is to be a zero of $\widetilde{L}(k,\Omega)$ then to lowest order

$$\delta k^2 = \delta\Omega \frac{2ZB}{A^2(1+Z\sum_{n\neq 0,N}\frac{1}{Q(N\pi-2n\pi,\Omega)})-2ZC}. \qquad (4.7.17)$$

We note that $\delta\Omega > 0$ gives real δk whilst $\delta\Omega < 0$ gives imaginary δk provided that $N = 1$. If N is even or if $k_0 > \pi$ then one or more terms in the infinite sum are complex and so δk is complex.

For $k_p = K + \delta k_p$, $\Omega = \Omega_0 + \delta\Omega$ to be a zero of $Q(k,\Omega)$ we must have to lowest order

$$A\delta k_p + B\delta\Omega = 0,$$

that is

$$\delta k_p = -\frac{B}{A}\delta\Omega = 0(\delta\Omega). \qquad (4.7.18)$$

Thus, if Ω is $\Omega_0 + \delta\Omega$ then a zero of $\widetilde{L}(k,\Omega)$ is $k = k_f = K + 0(\delta\Omega)^{\frac{1}{2}}$ and a zero of $Q(k,\Omega)$ is $k = k_p = K + 0(\delta\Omega)$. The residue contribution corresponding to the pole at $k = k_f$ is proportional to $\left[\frac{\partial L}{\partial k}\Big|_{k_f} Q(k_f)\right]^{-1}$. However,

$$\frac{\partial L}{\partial k}\Big|_{k_f} = \frac{-ZQ_k(k_f,\Omega)}{Q^2(k_f,\Omega)} + \frac{ZQ_k(k_f-2N\pi,\Omega)}{Q^2(k_f-2N\pi,\Omega)} + 0(1) \qquad (4.7.19)$$

and we can expand about K,Ω_0 to give

$$\left. \frac{\partial L}{\partial k} \right|_{k_f} = \frac{-ZA}{A(A\delta k^2 + 2B\delta k\delta\Omega + 2C\delta k^2)} + \frac{+ZA}{A(A\delta k^2 - 2B\delta k\delta\Omega - 2C\delta k^2)} + O(1)$$

$$= \frac{-Z4\delta k(B\delta\Omega + C\delta k)}{A^2\delta k^2} + O(1) \tag{4.7.20}$$

but δk is $O(\delta\Omega)^{\frac{1}{2}}$ and so we have

$$\left. \frac{\partial L}{\partial k} \right|_{k_f} = O(\delta\Omega)^{-\frac{1}{2}}. \tag{4.7.21}$$

Similarly,

$$Q(k_f) = (k_f - k_p)Q_k(K,\Omega_0) + O(\delta\Omega) = O(\delta\Omega)^{\frac{1}{2}}. \tag{4.7.22}$$

However, for all the other zeros, $k_f - 2n\pi$, of $\tilde{L}(k,\Omega)$, except $k_f - 2n\pi$, we have

$$Q(k_f - 2n\pi) = O(1),$$

but

$$Q(k_f - 2N\pi) = O(\delta\Omega)^{\frac{1}{2}}. \tag{4.7.23}$$

Hence the residue contributions from all the poles except those near to $\overset{+}{-} K$ are $O(\delta\Omega)^{\frac{1}{2}}$. Those from the poles near to $\overset{+}{-} K$ are $O(1)$, but since $K > k_0$ always, the corresponding pressure in the fluid decays exponentially with z. Also for $\delta\Omega \neq 0$ we either have $k_f > K > k_0$ or δk is complex so pole contributions near to the critical frequency Ω_0 are exponentially decaying with z.

Thus, for a given position and frequency we can find the farfield pressure in the fluid using (4.7.2) and (4.7.13), which does not necessitate the evaluation of inversion integrals.

The plate displacement far from any point of excitation can be found asymptotically from (4.3.12) by using the method of

stationary phase and the Riemann - Lebesgue lemma.

From (4.3.12) the normalized displacement $u(x,y)$ is given by

$$u(x,y) = \frac{1}{4\pi^2} \int\int_{-\infty}^{\infty} \bar{u}(k_x,k_y)e^{-i(k_x x + k_y y)}dk_x dk_y. \qquad (4.7.24)$$

The term $\bar{u}(k_x,k_y)$ has poles and branch cuts which all contribute

to the integral at finite x and y, however, for large values of x

the Riemann - Lebesgue lemma can be invoked to obtain an

asymptotic evaluation of the k_x integral as a sum of residue

contributions from the poles near to the real k_x axis.

For example, consider the integral of a function $F(k)/(k-K)$,

which has a single pole at $k = K$

$$\int_{-\infty+oi}^{\infty+oi} \frac{F(k)}{k-K} e^{-ikx} dk = \int_{-\infty+oi}^{\infty+oi} \left\{\frac{F(k)}{k-K} - \frac{F(K)}{k-K}\right\}e^{-ikx}dk + F(K)\int_{-\infty+oi}^{\infty+oi} \frac{e^{-ikx}}{k-K} dk.$$
$$(4.7.25)$$

The first integral in the right hand side tends to zero as x

increases by the Riemann - Lebesgue lemma, the second integral

can be evaluated by contour integration to give

$$\int_{-\infty+oi}^{\infty+oi} \frac{F(k)}{k-K} e^{-ikx}dk \simeq 2\pi i \, F(K)e^{-ikx} \text{ for large } x. \qquad (4.7.26)$$

At fixed k_y, the transform $\bar{u}(k_x,k_y)$ has three sets of poles. Two

of these sets are complex and give rise to exponentially decaying

terms. The third set may be either real, complex with real part

$n\pi$, or generally complex, corresponding respectively to waves in

pass bands, in stop bands or to acoustically damped waves. If

we denote the value of k_x at one of the poles by $k_x = k_f(k_y)$ then

by the periodicity of $\tilde{L}(k)$, $k_x = k_f(k_y) \pm 2n\pi$ $n=1,2,3,\ldots$ is also

a solution. k_f is assumed to be a pole that could lie in the upper half plane if the plate had finite internal damping. For $x > 0$ the contour can be closed in the lower half plane to give the k_x integral as a sum of branch cut integrals, which tend to zero by the Riemann - Lebesgue lemma for large x, plus a sum of residue contributions from the poles in the lower half plane. Similarly, for $x < 0$ we can close the contour in the upper half plane to give, generally,

$$u(x,y) \simeq \frac{i}{2\pi} \int_{-\infty}^{\infty} e^{i(k_f(k_y)|x| - k_y y)} \sum_n \bar{u}^*(k_f + 2n\pi, k_y) e^{i2\pi n |x|} dk_y,$$

(4.7.27)

where $\bar{u}^*(k_f, k_y)$ denotes the residue of $\bar{u}(k_x, k_y)$ at $k_x = k_f$.

The remaining integral can be evaluated by the method of stationary phase. (See Whitham (74)). The stationary phase points are given by

$$\frac{\partial}{\partial k_y} \left[k_f(k_y)|x| - k_y y \right] = 0,$$

i.e. $\frac{\partial k_f}{\partial k_y} |x| - y = 0.$ (4.7.28)

The partial derivative can be found from

$$\tilde{L}(k_x, k_y) = 1 + Z \sum_n \bar{G}(k_x - 2n\pi, k_y), \quad \text{since} \quad \tilde{L}(k_f, k_y) = 0.$$

Differentiating gives

$$\frac{\partial \tilde{L}}{\partial k_x} \bigg|_{k_x = k_f} \cdot \frac{\partial k_f}{\partial k_y} + \frac{\partial \tilde{L}}{\partial k_y} = 0,$$ (4.7.29)

from which

$$\frac{\partial k_f}{\partial k_y} = - \frac{\partial \tilde{L}}{\partial k_y} \bigg/ \frac{\partial \tilde{L}}{\partial k_x} \bigg|_{k_x = k_f} . \tag{4.7.30}$$

It has been shown by Hayes (77) that the energy flux vector is in the same direction as the group velocity and it can be shown that (4.7.28) is satisfied only by those waves whose group velocity $\left(\frac{\partial \omega}{\partial k_x}, \frac{\partial \omega}{\partial k_y} \right)$ is in the same direction (x,y) as follows;

The dispersion relation for the plate is

$$\tilde{L}(k_x, k_y, \omega) = 0; \tag{4.7.31}$$

hence,

$$\frac{\partial \tilde{L}}{\partial k_x} + \frac{\partial \tilde{L}}{\partial \omega} \cdot \frac{\partial \omega}{\partial k_x} = 0,$$

and

$$\frac{\partial \omega}{\partial k_x} = - \frac{\partial \tilde{L}}{\partial k_x} \bigg/ \frac{\partial \tilde{L}}{\partial \omega} . \tag{4.7.32}$$

Similarly

$$\frac{\partial \omega}{\partial k_y} = - \frac{\partial \tilde{L}}{\partial k_y} \bigg/ \frac{\partial \tilde{L}}{\partial \omega} . \tag{4.7.33}$$

If the group velocity is in the direction (x,y) then

$$\frac{\partial \omega}{\partial k_x} \bigg/ \frac{\partial \omega}{\partial k_y} = \frac{x}{y} , \tag{4.7.34}$$

i.e. $\frac{\partial \tilde{L}}{\partial k_x} \bigg/ \frac{\partial \tilde{L}}{\partial k_y} = \frac{x}{y} .$

Hence, using (4.7.30)

$$\frac{\partial k_f}{\partial k_y} x + y = 0. \tag{4.7.35}$$

This agrees exactly with (4.7.28) since k_f was a pole corresponding to $x < 0$, and $-k_f$ corresponded to $x > 0$. In the corresponding analysis in chapter 3, the phase velocity and the group velocity were in the same direction, which simplified the calculations.

If we denote the root of (4.7.28) by $k_y = k_s$, then (4.7.27) can be written as

$$u(x,y) \simeq \frac{i}{2\pi} e^{ig(k_s)} \sum_n \bar{u}^*(k_f + 2n\pi, k_s) e^{i2\pi m|x|} \int_{-\infty}^{\infty} e^{i(k_y - k_s)^2 g''(k_s)/2} dk_y$$
(4.7.36)

$$\simeq \frac{ie^{i\pi/4}}{2} \left(\frac{2\pi}{g''(k_s)} \right)^{\frac{1}{2}} e^{ig(k_s)} \sum_n \bar{u}^*(k_f + 2n\pi, k_s) e^{i2\pi m|x|}, \qquad (4.7.37)$$

where $g(k_y) = k_f(k_y)|x| - k_y y$.

The x component of (4.7.37) represents a Floquet wave which may or may not propagate to large distances, depending on whether k_f has an imaginary part. The y component represents a harmonic plane wave.

The function $g(k_y)$ can be written as

$$g(k_y) = (k_f(k_y)|\hat{x}| - k_y \hat{y})r \qquad (4.7.38)$$

where $r^2 = x^2 + y^2$, $\hat{y} = y/r$ and $|\hat{x}| = |x|/r$. Thus, k_s, the zero of (4.7.38), is a function of the direction defined by the unit vector $(|\hat{x}|, \hat{y})$.

The term $g''(k_s)$ occurring in (4.7.37) is given by

$$g''(k_s) = \frac{\partial^2 k_f}{\partial k_y^2} \bigg|_{k_y = k_s} |\hat{x}| \cdot r , \qquad (4.7.39)$$

and

$$\frac{\partial^2 k_f}{\partial k_y^2} = -\left[\tilde{L}_{11}\left(\frac{\tilde{L}_2}{\tilde{L}_1}\right)^2 - 2L_{12}\left(\frac{\tilde{L}_2}{\tilde{L}_1}\right) + \tilde{L}_{22}\right]/\tilde{L}_1 \quad , \tag{4.7.40}$$

where subscript 1 or 2 denotes partial differentiation with respect to k_x or k_y respectively, and all derivatives are evaluated at $k_x = k_f$. Thus the displacement given by (4.7.37) decays like $r^{-\frac{1}{2}}$, corresponding to the expected cylindrical spreading.

The residue term $\bar{u}(k_f, k_y)$ can be found from (4.3.12), and is given by

$$\bar{u}^*(k_f, k_y) = -\frac{Z\bar{G}(k_f, k_y)\,\tilde{\Psi}(k_f, k_y)}{\left.\dfrac{\partial \tilde{L}(k_x, k_y)}{\partial k_x}\right|_{k_x=k_f}} \tag{4.7.41}$$

For the special case $x = n$ (4.7.37) can be simplified since, using the periodicity of $\tilde{\Psi}$ and $\tilde{L}$,

$$\sum_n{}' \bar{u}^*(k_f+2n\pi, k_y) = -\frac{Z\tilde{\Psi}(k_f, k_y)}{\left.\dfrac{\partial \tilde{L}(k_x, k_y)}{\partial k_x}\right|_{k_x=k_f}} \cdot \sum_n \bar{G}(k_f+2n\pi, k_y). \tag{4.7.42}$$

Also

$$\tilde{L}(k_f, k_y) = 1 + Z(k_y)\sum_n \bar{G}(k_f+2n\pi, k_y) = 0$$

and so the value of the infinite sum in (4.7.42) is $-1/Z$. Hence

$$u(n, y) \simeq e^{i3\pi/4}(2\pi g''(k_s))^{-\frac{1}{2}} e^{ig(k_s)} \frac{\tilde{\Psi}(k_f, k_s)}{\left.\dfrac{\partial \tilde{L}}{\partial k_x}\right]_{k_x=k_f, k_y=k_s}} \cdot , \tag{4.7.43}$$

where it is noted that k_s depends upon nd and y.

The asymptotic expression (4.7.37) could have been obtained from the modified discrete Fourier transform using

$$u(x,y) = \frac{1}{4\pi^2} \int_{-\infty}^{\infty} e^{-ik_y y} \int_{-\pi}^{\pi} \widetilde{u}(x,a,k_y) da \, dk_y. \qquad (4.7.44)$$

The analysis would have been slightly easier since we need only have considered a single pole contribution when evaluating the a integral. Expression (4.7.42) can similarly be obtained from the discrete Fourier transform $\widetilde{u}(a,k_y)$. The resulting expressions for u(x,y) are no easier to calculate since the infinite sum in (4.7.37) is implicitly contained in the modified discrete transform $\widetilde{u}(x,k_f,k_s)$.

4.8 COMPUTATION

The calculation of the discrete Fourier transforms, which occur in the asymptotic expressions obtained in the previous section, require the evaluation of infinite sums. The summations must be done numerically with truncation after a finite number of terms, but convergence may be accelerated as follows. Consider the expression for $\tilde{L}(0,a)$,

$$\tilde{L}(0,a) = 1 + \bar{Z}_B(k_y) \sum_{n=-\infty}^{\infty} 1/\bar{Z}_p(a-2n\pi,k_y) \tag{4.8.1}$$

where $\bar{Z}_B$ and $\bar{Z}_p$ are given by (4.5.14) and (4.5.15) respectively.

Let the infinite sum be denoted by S, then S can be written as

$$S = \sum_{n} T_n + \sum_{n} \frac{1}{\left[(a-2n\pi)^2+k_y^2\right]^2} \quad , \tag{4.8.2}$$

where

$$T_n = \frac{1}{\bar{Z}_p(a-2n\pi,k_y)} - \frac{1}{\left[(a-2n\pi)^2+k_y^2\right]^2} \quad .$$

The second summation can be evaluated analytically, and $\sum_{n} T_n$ converges more rapidly than S.

Consider then

$$S_1(a,k_y) = \sum_{n} \frac{1}{\left[(a-2n\pi)^2+ k_y^2\right]^2} \quad , \tag{4.8.3}$$

which can be written as

$$S_1(a,k_y) = -\frac{1}{2k_y} \frac{\partial}{\partial k_y} \sum_{n} \left(\frac{1}{(a-2n\pi)^2+k_y^2} \right). \tag{4.8.4}$$

The summation can be evaluated by contour integration since

$$\sum_n \frac{1}{(a-2n\pi)^2+k_y^2} = \frac{1}{4\pi i} \oint \frac{\cot\left(\frac{t-a}{2}\right)}{t^2+k_y^2} \, dt, \qquad (4.8.5)$$

where the contour encloses the poles of the numerator of the integrand.

The integral around the contour at infinity is zero and so, by Cauchy's theorem, the integral can be evaluated as the sum of the two residue contributions from the zeros of the denominator. Hence,

$$S_1(a,k_y) = \frac{i}{8k_y} \frac{\partial}{\partial k_y} \left\{ \frac{1}{k_y} \left(\cot\left(\frac{a-ik_y}{2}\right) - \cot\left(\frac{a+ik_y}{2}\right) \right) \right\}$$

$$= \frac{1}{4k_y} \frac{\partial}{\partial k_y} \left\{ \frac{\sinh k_y}{k_y(\cos a - \cosh k_y)} \right\}$$

$$= \frac{\cos a \,(k_y \cosh k_y - \sinh k_y) + \sinh k_y \cosh k_y - k_y}{4k_y^3(\cos a - \cosh k_y)^2}$$
$$\qquad (4.8.6)$$

$\tilde{L}(0,a)$ can now be written as

$$\tilde{L}(0,a) \simeq 1 + \tilde{Z}_B (k_y) \sum_{n=M}^{N} T_n + \tilde{Z}_B(k_y)S_1(a,k_y) \qquad (4.8.7)$$

where N and M are chosen to give the required accuracy.

In practice, because of the periodicity of $\tilde{L}(0,a)$ we need only evaluate (4.8.7) for $-\pi \leq a \leq \pi$, and N = -M = 10 gave sufficient accuracy for the range of parameters considered in the next section. Expressions for the partial derivatives of $\tilde{L}(0,a)$ can be obtained by explicit differentiation of (4.8.7).

The Floquet wavenumbers, k_f, are found from $\tilde{L}(0,a)$ using

a standard N.A.G. routine for the solution of a pair of
transcendental equations by Powell's (68) method, the two equations
being the real and imaginary parts of $\widetilde{L}(0,a)$ set equal to zero.

For comparison with the results in chapter 3 we shall
consider harmonic point excitation of the plate, so that the
normalized force is

$$f(x,y) = f_0 \, \delta(x) \, \delta(y) \tag{4.8.9}$$

and

$$\widetilde{\psi}(x,a) = f_0 e^{-i\pi x} \sum_n \widetilde{G}(a-2n\pi,k_y)e^{i2n\pi x}. \tag{4.8.10}$$

The transformed displacement $\bar{u}(k)$ given in (4.3.12) reduces to

$$\bar{u}(k) = f_0 \bar{G}(k)/\widetilde{L}(k). \tag{4.8.11}$$

In general we note that the solution of (4.7.28), together with
$\widetilde{L}(k_f,k_y) = 0$ is complicated; however, for the special case $y = 0$
(4.7.28) is clearly satisfied by $k_y = 0$, from the symmetry of
the problem.

The infinite sum $S_1(a,0)$ given in (4.8.6) takes the value

$$S_1(a,0) = \frac{(2 + \cos a)}{12(1 - \cos a)^2} , \tag{4.8.12}$$

which is singular at $a = 2n\pi$. However, (4.8.7) can be written

$$\widetilde{L}(0,a) \simeq 1 + \bar{Z}_B(0)\sum_{\substack{n=M \\ n\neq 0}}^{N} T_n + \frac{\bar{Z}_B(0)}{\bar{Z}_p(a,0)} + \bar{Z}_B(0)\left[S_1(a,0) - \frac{1}{a^4}\right]. \tag{4.8.13}$$

The term in square brackets is regular at $a = 0$ and takes the
value 1/720.

4.9 RESULTS

In order that comparisons may be made with the results of
chapter 3, the same physical and material constants have been
used to generate the results presented in this section. As in
chapter 3, the results for the farfield fluid pressure and plate
displacement have been normalized to the corresponding results
for a plate with no stiffening beams.

The results for the plate displacement require the calculation
of the so called Floquet wavenumber, k_f. We choose k_f so that
$-\pi < \mathrm{Re}(k_f) < \pi$ and $\mathrm{Im}(k_f) \geq 0$. If the imaginary part of k_f is non-
zero the Floquet wave in the plate decays exponentially and ,
to lowest order in $|x|$, there is no displacement in the plate
farfield. Hence, we need only calculate the real values of k_f.
It has also been noted previously that, if the wavenumber in the
fluid is greater than π, then k_f necessarily has an imaginary
part and the Floquet wave is "acoustically damped". However, this
acoustic damping may be small, and, as argued by Mace (80a),
the damped Floquet wave may still be important at finite distances.
By neglecting the imaginary part of $L(k)$ we can find a wavenumber,
k_a, which satisfies

$$\mathrm{Re}\left[\tilde{L}(k_a)\right] = 0, \qquad\qquad (4.9.1)$$

and corresponds to a Floquet wavenumber found by neglecting the
acoustic damping of the fluid. For real k_a, if $\mathrm{Im}\left[\tilde{L}(k_a)\right] = 0$ then
$k_a = k_f$, and the corresponding wave in the plate is a
propagating Floquet wave. However, if $\mathrm{Im}\left[\tilde{L}(k_a)\right] \neq 0$ then the
wave is termed a "pseudo" propagating wave, (Mace(80)), and the
corresponding frequency range is called a "pseudo pass band".

Plots of real k_f and k_a against frequency are shown in figure 4.1.
For comparison with results in chapter 3 the frequency is normalized
to the classical coincidence frequency for the unstiffened plate.
Plots showing the behaviour of k_f in the pseudo pass bands and
the stop bands will be given in chapter 5. When the plate wave-
number k_p is a multiple of π, then $k_f + 2N\pi = k_p$ for some N. A
plot of $k_p - 2m\pi$ is also shown in figure 4.1 (the dotted lines),
where m is chosen so that $-\pi < k_p - 2m\pi \leq \pi$. Also shown are the
two straight lines denoting the acoustic wavenumbers $\pm k_o$.
When k_f (depicted by the solid line) is either above or below
both of these straight lines the Floquet wave is undamped and
k_f coincides with k_a (depicted by the "dashed " line). The
frequency bands for which there exists a real k_a but no real
k_f are pseudo pass-bands, those for which neither real k_a nor
k_f exist are stop-bands.

The response of the periodically stiffened plate to a line
source, applied along the beam at x = 0, may be obtained from
(4.7.27) by omitting the integral with respect to k_y and the
factor $1/2\pi$, and substituting $k_y = 0$. The resulting displacement
for large x = n is shown in figure 4.2 as a function of normalized
frequency. The displacements, u, are normalized to the
corresponding response, u_o, of an unstiffened plate to the same
line force. The solid lines show the displacement as calculated
using the actual Floquet wavenumber k_f; the vertical scale is
10 log $|u/u_o|$ and the plot shows the predicted pass- and stop-
bands. Above a normalized frequency of 0.019 the acoustic
wavenumber is greater than π (see figure 4.1) and so the Floquet
wave is always damped; hence there is no response, to this order,
at higher frequencies. The dashed lines depict the displacement
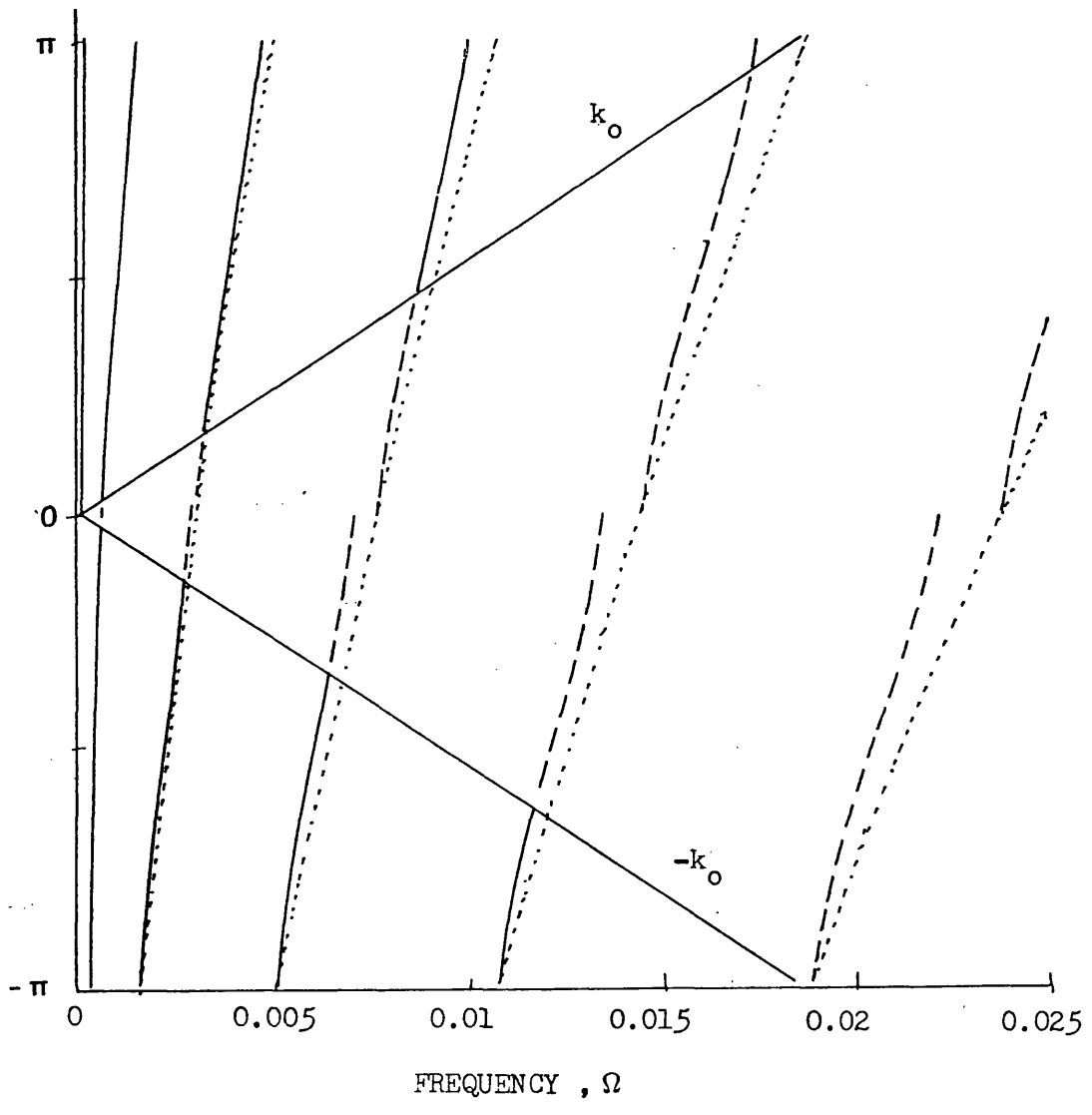
Figure 4.1. The real wavenumbers against frequency.

——————— k_f.

— — — — — k_a.
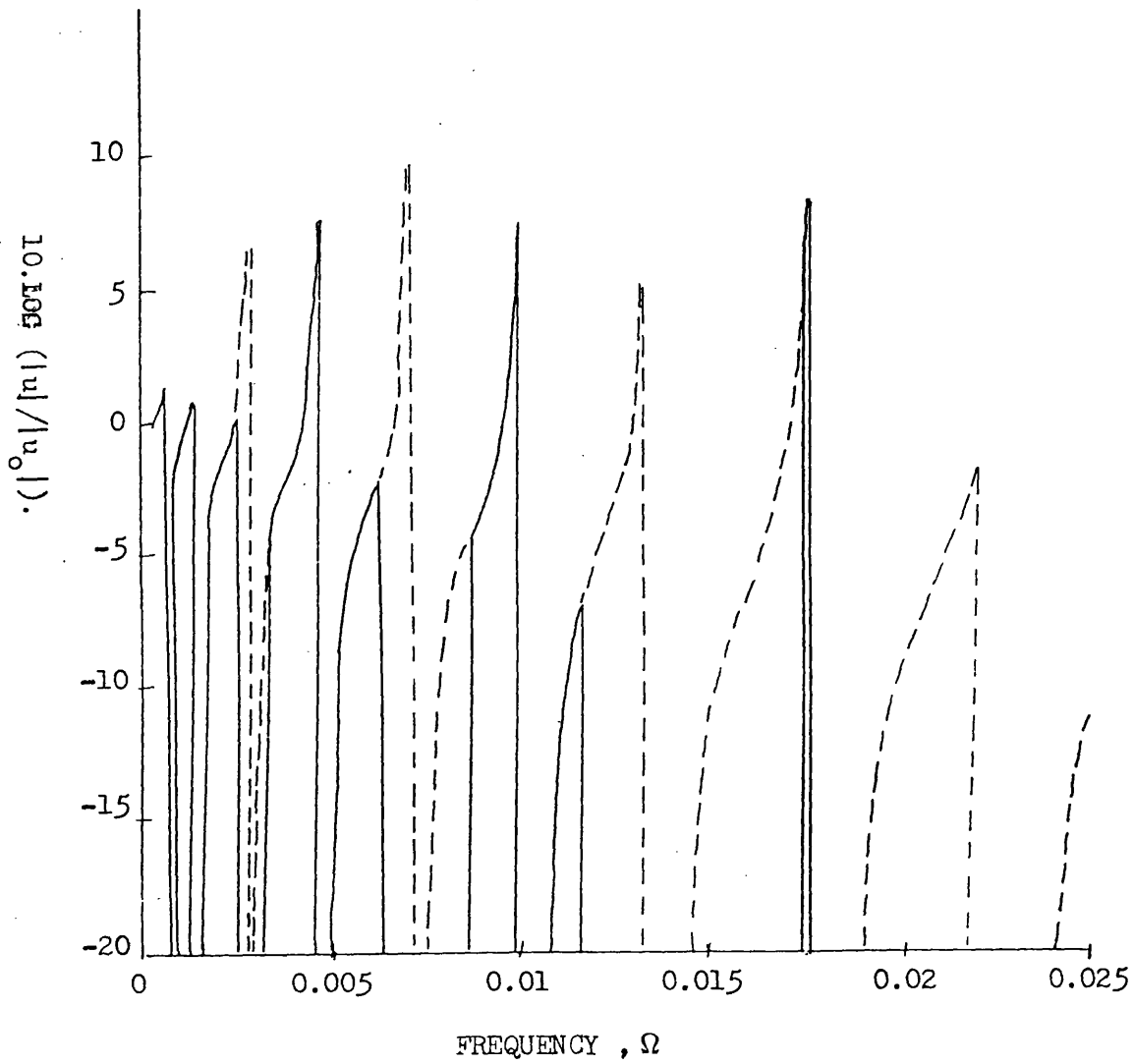
............— k_p - $2n\pi$.

Figure 4.2.   Plate displacement at a beam against frequency

for a line force excitation.

——————   using k_f.

- - - - - -   using k_a (neglecting acoustic damping).

as calculated using k_a instead of k_f. The acoustic damping thus

plays no part, and we have a non-zero response in the pseudo pass-

bands. This latter plot may be compared with figure 3.2. The

plot for $N = 9$ in figure 3.2 shows "troughs" in the frequency

bands corresponding to stop-bands; thus, the plate stiffened with

a finite number of beams is tending to produce the stop-bands

of the periodic structure. Although not shown, the corresponding

plot for $N = 5$ already shows the same structure. Figure 4.2 shows

the displacement at a beam. Near to $k_f = n\pi$ this displacement

will always be near to zero because the plate is excited into a

standing wave with nodes at the beam positions. A plot of the

maximum displacement of the plate between the beams may have

produced a plot more closely resembling those in figure 3.2,

however, at the end of a pass-band, the maximum displacement

is at the beam position and it is here that we have closest

correspondence between figure 4.2 and figure 3.2. Figure 4.3

shows the displacement of the plate, at large $|x| = n$ and $y = 0$,

caused by a point force excitation. As in the previous figure,

the solid lines depict the displacement, u, calculated using

the actual Floquet wavenumber, k_f, and the dashed lines using

k_a. Again the displacements are normalized to the response,

u_o, of an unstiffened plate, and can be compared with figure

3.2. The addition of a finite number of beams did not change

the nature of the free wave in the plate but merely modified

its amplitude, however the addition of the periodic array of

beams changes the problem. In both problems the beams can be

replaced by equivalent forces; with a finite array of beams the

only way for the effect of these forces to reach the plate

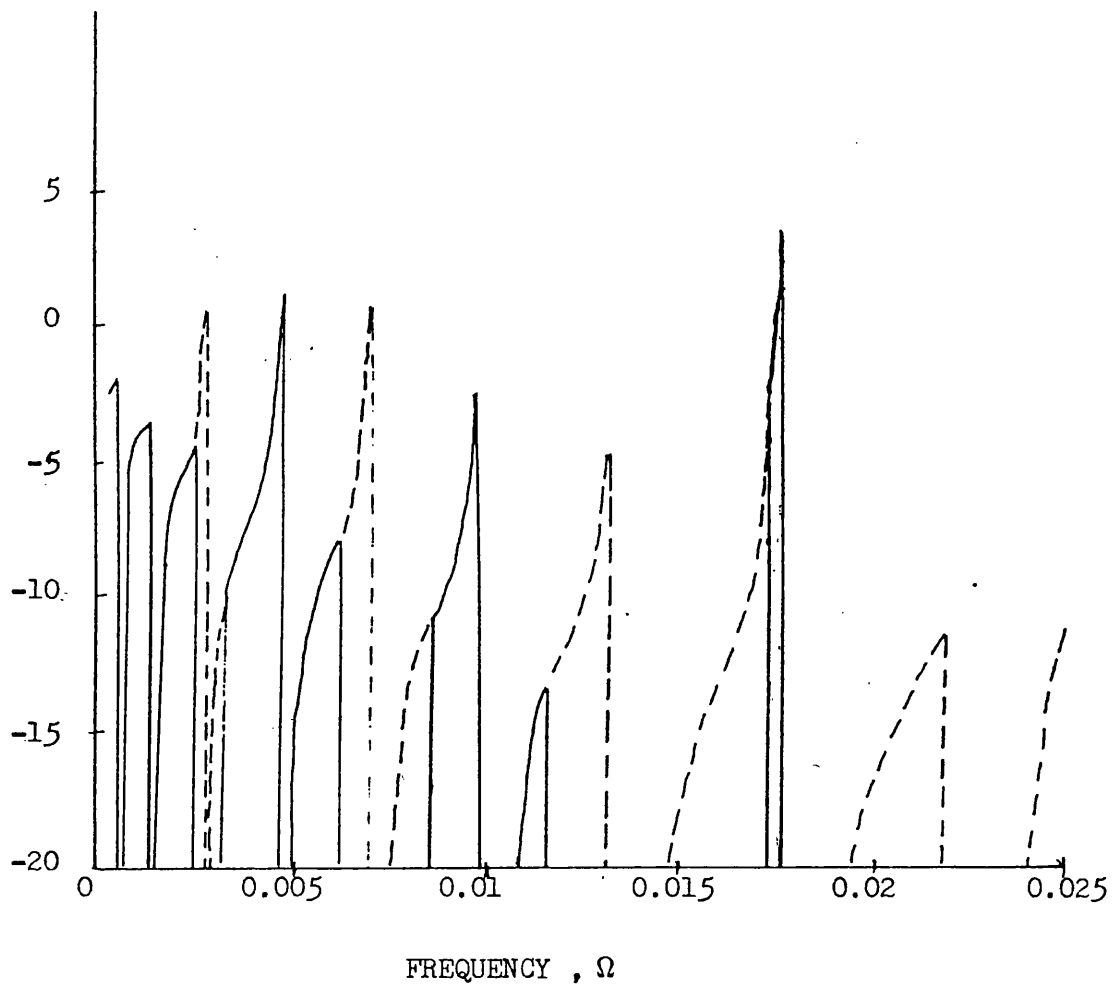farfield is through the flexural wave in the plate and so the

Figure 4.3. Plate displacement at a beam against frequency for a point force excitation.

———————— using k_f.

— — — — — using k_a (neglecting acoustic damping).

asymptotic result can be obtained by considering this one

flexural mode. However, a corresponding statement cannot be made

for the periodically stiffened plate, since the receiver is always

close to a beam, that is, close to a line of force. Thus, the

nature of the free wave is changed by the addition of the beams,

and the problem is further complicated because the free mode

is dependent upon the direction considered. In all then, the

nature of the wave propagation in the plate farfield has been

fundamentally changed by the addition of a periodic array of

beams, and it is not surprising, therefore, that the results

in this chapter, whilst having some features in common with

those in chapter 3, are not directly comparable. The nature

of the free wave propagation in the fluid, however, is

unchanged by the addition of periodic stiffening. Figure 4.4

shows the farfield fluid pressure at a point directly above

the point of excitation, relative to the corresponding pressure

radiated by an unstiffened plate. The maxima and minima could

probably be matched, as those in figure 3.6, to corresponding

extrema in the input impedance of the stiffened plate, and

it is expected that if N were increased, the corresponding plots

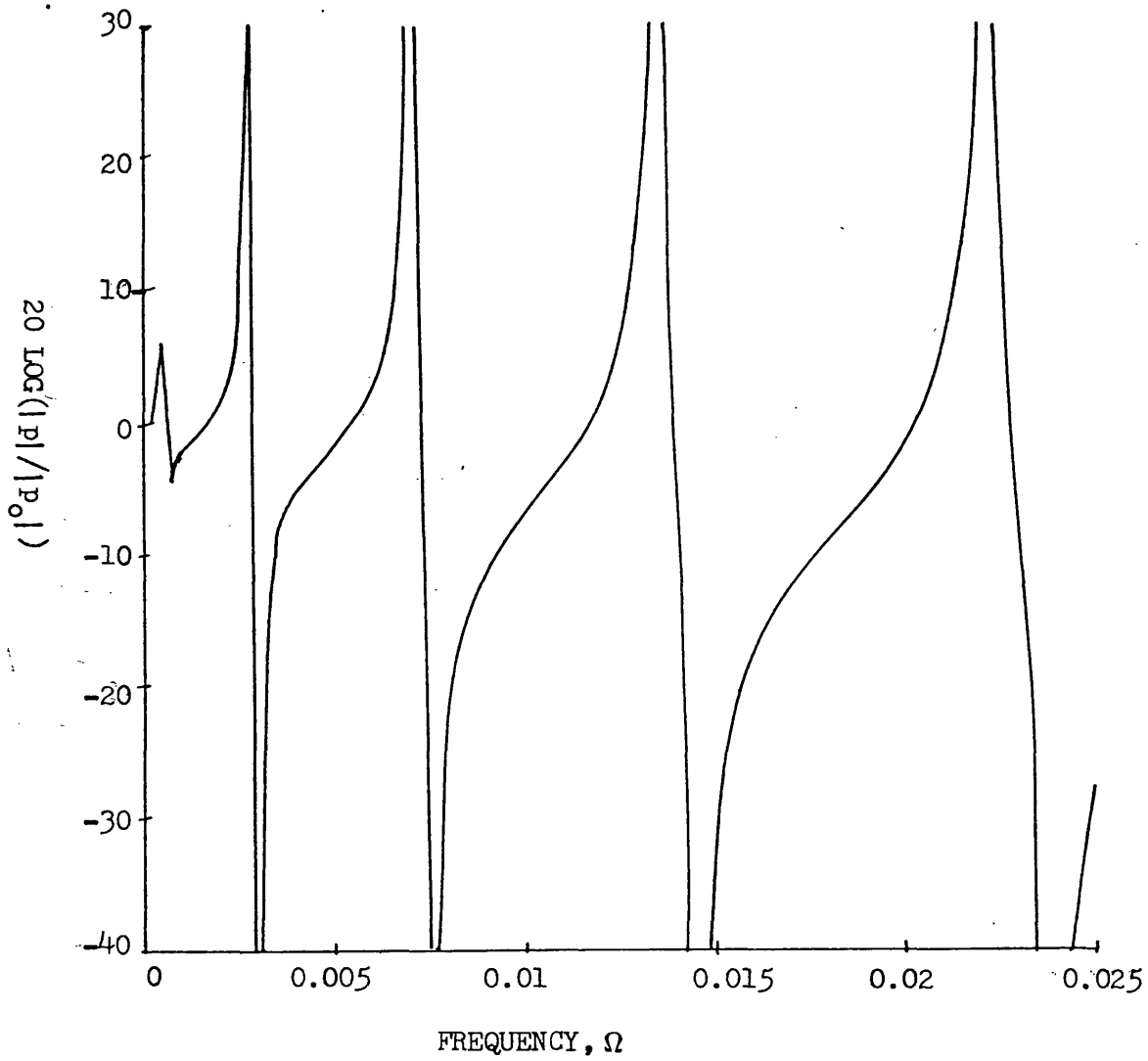in figure 3.6 would increasingly resemble figure 4.4.

Figure 4.4. The farfield radiated pressure against frequency, at a point directly above the point of excitation.

4.10 EXTENSIONS

The methods of this chapter can be combined with those of

chapter 3 to find the response of a more complicated structure

consisting of a periodically stiffened plate with a finite

number of additional stiffeners. Such a structure might be a

model for a periodically stiffened ship's hull with a finite number

of bulkheads. One interesting special case is when the additional

stiffeners are placed with the same spacing as the periodic array

of beams and are given an impedance equal and opposite to them.

This produces a model for a plate periodically stiffened except

for a gap. Similarly several gaps could be included into the model.

Corresponding to equation (4.2.4) we have

$$u(x) = \psi(x) - Z_1(G \square u)(x) - G * \sum_{n=1}^{N} Z_2^n \delta(x-x_n) u(x_n) \qquad (4.10.1)$$

where Z_1 and Z_2^n are the spectral impedances of the periodic

stiffeners and the nth additional stiffener respectively. Each

of the N additional stiffeners is assumed to lie along one of

the periodic stiffeners, and rotational impedances have been

neglected.

At $x = m$ (4.10.1) can be written

$$(L \square u)(m) = \psi(m) - \sum_{n=1}^{N} Z_2^n G(m-x_n) u(x_n), \qquad (4.10.2)$$

where

$$L(n) = \delta_{no} + Z_1 G(n).$$

Introducing the inverse operator M, which can be found using

discrete Fourier transforms, where

$$(M \square L)(n) = \delta_{no}, \tag{4.10.3}$$

gives

$$u(m) = (M \square \psi)(m) - \sum_{n=1}^{N} z_2^n (M \square G_n)(m)u(x_n) \tag{4.10.4}$$

where

$$G_n(x) = G(x-x_n).$$

Equation (4.10.4) is valid at $m = x_n$, $n = 1, \ldots, N$ so we can write

$$\sum_{n=1}^{N} K_{mn} u(x_n) = (M \square \psi)(x_m), \quad m=1, \ldots, N \tag{4.10.5}$$

where

$$K_{mn} = \delta_{mn} + z_2^n (M \square G_n)(x_m).$$

This is a set of N simultaneous equations for the displacements $u(x_n)$, the solution of which enables $u(x)$ to be found from the original equation (4.10.1).

Another extension to the model is the addition of a periodic array of stiffeners, so that we have stiffeners of impedance Z_1 at $x = n$ and stiffeners of impedance Z_2 at $x = np$, where n and p are integers (x has been suitably non-dimensionalized). This problem has already been studied by Mace (80b) using ordinary Fourier transforms, but it is interesting to note here how the use of discrete Fourier transforms simplifies the analysis.

We define the discrete convolution operator $\square_p$ by

$$(G \square_p u)(x) = \sum_{n=-\infty}^{\infty} G(x-np)u(np), \tag{4.10.6}$$

and the corresponding discrete transform by

$$\tilde{u}^p(x,a) = \sum_{n=-\infty}^{\infty} e^{ianp} u(np + x).$$ (4.10.7)

In terms of the ordinary Fourier transform $\bar{u}(k)$

$$\tilde{u}(0,a) = \sum_{n=-\infty}^{\infty} \bar{u}(a-2n\pi)$$ (4.10.8)

and

$$\tilde{u}^p(0,a) = \frac{1}{p} \sum_{n=-\infty}^{\infty} \bar{u}(a-\frac{2n\pi}{p}),$$ (4.10.9)

from which we deduce that

$$\tilde{u}^p(0,a) = \frac{1}{p} \sum_{n=0}^{p-1} (0,a-\frac{2n\pi}{p}).$$ (4.10.10)

Corresponding to (4.2.6) we have

$$u(x) = \psi(x)-z_1(G \square u)(x)-z_2(G \square_p u)(x).$$ (4.10.11)

Taking the modified discrete Fourier transform gives

$$\tilde{u}(x,a) = \tilde{\psi}(x,a)-z_1\tilde{G}(x,a)\tilde{u}(0,a)-z_2\tilde{G}(x,a)\tilde{u}^p(0,a).$$ (4.10.12)

Substituting for $\tilde{u}^p(0,a)$ from (4.10.10) gives

$$\tilde{u}(x,a) = \tilde{\psi}(x,a)-z_1\tilde{G}(x,a)\tilde{u}(0,a)-\frac{z_2}{p}\tilde{G}(x,a)\sum_{n=0}^{p-1}\tilde{u}(0,a-\frac{2n\pi}{p}).$$ (4.10.13)

Putting $x = 0$ in this equation and rearranging produces

$$\tilde{u}(0,a) = \frac{\tilde{\psi}(0,a)-\frac{z_2}{p}\tilde{G}(0,a)\sum_{n=0}^{p-1}\tilde{u}(0,a-\frac{2n\pi}{p})}{1 + z_1\tilde{G}(0,a)}$$ (4.10.14)

If we replace a by $a_r = a - \dfrac{2r\pi}{p}$ and then sum over r from 0 to

p-1 we obtain

$$\sum_{r=0}^{p-1} \widetilde{u}(0,a_r) = \sum_{r=0}^{p-1} \frac{\widetilde{\psi}(0,a_r)}{1+z_1\widetilde{G}(0,a_r)}$$

$$- \frac{z_2}{p} \sum_{r=0}^{p-1} \frac{\widetilde{G}(0,a_r)}{1+z_1\widetilde{G}(0,a_r)} \cdot \sum_{n=0}^{p-1} \widetilde{u}(0,a_n). \qquad (4.10.15)$$

Hence

$$\sum_{r=0}^{p-1} \widetilde{u}(0,a_r) = \sum_{r=0}^{p-1} \frac{\widetilde{\psi}(0,a_r)}{1+z_1\widetilde{G}(0,a_r)} \Bigg/ \widetilde{L}^p(0,a), \qquad (4.10.16)$$

where

$$\widetilde{L}^p(0,a) = 1 + \frac{z_2}{p} \sum_{r=0}^{p-1} \frac{\widetilde{G}(0,a_r)}{1+z_1\widetilde{G}(0,a_r)} \quad . \qquad (4.10.17)$$

Equation (4.10.16) can be used together with (4.10.13) and

(4.10.14) to give $\widetilde{u}(x,a)$ which can then be inverted to give $u(x)$.

Alternatively, we note that if the Green's function for a

plate with a periodic array of stiffeners is $G(x;x')$, then

$G(n;m) = G_s(n-m)$ and G_s can be found using discrete transforms.

The transform of G_s in terms of the plate Green's function

$G(x-x')$ is

$$\widetilde{G}_s(0,a) = \frac{\widetilde{G}(0,a)}{1+z_1\widetilde{G}(0,a)} \quad . \qquad (4.10.18)$$

In terms of G_s the response of a plate with two sets of stiffeners

can be written

$$u(n) = \psi(n) - Z_2(G_s \square_p u)(n), \qquad (4.10.19)$$

where

$$\psi(n) = (G_s * f)(n).$$

Taking the modified transform $(\widetilde{})^p$ of this equation gives

$$\tilde{u}^p(n,a) = \tilde{\psi}^p(n,a) - Z_2 \tilde{G}_s^p(n,a)\tilde{u}^p(0,a). \qquad (4.10.20)$$

We can use (4.10.9) to find G_s^p from G_s, and so at $n = 0$

$$\tilde{u}^p(0,a) = \tilde{\psi}^p(0,a)\big/\tilde{L}^p(0,a), \qquad (4.10.21)$$

where

$$\tilde{L}^p(0,a) = 1 + Z_2 \tilde{G}_s^p(0,a) = 1 + \frac{Z_2}{p} \sum_{n=0}^{p-1} \tilde{G}_s(0,a),-2n\pi$$

which is equivalent to (4.10.17).

This expression for $\tilde{u}^p(0,a)$, (4.10.20), can be inverted to give the displacement $u(x)$ at $x = np$, or used together with (4.10.13) and (4.10.14) to find the displacement at any x.

This model has been used by Mace (80b) to study a ship's hull with stiffeners and bulkheads, but could possibly be used to study other periodic structures (e.g. a turbine with a blade missing). It is noted that in the absence of fluid loading the infinite sums required in the calculation of the discrete transforms can be evaluated analytically.

4.11 CONCLUSIONS

In this chapter the response of a fluid-loaded, periodically stiffened plate has been studied. The problem was reduced to a single equation involving a discrete convolution operator, (or a pair of such equations if the moments produced by the beam are included), which was then solved by application of the discrete Fourier transform or the modified discrete Fourier transform. This latter transform represents a given function as a superposition of Floquet waves and reduces the convolution equation to an algebraic equation for the transformed variable. For a plate with no fluid loading the inverse transform can be found using residues, while for the fluid-loaded plate the inverse may either be evaluated numerically or expanded as an asymptotic series. In this chapter we have, as an example, found the first terms in the series for the plate displacement and the fluid pressure at large distances from a point or line of excitation. As in chapter 3, the pressure in the farfield of the fluid takes the form of either a spherically or a cylindrically spreading harmonic wave. The farfield motion of the plate, however, takes the form of a Floquet wave, a wave well known in the study of periodic structures. At some frequencies this wave may be exponentially decaying because of the periodicity of the structure or because of acoustic damping, or both. At other frequencies the wave may propagate unattenuated to large distances.

These propagation and attenuation zones are already becoming apparent in the results in chapter 3 for a plate stiffened with a finite number of equally spaced beams.

If the intention is to develop a model of an actual structure, the model developed in this chapter is physically more reasonable for the calculation of plate displacements, since the stiffening beams are likely to extend over the whole of the structure. For the calculation of fluid pressures there is little to choose between the two models. The first model has the advantage, however, of being able to deal with unequally spaced beams, but is numerically more complicated since it requires the solution of a system of algebraic equations.

The techniques developed in this chapter for studying this particular periodic system may well have applications to other periodic systems.

CHAPTER 5   THE RESPONSE OF A FLUID-LOADED PLATE STIFFENED BY

A SEMI-INFINITE ARRAY OF BEAMS

5.1   INTRODUCTION

Chapter 4 examined the behaviour of a periodically stiffened
fluid-loaded plate. Although in real structures, such as ship's
hulls or aircraft, stiffening often takes the form of equally
spaced uniform beams, the spacing and properties of the beam may
be different in adjacent regions of the structure, or indeed the
structure may have an unstiffened region. In order to gain some
insight into the behaviour of a structure with such a discontinuity
in the periodicity, this chapter examines the behaviour of a fluid-
loaded plate stiffened on one half by a semi-infinite array of
attached beams.

As in the previous chapter, the problem is first solved
formally using discrete convolutions. The actual technique for
finding the functions defined in the formal solution involves
the use of the discrete Fourier transform, introduced in chapter
4, together with an application of the Wiener-Hopf technique.

The solution for a general excitation is derived, although
details and results are given only for the case when the
excitation takes the form of a free plane wave in the unstiffened
half of the plate, incident upon the array of beams.

5.2 THE FORMAL SOLUTION

The transformed displacement of an elastic plate stiffened

by a semi-infinite array of beams attached along the lines

$x = n$, $n \geq 0$ is given by

$$\bar{u}(x,k_y) = \bar{G}(x,k_y)*\bar{f}(x,k_y) + \bar{G}(x,k_y)*\sum_{n=0}^{\infty}\bar{F}(k_y)\,\delta(x-n), \qquad (5.2.1)$$

where, as in previous chapters, $\bar{u}(x,k_y)$ denotes the ordinary

Fourier transform of $u(x,y)$ with respect to y, $G(x,y)$ is the

Green's function for the unstiffened plate and $F_n(y)$ is the force

on the plate due to the nth beam. The $*$ denotes convolution with

respect to x. As before we shall simplify the notation by assuming

the k_y dependence implicitly and write $u(x) = \bar{u}(x,k_y)$.

The force $\bar{F}_n(k_y)$ is related to the displacement at the nth

beam by

$$\bar{F}_n(k_y) = -\bar{Z}(k_y)\bar{u}(x,k_y) = -Zu(x), \qquad (5.2.2)$$

so (5.2.1) can be written as

$$u(x) = G(x)*f(x)-Z\sum_{n=0}^{\infty}G(x-n)u(n). \qquad (5.2.3)$$

We now introduce the notation

$$u_+(x) = \begin{cases} u(x), & x \geq 0 \\ 0, & x < 0 \end{cases} \qquad (5.2.4a)$$

and

$$u_-(x) = \begin{cases} 0, & x \geq 0 \\ u(x), & x < 0. \end{cases} \qquad (5.2.4b)$$

Using this notation together with the discrete convolution

introduced in the previous chapter, (5.2.3) reduces to

$$u(x) = \psi(x) - Z(G \square u_+)(x), \qquad (5.2.5)$$

where $\psi(x) = G(x) * f(x)$.

The remainder of this section is devoted to the formal solution of (5.2.5) using the discrete convolution operator. From the definitions (5.2.4) we note that $u(x) = u_+(x) + u_-(x)$, so that at $x = n$ (5.2.5) can be written

$$u_+(n) + u_-(n) = \psi(n) - Z(G \square u_+)(n)$$

which can be rearranged to give

$$(L \square u_+)(n) + u_-(n) = \psi(u), \qquad (5.2.6)$$

where

$$L(n) = \delta_{no} + ZG(n). \qquad (5.2.7)$$

We now assume that we can define $L_+(n)$ and $L_-(n)$ such that;

$$L_+(n) = 0 , n < 0,$$

$$L_-(n) = 0 , n > 0 \qquad (5.2.8)$$

and

$$(L_- \square L_+)(n) = L(n), \text{ for all } n. \qquad (5.2.9)$$

We also assume that the corresponding inverses M_+ and M_- exist so that

$$(M_+ \square L_+)(n) = (M_- \square L_-)(n) = \delta_{no}. \qquad (5.2.10)$$

We note that these equations do not define L_+ and L_- uniquely.

Applying the convolution operator $M\_\square$ to (5.2.6) yields

$$(L_+\square\, u_+)(n) + (M\_\square\, u\_)(n) = (M\_\square\, \psi)(n). \qquad (5.2.11)$$

If $n \geq 0$ then $(M\_\square\, u\_)(n) = 0$, since

$$(M\_\square\, u\_)(n) = \sum_m M\_(n-m) u\_(m)$$

and $u\_(m) = 0$ for $m \geq 0$, while $M\_(n-m) = 0$ for $m < n$.

Hence, for $n \geq 0$, (5.2.11) gives

$$(L_+\square\, u_+)(n) = (M\_\square\, \psi)(n), \quad n \geq 0, \qquad (5.2.12)$$

while for $n < 0$

$$(L_+\square\, u_+)(n) = 0. \qquad (5.2.13)$$

(5.2.12) and (5.2.13) can be combined to give

$$(L_+\square\, u_+)(n) = (M\_\square\, \psi)_+(n), \quad \text{for all } n, \qquad (5.2.14)$$

where

$$(M\_\square\, \psi)_+ = \begin{cases} (M\_\square\, \psi)(n), & n \geq 0 \\ 0, & n < 0 \end{cases}$$

Finally, application of $M_+\square$ gives

$$u_+(n) = (M_+\square\, (M\_\square\, \psi)_+)(n). \qquad (5.2.15)$$

We can now substitute for $u_+(n)$ in (5.2.5) to give the formal solution

$$u(x) = \psi(x) + Z(G\square M_+\square\, (M\_\square\, \psi)_+)(x). \qquad (5.2.16)$$

Thus the problem has been reduced to one of finding $L_+(n)$ and $L\_(n)$, from the known function $L(n)$ and finding their corresponding inverses $M_+(n)$ and $M\_(n)$.

5.3   THE DISCRETE FOURIER TRANSFORM AND THE WIENER-HOPF TECHNIQUE

As in section 4.3 of the preceding chapter the discrete Fourier transform of a function $F(x)$ is defined by

$$\widetilde{F}(k) = \sum_{n=-\infty}^{\infty} e^{ikn}F(n),$$ (5.3.1)

and the corresponding inverse is

$$F(n) = \frac{1}{2\pi} \int_{-\pi}^{\pi} e^{-ikn}\widetilde{F}(k)dk.$$ (5.3.2)

In addition to the properties of $\widetilde{F}(k)$ described in section 4.3, $\widetilde{F}(k)$ has the following property; if a function $F_+(n)$ satisfies $F_+(n) = 0$ for $n < 0$, then $\widetilde{F}_+(k)$, the transform of $F_+(n)$, is analytic in the upper half of the complex k plane, $Im(k) > 0$, since then $\widetilde{F}_+(k)$ is a sum of decaying exponentials. Similarly, if $F_-(n) = 0$ for $n > 0$, then $\widetilde{F}_-(k)$ is analytic in $Im(k) < 0$.

The discrete Fourier transform of (5.2.6) is

$$\widetilde{L}(k).\widetilde{u}_+(k) + \widetilde{u}_-(k) = \widetilde{\psi}(k),$$ (5.3.3)

where $\widetilde{u}_+(k)$ and $\widetilde{u}_-(k)$ are analytic in $Im(k) > 0$ and $Im(k) < 0$ respectively. The equation is a standard Wiener-Hopf equation, the solution of which is discussed by Noble (58). The solution requires that $\widetilde{L}(k)$ be factorized into the product of two functions $\widetilde{L}_+(k)$ and $\widetilde{L}_-(k)$, analytic in $Im(k) > 0$ and $Im(k) < 0$ respectively, which clearly correspond to the transforms of $L_+(n)$ and $L_-(n)$ defined by (5.2.8) and (5.2.9). Thus, from the transform of (5.2.9)

$$\widetilde{L}_-(k).\widetilde{L}_+(k) = \widetilde{L}(k).$$ (5.3.4)

If $\widetilde{L}(k)$ is analytic and non-zero in some strip $|Im(k)| < \varepsilon$ containing the real axis then we can write

$$\log \tilde{L}(k) = \frac{1}{2\pi i} \oint_{\Gamma} \frac{\log \tilde{L}(t)}{t-k} dt , \qquad (5.3.5)$$

where Γ is a positively oriented contour contained within the strip and enclosing the point $t = k$. In particular, for $\delta < \epsilon$ we can write

$$\log \tilde{L}(k) = \frac{1}{2\pi i} \int_{-\infty-i\delta}^{\infty-i\delta} \frac{\log \tilde{L}(t) dt}{t-k} - \frac{1}{2\pi i} \int_{-\infty+i\delta}^{\infty+i\delta} \frac{\log \tilde{L}(t) dt}{t-k}. \qquad (5.3.6)$$

The first term is analytic in $\text{Im}(k) > 0$ and can be identified with $\log \tilde{L}_+(k)$, and the second is analytic in $\text{Im}(k) < 0$ and can be identified with $\log \tilde{L}_-(k)$. Hence,

$$\log \tilde{L}_+(k) = \pm \frac{1}{2\pi i} \int_{-\infty \mp i\delta}^{\infty \mp i\delta} \frac{\log \tilde{L}(t)}{t-k} dt. \qquad (5.3.7)$$

We can use the periodicity of $\tilde{L}(t)$ to write

$$\log \tilde{L}_+(k) = \pm \frac{1}{2\pi i} \int_{-\pi \mp i\delta}^{\pi \mp i\delta} \log \tilde{L}(t) \sum_{n=-\infty}^{\infty} \left(\frac{1}{t-2n\pi-k} \right) dt,$$

that is

$$\log \tilde{L}_+(k) = \pm \frac{1}{4\pi i} \int_{-\pi \mp i\delta}^{\pi \mp i\delta} \log \tilde{L}(t) \cot\left(\frac{t-k}{2}\right) dt. \qquad (5.3.8)$$

Thus we have a procedure for calculating $\tilde{L}_+(k)$ and $\tilde{L}_-(k)$. We can replace $\tilde{L}(k)$ in (5.3.3) by $\tilde{L}_-(k)\tilde{L}_+(k)$ and divide by $\tilde{L}_-(k)$ to give

$$\tilde{L}_+(k)\tilde{u}_+(k) + \frac{\tilde{u}_-(k)}{\tilde{L}_-(k)} = \frac{\tilde{\psi}(k)}{\tilde{L}_-(k)} . \qquad (5.3.9)$$

The right hand side can be split into a sum of functions analytic in the upper and lower half planes. These are given by

$$\left(\frac{\widetilde{\psi}(k)}{\widetilde{L}_-(k)}\right)_{\pm} = \pm \frac{1}{4\pi i} \int_{-\pi \mp i\delta}^{\pi \mp i\delta} \left(\frac{\widetilde{\psi}(k)}{\widetilde{L}_-(k)}\right) \cot\left(\frac{t-k}{2}\right) dt. \tag{5.3.10}$$

Hence (5.3.9) can be rearranged as

$$\widetilde{L}_+(k)\widetilde{u}_+(k) - \left(\frac{\widetilde{\psi}(k)}{\widetilde{L}_-(k)}\right)_+ = \left(\frac{\widetilde{\psi}(k)}{\widetilde{L}_-(k)}\right)_- - \frac{\widetilde{u}_-(k)}{\widetilde{L}_-(k)} = P(k). \tag{5.3.11}$$

$P(k)$ is defined in the strip $-i\delta < \text{Im}(k) < i\delta$, and may be extended by analytic continuation to the whole of the plane. $P(k)$ is bounded in the strip (since it is periodic) and so by Liouville's theorem $P(k) = $ constant. The value of this constant can be found by considering the value of $\left(\dfrac{\widetilde{\psi}(k)}{\widetilde{L}_-(k)}\right)_- - \dfrac{\widetilde{u}_-(k)}{\widetilde{L}_-(k)}$ as $k \to -i\infty$.

The decomposition of $\dfrac{\widetilde{\psi}(k)}{\widetilde{L}_-(k)}$ is not unique and we can redefine

$\left(\dfrac{\widetilde{\psi}(k)}{\widetilde{L}_-(k)}\right)_-$, if necessary, by addition of a constant so that $P(k) = 0$.

(5.3.11) then gives

$$\widetilde{L}_+(k)\widetilde{u}_+(k) = \left(\frac{\widetilde{\psi}(k)}{\widetilde{L}_-(k)}\right)_+ ,$$

that is

$$\widetilde{u}_+(k) = \frac{1}{\widetilde{L}_+(k)} \cdot \left(\frac{\widetilde{\psi}(k)}{\widetilde{L}_-(k)}\right)_+ . \tag{5.3.12}$$

Also from (5.3.11) we get

$$\widetilde{u}_-(k) = \widetilde{L}_-(k)\left(\frac{\widetilde{\psi}(k)}{\widetilde{L}_-(k)}\right)_- . \tag{5.3.13}$$

We can now find $u(x)$ from (5.3.12) by any of three possible methods.

(i) We can invert (5.3.12) to give $u_+(n)$ and then substitute into (5.2.5).

(ii) We can take the modified discrete Fourier transform of (5.2.5) to give

$$\widetilde{u}(x,k) = \widetilde{\psi}(x,k) - Z\widetilde{G}(x,k)\widetilde{u}_+(0,k),\tag{5.3.14}$$

where $\widetilde{u}_+(0,k) = \widetilde{u}_+(k)$ and is given by (5.3.12). Inverting gives

$$u(x) = \frac{1}{2\pi}\int_{-\pi}^{\pi}\widetilde{u}(x,k)\,dk.\tag{5.3.15}$$

(iii) We can take the ordinary Fourier transform of (5.2.5) to give

$$\bar{u}(k) = \bar{\psi}(k) - Z.\bar{G}(k)\widetilde{u}_+(k),\tag{5.3.16}$$

which can then be inverted to give

$$u(x) = \frac{1}{2\pi}\int_{-\infty}^{\infty}\left\{\bar{\psi}(k) - Z\bar{G}(k)\widetilde{u}_+(k)\right\}e^{-ikx}\,dk.\tag{5.3.17}$$

Since $\bar{\psi}(k)$ and $\bar{G}(k)$ are usually easy to find, we shall use (5.3.17) in the sequel to find $u(x)$ from $\widetilde{u}_+(k)$.

Thus, application of the discrete Fourier transform produces a standard Wiener-Hopf equation for the transformed displacement. This equation can be solved by the Wiener-Hopf technique and the solution used to find the displacement $u(x)$.

5.4 INCIDENT WAVE EXCITATION

In this section we shall consider the particular form of the solution for the case where the excitation takes the form of a free plane wave in the unstiffened half of the plate. We denote this incident wave by $u_-^i(x,y)e^{-i\omega t}$, where

$$u_-^i(x,y) = A \exp(ik_p(x \cos\theta + y \sin\theta)), \qquad (5.4.1)$$

where θ is the angle between the x-axis and the direction of propagation and $k_p(\omega)$ satisfies the dispersion relation for the unstiffened plate. $k_p(\omega)$ is assumed to have a small positive imaginary part induced by internal damping in the plate, so that $u_-^i(x,y)$ decays with increasing x.

This wave impinges on the array of beams producing a reflected wave, $u_-^s(x,y)$, in $x<0$ and a transmitted wave, $u_+^t(x,y)$, in the region $x>0$, as well as producing a scattered sound field in the fluid. We can write the transmitted wave as a sum of incident and scattered waves, $u_+^i(x,y)$ and $u_+^s(x,y)$ respectively, where $u_+^i(x,y)$ has the same form as $u_-^i(x,y)$.

The scattered field $u^s(x,y)$ is produced by the forces on the plate due to the beams. Hence, corresponding to (5.2.1), we have

$$\bar{u}^s(x,k_y) = -\bar{G}(x,k_y)\,\bar{Z}(k_y)\sum_{n=0}^{\infty}\bar{u}^t(x,k_y)\,\delta(x-n), \qquad (5.4.2)$$

where the bar denotes an ordinary Fourier transform in the y direction. However,

$$\bar{u}_+^i(x,k_y) = 2\pi A\,\delta(k_y - k_p \sin\theta)e^{ik_p x\cos\theta}, \qquad (5.4.3)$$

so

$$u^s(x,y) = \bar{u}^s(x, k_p \sin \theta) e^{ik_p y \sin \theta} . \qquad (5.4.4)$$

If we write

$$\bar{u}^s(x, k_p \sin \theta) = u^s(x), \qquad (5.4.5)$$

then $u^s(x,y) = u^s(x) e^{ik_p y \sin \theta}$ and (5.4.2) becomes

$$u^s(x) = -Z(G \square u_+^t)(x). \qquad (5.4.6)$$

Replacing $u_+^t(x)$ by $u_+^i(x) + u_+^s(x)$ gives

$$u^s(x) = -Z(G \square u_+^i)(x) - Z(G \square u_+^s)(x). \qquad (5.4.7)$$

At $x = n$, if we replace $u^s(n)$ by $u_+^s(n) + u_-^s(n)$ and rearrange we have

$$(L \square u_+^s)(n) + u_-^s(n) = -Z(G \square u_+^i)(n), \qquad (5.4.8)$$

where $L(n) = \delta_{no} + ZG(n)$.

This equation is of the form (5.2.6), with $-Z(G \square u_+^i)(n)$ as the known forcing term, and can be solved using the methods outlined previously as follows:

Application of the discrete Fourier transform gives

$$\tilde{L}(k).\tilde{u}_+^s(k) + \tilde{u}_-^s(k) = -Z\tilde{G}(k)\tilde{u}_+^i(k). \qquad (5.4.9)$$

However,

$$u_+^i(x) = Ae^{ik_p x \cos \theta} = Ae^{iKx} \quad \text{say, where } K = k_p \cos \theta, \text{ and hence}$$

$$\tilde{u}_+^i(k) = A\sum_{n=0}^{\infty} e^{ikn} e^{iKn} = \frac{A}{1 - e^{i(k+K)}} . \qquad (5.4.10)$$

Also,

$$\tilde{L}(k) = 1 + z\tilde{G}(k),$$

so that

$$- z\tilde{G}(k) = 1 - \tilde{L}(k). \tag{5.4.11}$$

We can use (5.3.8) to factorize $\tilde{L}(k)$ into $\tilde{L}_-(k)\tilde{L}_+(k)$, so that (5.4.9) can be written

$$\tilde{L}_-\tilde{L}_+\tilde{u}_+^s + \tilde{u}_-^s = (1 - \tilde{L}_-\tilde{L}_+)\tilde{u}_+^i,$$

that is

$$\tilde{L}_+\tilde{u}_+^s + \frac{\tilde{u}_-^s}{\tilde{L}_-} = \frac{\tilde{u}_+^i}{\tilde{L}_-} - \tilde{L}_+\tilde{u}_+^i . \tag{5.4.12}$$

To solve this equation we must split $\dfrac{\tilde{u}_+^i}{\tilde{L}_-}$ into the sum

$$\frac{\tilde{u}_+^i}{\tilde{L}_-} = \left(\frac{\tilde{u}_+^i}{\tilde{L}_-}\right)_+ + \left(\frac{\tilde{u}_+^i}{\tilde{L}_-}\right)_- . \tag{5.4.13}$$

However,

$$\frac{\tilde{u}_+^i}{\tilde{L}_-} = \frac{A}{\tilde{L}_-(k)(1-e^{i(k+K)})} ,$$

and so by inspection

$$\left(\frac{\tilde{u}_+^i}{\tilde{L}_-}\right)_+ = \frac{A}{\tilde{L}_-(-K)(1-e^{i(k+K)})} \tag{5.4.14}$$

and

$$\left(\frac{\tilde{u}_+^i}{\tilde{L}_-}\right)_- = \frac{A}{1-e^{i(k+K)}} \left\{ \frac{1}{\tilde{L}_-(k)} - \frac{1}{\tilde{L}_-(-K)} \right\} . \tag{5.4.15}$$

These expressions can be substituted into (5.4.12) and the result rearranged to give

$$\tilde{L}_+(k)\tilde{u}_+^s(k) + \tilde{L}_+(k)\tilde{u}_+^i(k) - \frac{A}{\tilde{L}_-(-K)(1-e^{i(k+K)})}$$

$$= \frac{A}{1-e^{i(k+K)}}\left\{\frac{1}{\tilde{L}_-(k)} - \frac{1}{\tilde{L}_-(-K)}\right\} - \frac{\tilde{u}_-^s(k)}{\tilde{L}_-(k)} = P(k), \text{ say.} \tag{5.4.16}$$

As $k \rightarrow -i\infty$, $\tilde{u}_-^s(k) = \sum_{n=-\infty}^{-1} e^{ikn}u_-(n) \rightarrow 0$ and also $\frac{1}{1-e^{i(k+K)}} \rightarrow 0.$

$P(k)$ is constant by Liouville's theorem and so

$$P(k) = \lim_{k \rightarrow -i\infty} P(k) = 0.$$

Hence, from (5.4.16), writing $\tilde{u}_+^t(k) = \tilde{u}_+^s(k) + \tilde{u}_+^i(k)$ we have

$$\tilde{u}_+^t(k) = \frac{A}{\tilde{L}_-(-K)\tilde{L}_+(k)(1-e^{i(k+K)})} \tag{5.4.17}$$

and

$$\tilde{u}_-^s(k) = \frac{A}{1-e^{i(k+K)}}\left\{1 - \frac{\tilde{L}_-(k)}{\tilde{L}_-(-K)}\right\}. \tag{5.4.18}$$

Finally, using (5.3.17) we have

$$u^s(x) = - \frac{Z}{2\pi}\int_{-\infty}^{\infty} dk\ e^{-ikx}\tilde{u}_+^t(k)\bar{G}(k)\Big|_{k_y=k_p\sin\theta} \tag{5.4.19}$$

and

$$u^s(x,y) = u^s(x)e^{ik_p y\sin\theta}. \tag{5.4.20}$$

Thus, we find the response of the plate to an incident free wave.

We can also use equations (4.7.1) and (4.7.2) to find the sound pressure generated in the fluid.

In general, the Wiener-Hopf split given by (5.3.10) will not have a simple form and may require numerical evaluation of the integral, but there are some other excitations, such as a point or line source at the origin, which can be dealt with analytically.

5.5 THE SOLUTION NEGLECTING FLUID - LOADING

As in section 4.6 of the preceding chapter, the problem is greatly simplified by the neglect of the fluid-loading. The function $\tilde{L}(k)$ can be evaluated analytically. In the simplest case of normal incidence we have $k_y = 0$ and $\tilde{L}(k)$ can be written as

$$\tilde{L}(k) = \frac{\cos^2 k - A \cos k + B}{(\cos k - \cos k_p)(\cos k - \cosh k_p)} \quad , \qquad (5.5.1)$$

where k_p is the free plate wavenumber (which has positive imaginary part for finite internal damping) and A and B are given by (4.6.9).

The numerator may be factorized to give

$$\tilde{L}(k) = \frac{(\cos k - \cos k_f)(\cos k - \cos a_f)}{(\cos k - \cos k_p)(\cos k - \cosh k_p)} \quad , \qquad (5.5.2)$$

where a_f is the root which is always complex and has positive imaginary part. The factorization of $\tilde{L}(k)$ into $\tilde{L}_+(k)\tilde{L}_-(k)$ can be done by inspection to give

$$\tilde{L}_\pm(k) = \frac{\sin\left(\frac{k \mp k_f}{2}\right) \sin\left(\frac{k \mp a_f}{2}\right)}{\sin\left(\frac{k \mp k_p}{2}\right) \sin\left(\frac{k \mp ik_p}{2}\right)} \quad . \qquad (5.5.3)$$

Hence,

$$\tilde{u}_+^t(k) = \frac{iAe^{-i\left(\frac{k+k_p}{2}\right)} \sin\left(\frac{k+ik_p}{2}\right) \sin(k_p)\sin(k_p(\frac{1+i}{2}))}{2 \sin\left(\frac{k+k_f}{2}\right) \sin\left(\frac{k+a_f}{2}\right) \sin\left(\frac{k_p+k_f}{2}\right) \sin\left(\frac{k_p+a_f}{2}\right)} \quad , \qquad (5.5.4)$$

where A, in (5.5.4), is the amplitude of the incident wave.

We can now evaluate $u^s(x)$ from (5.4.19) using contour integration.

For $x > 0$ we can close the contour in the lower half plane. Here the integrand is analytic except for poles at $k = -k_f + 2\pi$, $k = -\alpha_f + 2n\pi$ and at $k = -k_p$. Hence, by residues,

$$
u_+^t(x) = \frac{-ZAe^{-i\left(\frac{k_p-k_f}{2}\right)} \sin\left(\frac{ik_p-k_f}{2}\right)}{\tilde{L}_-(-k_p) \sin\left(\frac{\alpha_f-k_f}{2}\right)} e^{ik_f x} \sum_n \frac{e^{i2n\pi x}}{\bar{Q}(-k_f-2n\pi)}
$$

$$
\frac{-ZAe^{-i\left(\frac{k_p-\alpha_f}{2}\right)} \sin\left(\frac{ik_p-\alpha_f}{2}\right)}{\tilde{L}_-(-k_p)\sin\left(\frac{k_f-\alpha_f}{2}\right)} e^{i\alpha_f x} \sum_n \frac{e^{i2n\pi x}}{\bar{Q}(-\alpha_f-2n\pi)}
$$

$$
- Ae^{ik_p x} \; . \tag{5.5.5}
$$

Thus, $u_+^s(x) = u_+^t(x) + Ae^{ik_p x}$ is a sum of two Floquet waves.

However, α_f always has a positive imaginary part and so the second wave decays with x. If $k_f(\Omega)$ is real, then Ω is a frequency in a pass band for the corresponding periodic structures and the first Floquet wave propagates to large distances. If $k_f(\Omega)$ has an imaginary part, then Ω is in a stop band and the first wave also decays. It is noted that this problem without fluid-loading can easily be solved by assuming that the transmitted and reflected waves must be some combination of the free modes for each half of the plate (that is, plane harmonic waves in the unstiffened half and Floquet waves in the stiffened half) and

then satisfy the boundary conditions at $x = 0$ (and $x = \pm \infty$).

Finally, it is noted that $u_+^t(x)$ is well behaved near

$k_p = k_f = n\pi$, since if $k_p = n\pi + \delta$ then $k_f = n\pi + O(\delta^{\frac{1}{2}})$ and it

is easy to show that the first term in $(5.5.5)$ is

$O(1) \cdot \sin n\pi x + O(\delta^{\frac{1}{2}})$, the leading term being due solely to the

poles at $k_f = \pm k_p + O(\delta^{\frac{1}{2}})$. The remaining residue contributions

are $O(\delta^{\frac{1}{2}})$. Thus at $k_p = n\pi$, $u_+^t(x)$ is the sum of only two residue

contributions and takes the form of a standing wave, $B \sin n\pi x$,

which has nodes at the beams.

5.6 ASYMPTOTIC EVALUATION OF THE PLATE DISPLACEMENT AND THE FLUID PRESSURE

The calculation of $u^S(x,y)$ from (5.4.19) and (5.4.20) requires the numerical evaluation of an integral, and the evaluation of the integrand at any point also requires the evaluation of integrals to find $\tilde{u}_+^t(k)$.

In this section we shall obtain the leading term in the asymptotic expansion of (5.4.19), and the corresponding expression for the fluid pressure, for large values of x and z respectively.

Substituting $\tilde{u}_+^t(k)$ from (5.4.17), (5.4.19) becomes

$$u^S(x) = - \frac{ZA}{2\pi} \int_{-\infty}^{\infty} \frac{e^{-ikx} \, dk}{\tilde{L}_-(-K)\tilde{L}_+(k)(1-e^{i(k+K)})\bar{Q}(k)} \quad , \qquad (5.6.1)$$

where

$$\bar{Q}(k) = 1/\bar{G}(k). \qquad (5.6.2)$$

The term $\tilde{L}_+(k)(1-e^{i(k+K)})$ has zeros at the Floquet wavenumbers in the lower half plane, since $\tilde{L}_+(k) = \tilde{L}(k)/\tilde{L}_-(k)$ and $\tilde{L}_-(k)$ is well behaved and non-zero in the lower half plane. We denote these zeros by $k = - k_f + 2\pi n$, n=0, $\pm$ 1, $\pm$ 2,... However, the term $\tilde{L}_+(k)(1-e^{i(k+K)})$ is well behaved (non-zero) at $k = -K + 2\pi n$.

$\bar{Q}(k)$ has zeros in the upper and lower half planes, at $k = \pm K$ respectively, near to the real axis. In addition, both $\tilde{L}_+(k)$ and $\bar{Q}(k)$ have branch cuts and complex zeros, the zeros and branch cuts of $\tilde{L}_+(k)$ being confined to the lower half plane.

For large values of x we can close the contour in the lower half plane and use the Riemann-Lebesgue lemma, as in chapter 4, to show that the major contribution to the integral comes from

the poles at $k = -k_f + 2\pi n$ and at $k = - K$. Thus, for $x \gg 0$,

$$u^s(x) \simeq \frac{iAZ}{L_-(-K)} \left\{ \frac{e^{ik_f x} \sum_{n=-\infty}^{\infty} e^{i2\pi nx} / \overline{Q}(-k_f-2\pi n)}{(1-e^{i(K-k_f)}) \frac{\partial \tilde{L}_+}{\partial k} \Big|_{k=-k_f}} \right.$$

$$\left. + \frac{e^{ikx}}{\frac{\partial \overline{Q}}{\partial k} \Big|_{k=-K}} \cdot \lim_{k \to -K} \left[\frac{1}{\tilde{L}_+(k)(1-e^{i(k+K)})} \right] \right\} . \qquad (5.6.3)$$

The second term in the right hand side reduces to $-Ae^{ikx}(= - u^i(x))$, and so for $x \gg 0$,

$$u_+^t(x) \simeq iAZe^{ik_f x} \frac{\sum_n e^{i2\pi nx} / \overline{Q}(-k_f-2\pi n)}{\tilde{L}_-(-K)(1-e^{i(K-k_f)}) \frac{\partial \tilde{L}_+}{\partial k} \Big|_{k=-k_f}} . \qquad (5.6.4)$$

The sum term represents a function periodic in x; thus, $u_+^t(x)$ given by (5.6.4) is a Floquet wave. As in chapter 4 we can show that as k_f approaches $N\pi$ the residue terms all tend to zero except for the two corresponding to $k_f \simeq \pm K$. Hence, by symmetry, the solution for $u_+^t(x)$ when $k_f = N\pi$ is a standing wave in the x direction with nodes at the beam positions.

At $x = n$ we can evaluate the infinite sum, since

$$\tilde{L}(-k_f) = 1 + Z \sum_n \frac{1}{\overline{Q}(-k_f-2n\pi)} = 0 , \qquad (5.6.5)$$

and hence

$$u_+^t(n) = -\frac{iAe^{ik_f n}}{\tilde{L}_-(-K)(1-e^{i(K-k_f)}) \frac{\partial \tilde{L}_+}{\partial k} \Big|_{k=-k_f}} \qquad (5.6.6)$$

If k_f has a non-zero imaginary part then $u_+^t(x)$ given by (5.6.4)

tends to zero as x increases, showing that the Floquet wave

does not propagate energy. In this case the main contribution to

the integral in (5.6.1) will come from integration around the

branch cuts in the lower half plane. Thus, when k_f has an

imaginary part, energy can only reach the plate at $x \gg 0$ through

the fluid, but energy in the fluid is subject to cylindrical

spreading and so $u_+^t(x)$ is proportional to $x^{-\frac{1}{2}}$ for large x, and

can be found by the method of stationary phase.

For large negative values of x we can evaluate (5.6.1) by

closing the contour in the upper half plane, where, by definition,

$u_+^t(k)$ is analytic. We can again use the Riemann-Lebesgue lemma

to show that the main contribution to the integral is from the pole

in the upper half plane at $\bar{Q}(k) = 0$ near to the real axis, that is,

at k = K. Hence, for $x \ll 0$,

$$u^s(x) \simeq \frac{-AZe^{-iKx}}{\tilde{L}_+(K)\,\tilde{L}_-(-K)(1-e^{2iK})\,\frac{\partial \bar{Q}(k)}{\partial k}\bigg|_{k=K}} \qquad (5.6.7)$$

Thus, the reflected wave is of the same form as the incident wave

but with modified amplitude and x-component travelling in the

opposite direction.

The fluid displacement potential $\phi(x,z)$ is given by

$$\phi(x,z) = \frac{iZ}{2\pi} \int_{-\infty}^{\infty} dk\; \frac{e^{-ikx}e^{ik_z z}\tilde{u}_+^t(k)}{k_z\,\bar{Q}(k)} \qquad (5.6.8)$$

where $\phi(x,z) = \phi(x, k_y = k_p\sin\theta\,,\,z)$. The unnormalized fluid

pressure $p(x,y,z)$ is related to the displacement potential by

$$p(x,y,z) = - \rho_0 \omega^2 d^2 \phi(x,z) e^{i(k_p y \sin\theta - \omega t)}. \qquad (5.6.9)$$

The asymptotic evaluation of (5.6.8), for large values of z, is facilitated by the substitutions

$$x = R \sin\mu \cos\theta \,, \quad y = R \sin\mu \sin\theta \,, \quad z = R \cos\mu \,,$$

$$k_p \sin\theta / k_0 = \sin\beta \quad \text{and} \quad k = k_0 \sin\alpha \cos\beta \,,$$

where $R = (x^2 + y^2 + z^2)^{\frac{1}{2}}$.

With these substitutions $k_z = k_0 \cos\alpha \cos\beta$ and (5.6.8) becomes

$$\Phi(x,z) = \Phi(R,\mu,\theta) = \frac{iZ}{2\pi} \int_{-\pi/2 + i\infty}^{\pi/2 - i\infty} d\alpha \, \overset{t}{u}_+(k_0 \sin\alpha \cos\beta) e^{-ik_0 R \cos\beta \, g(\alpha,\mu,\theta)},$$

$$(5.6.10)$$

where

$$g(\alpha,\mu,\theta) = \sin\alpha \sin\mu \cos\theta - \cos\alpha \cos\mu \,. \qquad (5.6.11)$$

The contour in the complex α-plane is shown in figure 5.1. For large values of $k_0 R$, (5.6.10) can be evaluated asymptotically by the method of steepest descents. The saddle point α_0 of the function $g(\alpha,\mu,\theta)$ satisfies

$$\left. \partial g / \partial \alpha \right|_{\alpha = \alpha_0} = 0 \,,$$

which gives

$$\alpha_0 = - \tan^{-1}(\tan\mu \cos\theta) \,, \qquad (5.6.12)$$

and the original path of integration can be deformed to the steepest descent path, shown in figure 5.1, which is given by

$$\text{Re}\left\{\cos\beta \, g(\alpha,\mu,\theta)\right\} = \text{Re}\left\{\cos\beta \, g(\alpha_0,\mu,\theta)\right\} = \text{constant},$$
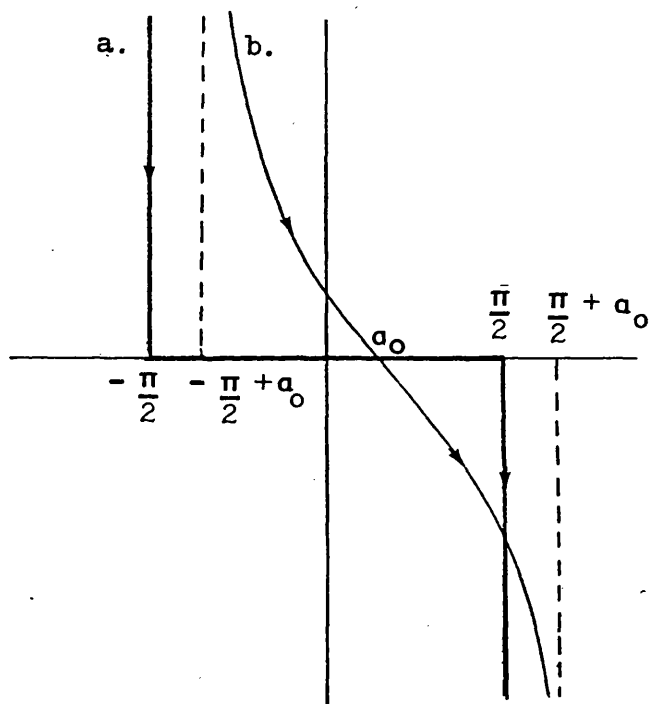
together with

Figure 5.1.   The original contour, (a) and steepest

descents contour (b) in the complex a-plane.

$$\text{Im} \left\{ \cos\beta \, \frac{\delta^2 g}{\delta a^2} \, (a,\mu,\theta) \right\} < 0. \qquad\qquad (5.6.13)$$

Account must be taken of any poles in the integrand which lie between the two contours. Any poles which do not lie on the real axis of the complex a-plane give rise to exponentially decaying terms which can be neglected. If a is real, then k is either complex, (when β is complex, and hence k_z is complex), or k is real and $|k| < k_0$. Thus, the only zeros of $\tilde{L}_+(k)$ which could give rise to non-decaying residue terms are real zeros, satisfying $|k| < k_0$, and these can only occur when $k_p = N\pi$. However, it has been shown in section 4.7 and section 5.5 that the residue contributions from such zeros are identically zero, since the Floquet wave is a standing wave formed by the superposition of two acoustically slow plane waves. In conclusion then, for large R, the residue terms can be neglected since they are exponentially small, and the integral in (5.6.10) can be approximated by the integral along the steepest descents contour. Approximating the integrand by its value at the saddle point and expanding $g(a,\mu,\theta)$ in a Taylor series about the saddle point gives

$$\Phi(R,\mu,\theta) \simeq iZe^{-ik_0 R\cos\beta} g_0 \cdot \frac{\tilde{u}_+^t(k_0\sin a_0\cos\beta)}{\bar{Q}(k_0\sin a_0\cos\beta)} \cdot \left(\frac{i}{2\pi R k_0 \cos\beta \, g_0} \right)^{\frac{1}{2}},$$

$$(5.6.14)$$

where $g_0 = g(a,\mu,\theta) \Big|_{a=-\tan^{-1}(\tan\mu\cos\theta)}$

and

$$\cos\beta = \left(1 - \frac{k_p^2}{k_0^2}\sin^2\theta\right)^{\frac{1}{2}}.$$

We note that $\cos\beta$ may be complex. If this is the case then
$\Phi(R,\mu,\theta)$, given by (5.6.14), decays exponentially with R and there
is no radiation to the fluid farfield. For large enough R, we
can use the steepest descents approximation (5.6.14) to compute
the farfield fluid pressure and we can use the residue
approximations (5.6.4) and (5.6.7) to compute the plate
displacement for $x \gg 0$ and $x \ll 0$ respectively.

If one were interested in computations at finite fixed R
(R "large"), then the pole contributions from poles with small
imaginary parts may be significant, both in the calculations of
pressure and displacement. In the remainder of this chapter,
however, R is considered to be large enough that any exponentially
decaying terms can be ignored.

5.7 COMPUTATION

The computation of $\tilde{L}_+(k)$ from (5.3.8) requires that $\tilde{L}(k)$

be analytic and non-zero in some strip containing the real axis.

Thus, it would appear that we must include some finite internal

damping (by assuming that the plate bending stiffness D is

complex) in the calculations. However, we can deal with the poles

and zeros of $\tilde{L}(k)$ near to the real axis explicitly by writing

$$\tilde{L}(k) = J(k) \left(\frac{\cos k - \cos k_f}{\cos k - \cos K} \right) \qquad (5.7.1)$$

where k_f and K are zeros and poles respectively of $\tilde{L}(k)$ in the

upper half plane. Further, we can use the Plemelj-Privalov

formula (Muskhelishvili (53)), to write

$$F_+(k) = \tfrac{1}{2}F(k) \pm \frac{1}{4\pi i} \text{ P.V.} \int_{-\pi}^{\pi} F(t)\cot\left(\frac{t-k}{2}\right) dt, \qquad (5.7.2)$$

where P.V. denotes the Cauchy Principal Value, and

$$F(k) = F_+(k) + F_-(k).$$

Hence,

$$\log J_+(k) = \tfrac{1}{2}\log J(k) \pm \frac{1}{4\pi i} \text{ P.V.} \int_{-\pi}^{\pi} \log J(t)\cot\left(\frac{t-k}{2}\right) dt. \qquad (5.7.3)$$

J(k) has branch points near to the real axis at

$k = \pm (k_o^2 - k_y^2)^{\frac{1}{2}} - 2n\pi$, but (5.7.3) is valid even as we let the

internal damping tend to zero provided $k_z(k)$ is chosen to have

a non-negative imaginary part.

The term $\left(\dfrac{\cos k - \cos k_f}{\cos k - \cos K} \right)$ may be factorized by inspection

and so

$$\tilde{L}_+(k) = J_+(k) \; \frac{\sin\left(\dfrac{k \mp k_f}{2}\right)}{\sin\left(\dfrac{k \mp K}{2}\right)} \quad , \tag{5.7.4}$$

where $J_+(k)$ is found from (5.7.3).

Having calculated $J_+(k)$, we can find $\dfrac{\partial \tilde{L}_+}{\partial k}$ simply by

differentiating (5.7.4), giving

$$\left.\frac{\partial \tilde{L}_+}{\partial k}\right|_{k=-k_f} = \frac{J_+(-k_f)}{2 \sin\left(\dfrac{K-k_f}{2}\right)} \quad . \tag{5.7.5}$$

The calculation of $\tilde{L}(k)$ and k_f has already been discussed in section 4.8.

The principal value integral is calculated as follows. Consider

$$I = P.V. \int_{-\pi}^{\pi} F(t) \cot\left(\frac{t-k}{2}\right) dt = \lim_{\varepsilon \to 0} \left\{ \int_{-\pi}^{k-\varepsilon} F(t) \cot\left(\frac{t-k}{2}\right) dt \right.$$

$$\left. + \int_{k+\varepsilon}^{\pi} F(t) \cot\left(\frac{t-k}{2}\right) dt \right\} \quad . \tag{5.7.6}$$

Substituting $h = k-t$ and $h = t-k$ in the first and second integrals respectively gives

$$I = \lim_{\varepsilon \to 0} \left\{ -\int_{\varepsilon}^{\pi+k} F(k-h) \cot(h/2)\, dh + \int_{\varepsilon}^{\pi-k} F(k+h) \cot(h/2)\, dh \right\}$$

$$= \lim_{\varepsilon \to 0} \int_{\varepsilon}^{\pi-|k|} \left[F(k+h) - F(k-h) \right] \cot(h/2)\, dh$$

$$- \operatorname{sgn}(k) \int_{\pi-|k|}^{\pi+|k|} F(k-h\, \operatorname{sgn}(k)) \cot(h/2)\, dh, \tag{5.7.7}$$

where $\text{sgn}(k) = k/|k|$.

The integrand in the first integral is well behaved and can be used for numerical calculations.

For the calculation of results in the next section, Simpson's rule has been used to evaluate (5.7.7) and the real and complex parts of the integral have been calculated separately.

5.8 RESULTS

As an example, results have been calculated for the following dimensionless constants, (defined in chapter 4),

$$\lambda^2 \left(= \frac{md}{M} \right) = 1.2, \qquad \beta^2 \left(= \frac{\rho_0 d^2}{M} \right) = 1.846,$$

$$s \left(= \frac{B}{Dd} \right) = 0.00477, \qquad \gamma^2 \left(= \frac{D}{Mdc^2} \right) = 0.004413. \qquad (5.8.1)$$

Any particular system is defined by knowledge of beam spacing together with the mass per unit length and the bending stiffness of the beams. For example, if $d = 0.6m$, $M = 195kg.m^{-1}$ and $B = 8.12kg.m^3.s^2$ then $\Omega = 1$ corresponds to a frequency of 885.5 Hz. The range of values used in chapters 3 and 4 was chosen so that the frequency range considered contained a number of pass and stop bands. In order to demonstrate all of the important features however, it suffices to choose a frequency range that contains a pass and stop band together with acoustically damped pseudo-pass and stop bands. The solid curves in figures 5.2a,b show respectively, the real and imaginary parts of the Floquet wavenumber k_f, as a function of the normalized frequency, Ω. The two solid lines in figure 5.2a are $\pm k_0$, the acoustic wavenumber, and the dashed curves are k_p and $k_p - 2\pi$. As described before, frequencies for which the imaginary part of k_f is zero correspond to pass bands, and if $-k_0 < Re(k_f) < k_0$ then the Floquet wave is acoustically damped and decays exponentially. The various frequency bands are shown in the figure. At higher frequencies the Floquet wave is always acoustically damped.

Figure 5.2. The Floquet wavenumber, k_f, against frequency.

(a).

(b).

FREQUENCY , Ω
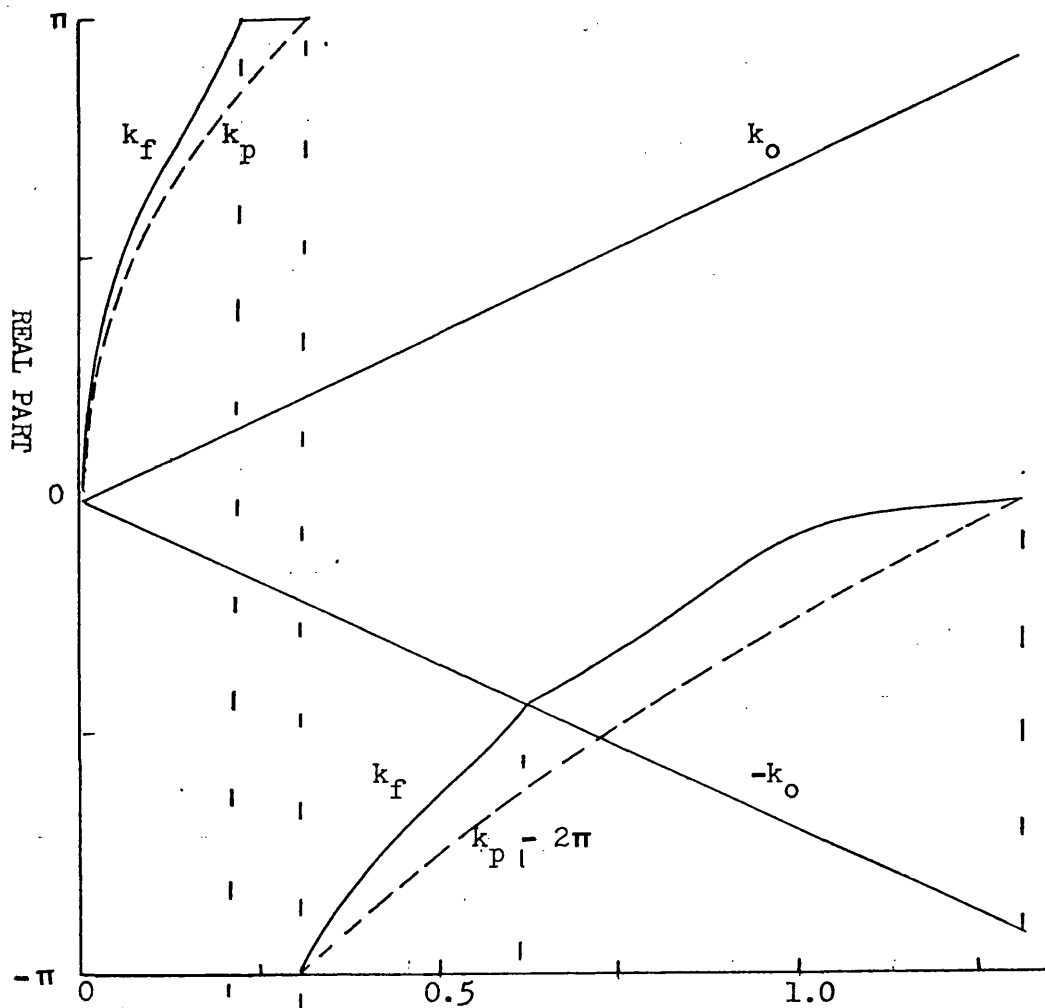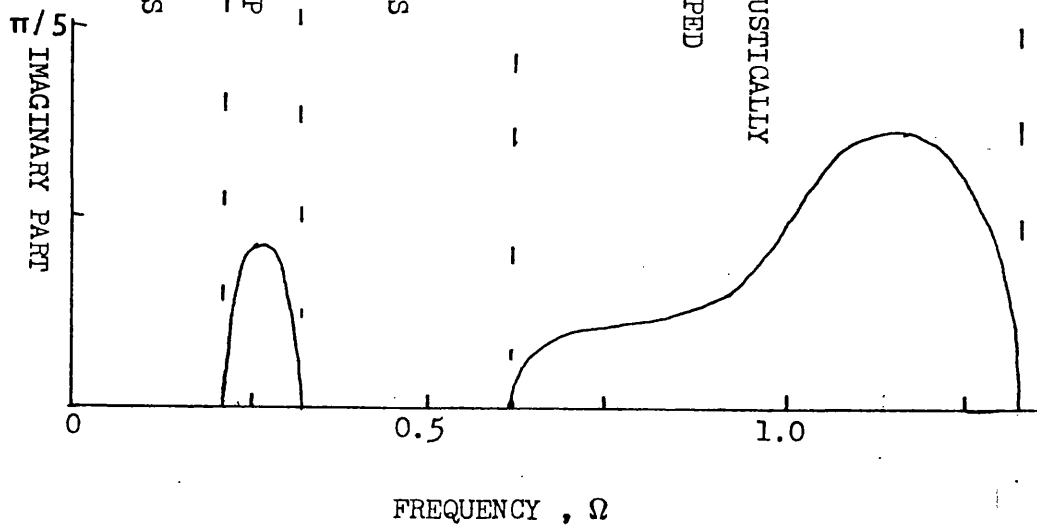
For the incident wave excitation considered here, we can

define reflection and transmission coefficients by $\left|u_-^s\right|/A$ and

$\left|u_+^t\right|$ /A, respectively, where A is the amplitude of the

incident wave and u_-^s , u_+^t are the displacements at large

negative x and large positive x. The solid curve in figure

5.3 shows the transmission coefficient and the broken curve,

the reflection coefficient, again as a function of the

frequency, for an incident wave travelling along the normal

to the beams. At low frequencies the structure is dominated by

the fluid loading and the relative effect of the stiffening

beams is small. Thus, the structure appears almost homogeneous.

The transmission coefficient in figure 5.3 tends to 1 and the

reflection coefficient to zero, as they should do. The

displacements in the stiffened half of the plate have been

calculated at a beam position, thus we have a maximum of the

transmission coefficient at the end of the first pass band,

which is at a frequency corresponding to the resonant frequency

of a single "element" of the structure with free ends. The

transmission coefficient is larger than unity but we have

only calculated the displacement at a single point. If the

coefficients were defined in terms of the energy in an "element"

we would expect them to be less than unity, but with the

definitions used here there is no physical contradiction,

indeed, for the problem without fluid-loading, analytic

results show the same phenomenon.

At the start of the second pass band the transmission

coefficient is zero, as it should be, since the Floquet wave is

predicted to have nodes at the beam positions when k_p = nπ.
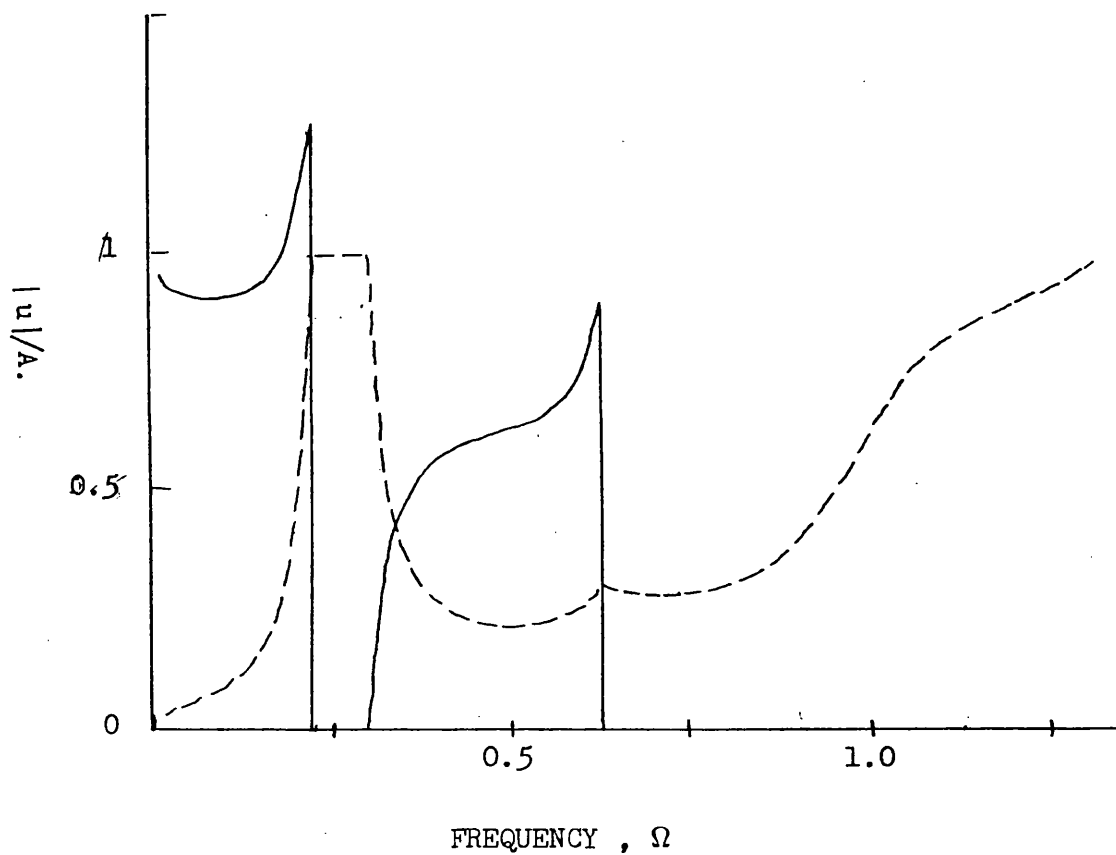
Outside of the pass bands the transmission coefficient is

Figure 5.3.   The transmission, (————) and reflection,

(— — — — —) coefficients against frequency.

for a normally incident plane wave.

zero (asymptotically for large x).

In the stop bands the stiffened plate is hard to excite and the reflection coefficient is almost unity since the region $x > 0$ will not allow energy propagation to large x. Above the frequency at which $k_f = k_o$ the Floquet wave is acoustically damped. Initially, the imaginary part of k_f is small and the Floquet wave may be slowly decaying with x; thus calculations for x large but not infinite, would not contain a sharp"cut-off" frequency, at which the transmission coefficient becomes zero. As we approach the frequency for which $k_p - 2\pi = 0$, that is the extreme right of the figure, the reflection coefficient approaches unity as it must do to produce the predicted standing wave. At higher frequencies the transmission coefficient is always zero, while it is expected that the reflection coefficient will peak to unity at frequencies for which $k_p = n\pi$, although calculations have not been made.

The farfield fluid pressure is shown in figure 5.4. The vertical scale is $20 \log(R^{\frac{1}{2}} | \phi(R,\mu,0)|/A)$, or, in terms of the unnormalized pressure, p', $20\log\left[R^{\frac{1}{2}}p'/(A \rho_o c^2 \gamma^2 \Omega^2)\right]$.
The plots show the pressure at a point directly above the origin and at points corresponding to $\mu = \pm 45^o$, produced by a wave, amplitude A, incident along the normal to the beams. All three plots show a local maximum at the end of the first pass band, when the displacement at the beams is largest, and a sharp minimum at the end of the first stop band, where the displacement, asymptotically at least, is a superposition of two acoustically slow plane waves. The plot for $\mu = -45^o$ shows a peak at $\Omega = 0.72$. At this frequency $Re(k_f) \simeq \sin(-45^o)k_o$. That is, the

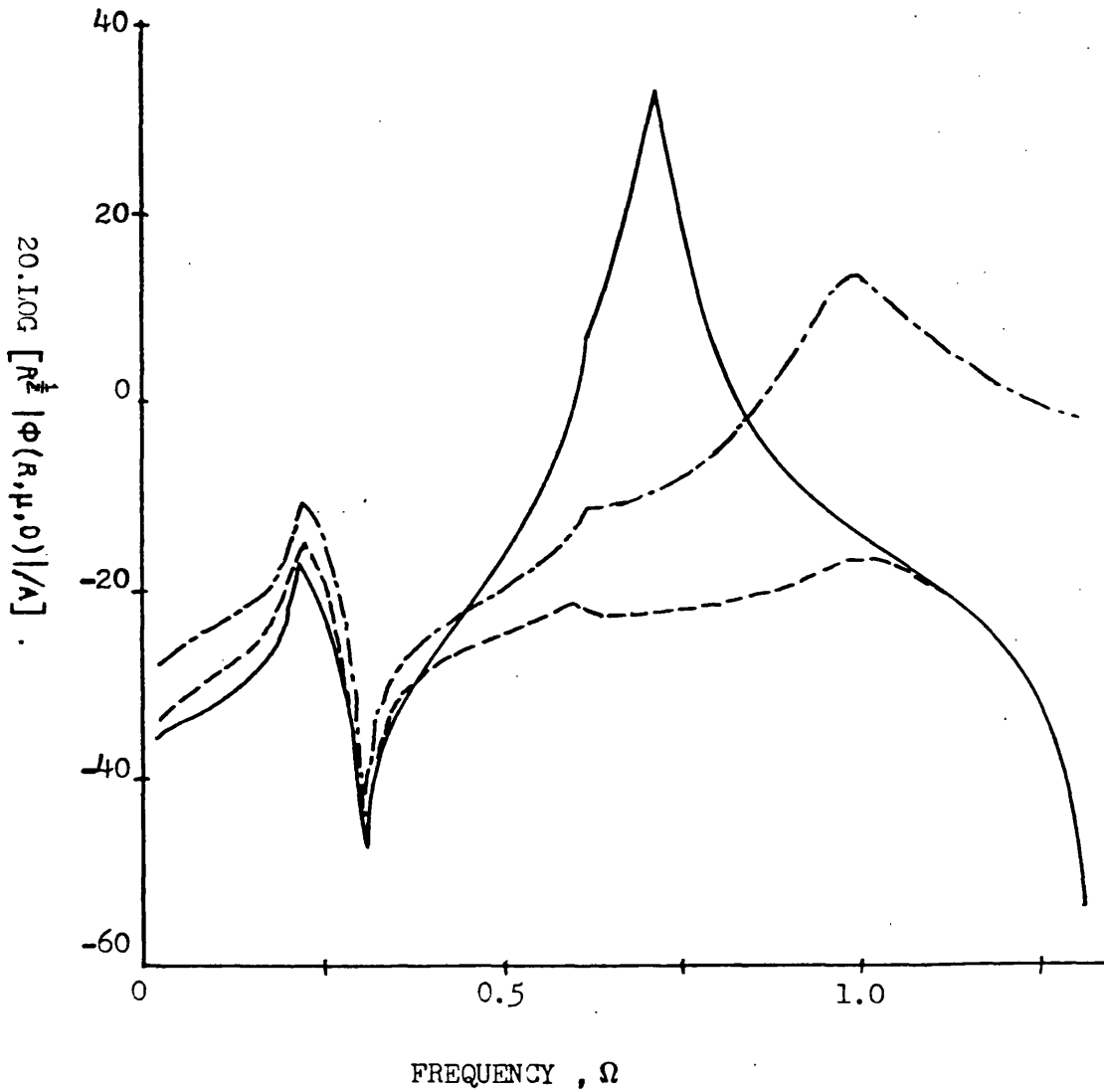Figure 5.4.   The farfield displacement potential against frequency due to an incident wave.

———————— $\mu = -45^\circ$

—·—·—·— $\mu = 0^\circ$

— — — — — $\mu = 45^\circ$

Floquet wave in the stiffened half of the plate is acoustically

fast, and therefore damped, and has a wavelength equal to

the trace wavelength of an acoustic wave in the fluid

travelling at an angle of -45° to the plate normal. The

maximum in the plot for $\mu = 0^{\circ}$ is at a frequency for which

$k_a = \sin \mu = 0$ where k_a, as defined in chapter 4, is the

Floquet wavenumber calculated by neglecting the acoustic

damping.

Figure 5.5 shows the radiated pressure as a function of μ ,

the angle from the plate normal, for five different frequencies.

Again the results are for a normally incident wave, and the

vertical scale is $20\log(R^{\frac{1}{2}}\Omega^2 \phi (R,\mu,0)/A)$. The lowest plot

is for a normalized frequency of 0.108, which is in the first

pass band, and the next is for a frequency of 0.280, which

is in the first stop band. Both plots are almost symmetrical

about $\mu = 0$. The plot for $\Omega = .561$, which is in the second

pass band, shows a maximum at negative μ. The Floquet wave

is still "acoustically slow", in that it is a superposition

of acoustically slow plane waves, but for negative angles, near

to $\mu = -90^{\circ}$, k_f is near to $k_o \sin \mu$. For the remaining two plots

the Floquet wave is acoustically fast, that is $| \text{Re}(k_f)| < k_o$

and the plots show peaks at $\text{Re}(k_f) \simeq k_o \sin \mu$. As the

frequency increases the peak moves to the right. If more

than one of the plane wave components of the Floquet wave is

acoustically fast then there will be more than one peak; the

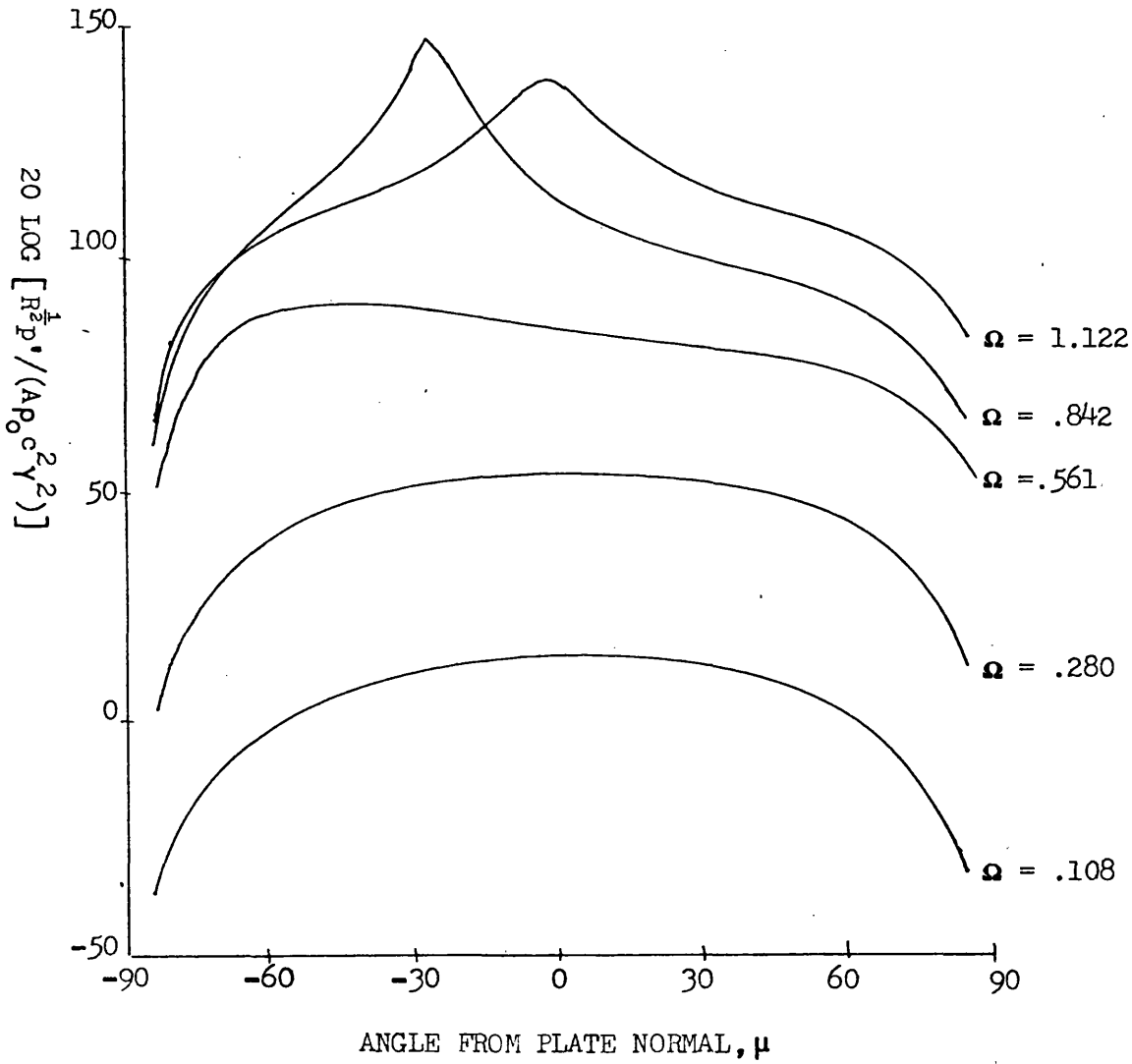peaks will occur at angles μ for which $\text{Re}(k_f - 2n\pi) \simeq k_o \sin \mu$.

Figure 5.5, The farfield pressure against μ, the angle from the plate normal.

The Floquet wavenumber k_f is a function of $k_y = k_p \sin\theta$.
For a fixed frequency k_p is constant and k_f is a function of
θ, the angle between the normal to the beams and the direction
of propagation of the incident wave. Figures 5.6 a,b show the
dependence of k_f upon θ for a frequency $\Omega = 0.068$. Also shown
in figure 5.6a is the acoustic wavenumber k_o and $K = k_p \cos\theta$,
the x-component of the wavenumber in the unstiffened plate. The
plots show that we have pass and stop bands dependent upon θ,
that is, at some angles the incident wave will excite a non-
decaying Floquet wave in the stiffened half of the plate while at
other angles the Floquet wave will be exponentially decaying in
the x-direction.

The corresponding reflection and transmission coefficients
are shown in figure 5.7. The reflection coefficient is shown by the
dashed curve. It is smallest when the x-components of the Floquet
wavenumber and the incident wavenumber are equal, that is, when
$k_f = K$. Throughout the stop band there is almost total reflection
since the stiffened half of the plate is hard to excite. The
transmission coefficient is shown by the solid curve. It is zero
throughout the stop band and is small at high angles of incidence.
At about 19°, where $k_f = K$, the transmission coefficient shows a
sharp drop which is preceded by a sharp peak. As before the
transmission is calculated at a beam position at large x. The
y-dependence of the coefficients is $e^{ik_p y \sin\theta}$ and so the modulus,
as shown in the figures, is independent of y. Clearly, the response
for $\theta < 0$ can be found by symmetry. The plot of transmission
coefficients bears some resemblance to the angular plots given in
chapter 3. Although for point excitation, the asymptotic method
used in chapter 3 is equivalent to looking at a plane wave travelling

in the appropriate direction. Hence, it is expected that the incident
wave excitation of a plate with a semi-infinite array of beams is
a limiting case of the same excitation when only a finite number
of equally spaced beams are present.

Finally, it is noted that except at very small angles of
incidence, $k_p \sin\theta > k_o$. Hence, the imaginary part of k_z is non-zero
and the resulting scattered field in the fluid is exponentially
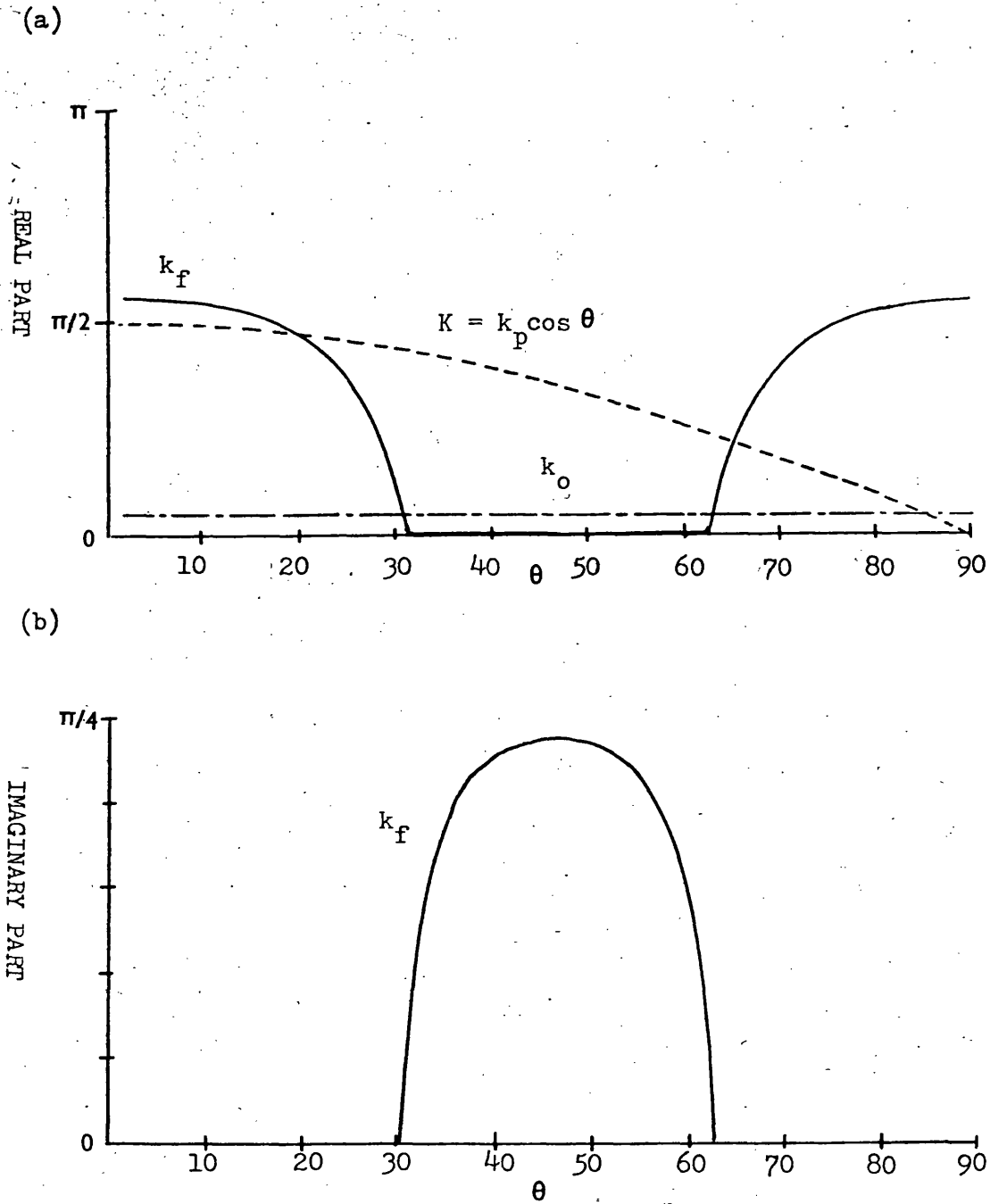decaying with distance.

(a)

(b)

Figure 5.6.   The real and imaginary parts of the Floquet

wavenumber k_f against θ, the angle of incidence

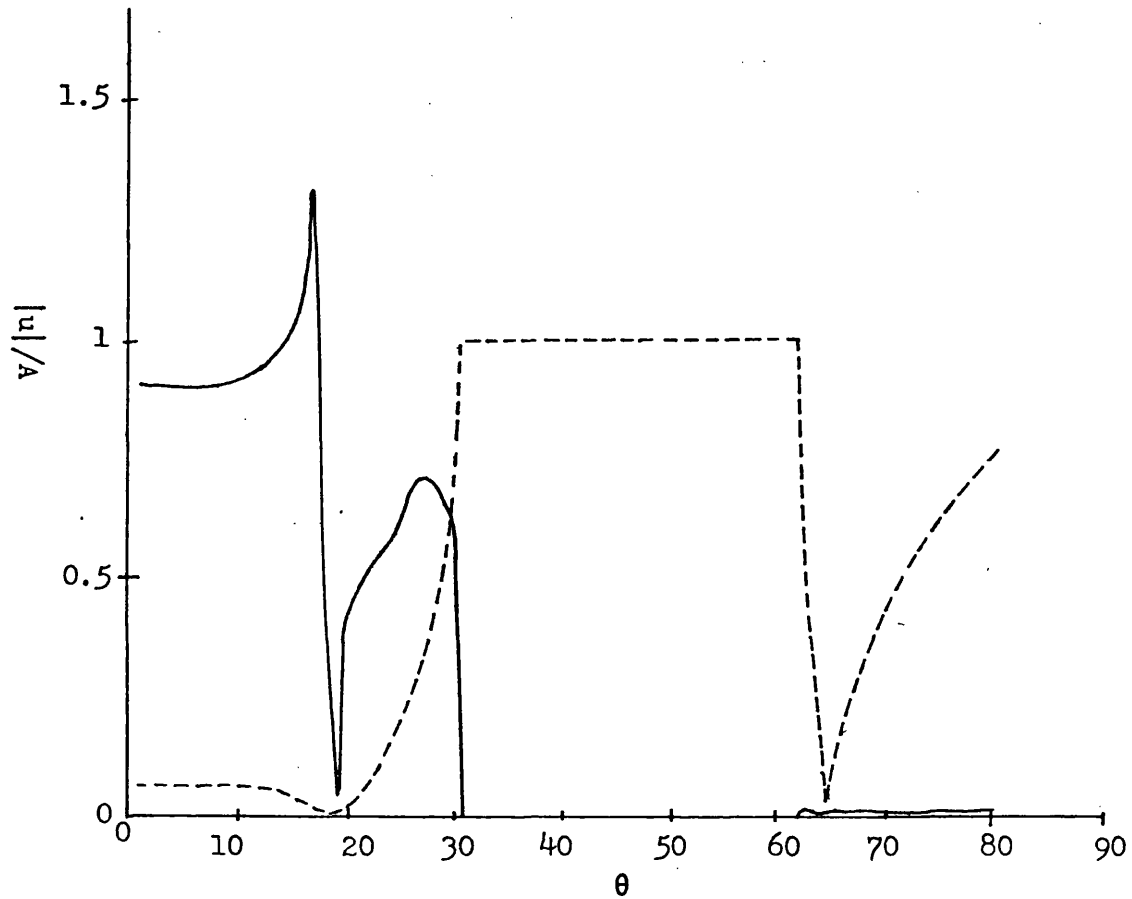from the normal to the beams for a frequency

$\Omega = 0.068$.

Figure 5.7. The transmission (————) and reflection (— — — —)
coefficients against θ, the angle of incidence
from the normal to the beams for a frequency
Ω = 0.068.

5.9 EXTENSIONS

We can extend the methods of this chapter to obtain the
response of a periodically stiffened plate with additional
stiffeners on one half of the plate. Consider a plate with
stiffeners of impedance Z_1 attached at $x = n$, for all n and with
additional stiffeners at $x = np$, $n \geq 0$, p being a fixed integer.

As in chapter 4 we can find the Green's function, $G_s(x,x^1)$,
for the periodically stiffened plate. It is given by

$$G_s(n,m) = G_s(n-m) = \frac{1}{2\pi} \int_{-\pi}^{\pi} \frac{\tilde{G}(k)e^{-ik(n-m)}}{1+Z_1\tilde{G}(k)} \, dk \quad , \tag{5.9.1}$$

where $\tilde{G}(k)$ is the discrete transform of the Green's function for
the unstiffened plate.

The displacement $u(np)$ satisfies

$$u_+(np) + u_-(np) = -Z_2(G_s \square_p u_+)(np) + \psi(np), \tag{5.9.2}$$

where

$$\psi(np) = (G_s \square_p f)(np) = \sum_{m=-\infty}^{\infty} G_s(np-mp)f(mp). \tag{5.9.3}$$

We define the discrete Fourier transform by

$$\tilde{u}^p(k) = \sum_{n=-\infty}^{\infty} e^{iknp}u(np) \tag{5.9.4}$$

and note that

$$\tilde{u}^p(k) = \frac{1}{p} \sum_{n=0}^{p-1} \tilde{u}(0,k-\frac{2n\pi}{p}). \tag{5.9.5}$$

Transforming (5.9.2) gives

$$\tilde{u}_+^p(k) + \tilde{u}_-^p(k) = -Z_2\tilde{G}_s^p(k)\tilde{u}_+^p(k) + \tilde{\psi}^p(k), \tag{5.9.6}$$

that is

$$\widetilde{L}^p(k)\ \widetilde{u}^p_+(k) + \widetilde{u}^p_-(k) = \widetilde{\psi}^p(k),$$

(5.9.7)

where

$$\widetilde{L}^p(k) = 1 + Z_2\widetilde{G}^p_s(k).$$

We know that $\widetilde{G}(k) = \widetilde{G}(k)/(1 + Z_1\widetilde{G}(k))$ and so we can use (5.9.5)

to find $\widetilde{G}^p_s(k)$. Equation (5.9.7) is a standard Wiener-Hopf equation

and can be solved by the methods already discussed in this chapter;

we write

$$\widetilde{L}^p(k) = \widetilde{L}^p_+(k)\ \widetilde{L}^p_-(k)$$

and

$$\widetilde{\psi}^p(k)/\widetilde{L}_-(k) = \widetilde{F}^p_+(k) + \widetilde{F}^p_-(k),$$

(5.9.8)

where the subscripts +, - denote functions analytic in the upper

or lower half planes respectively. (5.9.7) can then be rearranged

to give

$$\widetilde{L}^p_+(k)\ \widetilde{u}^p_+(k) - \widetilde{F}^p_+(k) = \widetilde{F}^p_-(k) - \frac{\widetilde{u}^p_-(k)}{\widetilde{L}^p_-(k)} = P(k).$$

(5.9.9)

As before, the left hand side of the equation is bounded in some

strip containing the real axis and so by Liouville's theorem

$P(k) = C$, a constant and we can choose $\widetilde{F}^p_+(k)$ so that $C = 0$.

Hence,

$$\widetilde{u}^p_+(k) = \widetilde{F}^p_+(k)/\widetilde{L}^p_+(k).$$

(5.9.10)

The displacement at any position is

$$u(x) = \psi(x) - Z_1(G \square u)(x) - Z_2(G \square_p u_+)(x),$$

(5.9.11)

which transforms under the modified discrete transform to

$$\tilde{u}(x,k) = \tilde{\psi}(x,k) - z_1 \tilde{G}(x,k)\tilde{u}(0,k) - z_2 \tilde{G}(x,k)\tilde{u}_+^p(0,k). \qquad (5.9.12)$$

At $x = 0$ we have

$$\tilde{u}(0,k) = (\tilde{\psi}(0,k) - z_2 \tilde{G}(0,k)\tilde{u}_+^p(0,k))/\tilde{L}(0,k), \qquad (5.9.13)$$

where $\tilde{L}(0,k) = 1 + z_1 \tilde{G}(0,k)$.

Thus we can substitute into (5.9.12) for $\tilde{u}(0,k)$ and $\tilde{u}_+^p(0,k)$ from (5.9.13) and (5.9.10) respectively, and then invert to give the displacement $u(x)$ at any position.

Two interesting special cases of the above problem are;

(i) $p = 1$, that is, we have equally spaced beams with a different impedance on each half of the plate.

(ii) $p = 2$ and $Z_2 = -Z_1$, which gives beams of the same impedance on each side of the plate, but with different spacings.

5.10 CONCLUSIONS

The response of a fluid-loaded plate, stiffened on one half
by a semi-infinite array of beams, can be formulated and
formally solved in terms of discrete convolutions. Application
of the discrete Fourier transform reduces the equation for
the plate displacement to a Wiener-Hopf equation, which can
be solved using the Wiener-Hopf technique. If however, the
moments of the beams on the plate are included, application
of the discrete Fourier transform produces a pair of simultaneous
Wiener-Hopf equations, which cannot be solved unless the fluid
loading is neglected. Similarly, except for the structures
considered in section 5.9, the problem of a plate stiffened
by two dissimilar semi-infinite arrays reduces to a set of
simultaneous Wiener-Hopf equations which cannot be solved.

The exact solution obtained in this chapter requires
lengthy computation but, at large distances from the boundary
between the stiffened and unstiffened halves of the plate,
asymptotic methods can be used to simplify the computation.
An asymptotic expansion for the plate displacement has been
obtained showing that, asymptotically, the displacement in the
unstiffened half of the plate has the form of a plane harmonic
wave, while in the stiffened half it has the form of a Floquet
wave.

The method may be used to find the response to any
excitation. As an example, the response to a free plane wave in
the unstiffened half of the plate has been discussed in detail.
The amplitudes of the transmitted and reflected fields relative
to the incident wave is used to define transmission and

reflection coefficients, which, together with the scattered pressure field, have then been calculated from the asymptotic expressions.

It has been shown that the incident wave, which is acoustically slow at all frequencies and therefore non-radiating, is scattered by the beams and radiates sound into the fluid. If the wavelength in the fluid is shorter than the beam spacing, that is, if $k_o > \pi$, then the pressure field peaks at angles for which the "trace" acoustic wavelength matches the "undamped" Floquet wavelength $(2\pi/(k_a \overset{+}{-} 2n\pi), n=0,1,2,..)$, which is calculated by ignoring the acoustic damping. The actual Floquet wave is damped, since it is radiating energy, and no energy can reach the farfield of the stiffened half of the plate, except through the fluid. At low frequencies the mass loading of the fluid dominates the structure and the effect of the stiffening is small; the reflected and scattered fields are small and the incident wave is transmitted almost unattenuated.

REFERENCES

Bedding, R.J. and Willis, J.R. (80), "The elastodynamic Green's tensor for a half-space with an embedded anisotropic layer". Wave Motion 2, 51 (1980).

Burridge, R. (71), "Lamb's problem for an anisotropic half-space". Quart. J. Mech. Appl. Math. 24, 81 (1971).

Cagniard, L. (39), "Reflexion et Refraction des Ondes Seismiques Progressives".
Gauthier-Villars, Paris (1939).
(Translated into English by E.A. Flynn and C.H. Dix, McGraw-Hill, New York (1962)).

Crighton, D.G. (79), "The free and forced waves on a fluid-loaded elastic plate".
J. Sound and Vibration, 63(2), 225-235 (1979).

Eason, G. (66), "The displacements produced in an elastic half-space by a suddenly applied surface force".
J. Inst. Maths. Applics. 4, 299 (1966).

Evseev, V.N. (73), "Sound radiated from an infinite plate with periodic inhomogeneities".
Sov. Phys. Acoust. 19(3), 226-229 (1973).

Garrelick, J.M. and Lin, G-F. (75), "Effect of the number of frames on the sound radiated by fluid-loaded, frame-stiffened plates".

J. Acoust. Soc. Am. 58(2), 499-500 (1975).

Hayes, M. (77), "A note on group velocity".
Proc. R. Soc. Lond. A, 354, 533-535 (1977).

Heckl, M. (61), "Wave propagation on beam-plate systems".
J. Acoust. Soc. Am. 33(5), 640-651 (1961).

de Hoop, A.T. (60), "A modification of Cagniard's method for
solving seismic pulse problems".
Appl. Sci. Res. B8, 349 (1960).

Johnson, L.R. (74), "Green's function for Lamb's problem".
Geophys. J. R. Astr. Soc. 37, 99 (1974).

Kennett, B.L.N. (80), "Seismic waves in stratified medium II -
Theoretical seismograms".
Geophys. J.R. Astr. Soc. 61, 1 (1980).

Kennett, B.L.N. and Kerry, N.J. (79), "Seismic waves in a
stratified half-space".
Geophys. J.R. Astr. Soc. 57, 557 (1979).

Knopoff, L., Gilbert, F., and Pilant, W.L. (60), "Wave
propagation in a medium with a single layer".
J. Geophys. Res. 65, 265-278 (1960).

Kovinskaya, S.I. and Nikiforov, A.S. (73), "Flexural wave
fields in infinite beam-reinforced plates under point excitation".
Sov. Phys. Acoust. 19(1), 32-35 (1973).

Lamb, G.L. (61), "Input impedance of a beam coupled to a plate".
J. Acoust. Soc. Am. 33(5), 628-633 (1961).

Leppington, F.G. (78), "Acoustic scattering by membranes and plates with line constraints".
J. Sound and Vibration 58(3), 319-332 (1978).

Lighthill, M.J. (58), "Fourier Analysis and Generalized Functions".
Cambridge Uni. Press (1958).

Lin, G-F. and Hayek, S.I. (77), "Acoustic radiation from point excited rib-reinforced plate".
J. Acoust. Soc. Am. 62(1), 72-83 (1977).

Love, A.E.H. (44), "A Treatise in the Mathematical Theory of Elasticity".
Dover, New York (1944).

Mace, B.R. (80a), "Periodically stiffened fluid-loaded plates, I and II".
J. Sound and Vibration, 73(4), 473-504 (1980).

Mace, B.R. (80b), "Sound radiation from a plate reinforced by two sets of parallel stiffeners".
J. Sound and Vibration, 71(3), 435-441 (1980).

Mead, D.J. (73), "A general theory of harmonic wave propagation in linear periodic systems with multiple coupling".
J. Sound and Vibration 27(2), 235-260 (1973).

Mead, D.J. (75), "Wave propagation and natural modes in periodic

systems: I, II".

J. Sound and Vibration 40(1), 1-39 (1975).

Mead, D.J. (76), "An approximate method of predicting the response of periodically supported beams subjected to random convected loading".

J. Sound and Vibration 47(4), 457-471 (1976).

Muskhelishvili, N.I. (53), "Singular integral equations".
P. Noordhoff, Groningen (1953).

Noble, B. (58), "The Wiener-Hopf Technique".
Pergamon Press, New York (1958).

Pao, Y-H and Gajewski, R.R. (77), "The generalized ray theory and transient responses of layered elastic solids".
In: W.P. Mason and R.N. Thurstone, eds., New York (1977), 184.

Pekeris, C.L., Alterman, Z., Abramovici, F. and Jarosch, H. (65), "Propagation of a compressional pulse in a layered solid".
Rev. Geophys. 3, 25-47 (1965).

Powell, M.J.D. (68), "A FORTRAN method for solving systems of non-linear algebraic equations".
Harwell report AERE - R5947, H.M.S.O. (1968).
Also in Rabinowitz, P. "Numerical Methods for Non-linear Algebraic Equations".
Gordon and Breach (1970).

Romanov, V.N. (71), "Radiation of sound by an infinite plate with reinforcing beams".
Sov. Phys. Acoust. 17(1), 92-96 (1971).

Romanov, V.N. (77), "Sound radiation from an infinite plate reinforced with a finite set of beams and driven by a point source".
Sov. Phys. Acoust. 23(1), 64-68 (1977).

Rumerman, M.L. (75), "Vibration and wave propagation in ribbed plates".
J. Acoust. Soc. Am. 57(2), 370-373 (1975).

Sinclair, J.E. (79), "Epicentre solutions for point multipole sources in an elastic half-space".
J. Phys. D: Appl. Phys. 12, 1309-1315 (1979).

Spencer, T.W. (60), "The method of generalized reflection and transmission coefficients".
Geophysics 25, 625-641 (1960).

Stepanishen, P.R. (78), "The acoustic transmission and scattering characteristics of a plate with line impedance discontinuities".
J. Sound and Vibration 58(2), 257-272 (1978).

Whitham, G.B. (74), "Linear and Non-linear Waves".
Wiley, New York (1974).

Willis, J.R. (73), "Self-similar problems in elastodynamics".
Phil. Trans. R. Soc. A274, 435 (1973).

Willis, J.R. and Bedding, R.J. (75), "Arrivals associated
with a class of self-similar problems in elastodynamics".
Math. Proc. Camb. Phil. Soc. 77, 591 (1975).